UNIVERSIDAD NACIONAL AUTÓNOMA DE MÉXICO

PROGRAMA DE MAESTRÍA Y DOCTORADO EN INGENIERÍA
ENERGÍA - DISEÑO BIOCLIMÁTICO

EVALUACIÓN DEL DESEMPEÑO TÉRMICO DE SISTEMAS CONSTRUCTIVOS CON MATERIALES DE CAMBIO DE FASE

THERMAL PERFORMANCE EVALUATION OF CONSTRUCTIVE SYSTEMS WITH PHASE CHANGE MATERIALS

TESIS
QUE PARA OPTAR POR EL GRADO DE:
DOCTOR EN INGENIERÍA

PRESENTA:
LUIS EFRAÍN MORELES VÁZQUEZ

TUTOR PRINCIPAL:
DRA. GUADALUPE HUELSZ LESBROS, IER-UNAM

COMITÉ TUTOR:
DR. JORGE ANTONIO ROJAS MENÉNDEZ, IER-UNAM
DR. GUILLERMO BARRIOS DEL VALLE, IER-UNAM
DR. ABEL HERNÁNDEZ GUERRERO, DIM-UG
DR. LUIS MIGUEL DE LA CRUZ SALAS, IGF-UNAM

TEMIXCO, MOR., DICIEMBRE 2017

Examination Committee

Examination Chair:	Dr. Jorge Antonio Rojas Menéndez
Secretary:	Dr. Guillermo Barrios del Valle
1st Member (Thesis Supervisor):	Dr. Guadalupe Huelsz Lesbros
2nd Member (External Examiner):	Dr. Abel Hernández Guerrero
3rd Member (External Examiner):	Dr. Luis Miguel De la Cruz Salas

Instituto de Energías Renovables, UNAM, Temixco, Mor., Mexico

Thesis Supervisor

Dr. Guadalupe Huelsz Lesbros

_____

Signature

Dedicated to
my daughter Rebeca and my wife Aurea

Acknowledgments

To my thesis supervisor, Dr. Guadalupe Huelsz Lesbros, for her invaluable guidance, support and trust. The knowledge and experience I learned from her are priceless to me

To Dr. Guillermo Barrios del Valle for his support and knowledge in numerical modeling. I really appreciate his invaluable advice and friendship during my doctoral studies

To the Universidad Nacional Autónoma de México UNAM and the Instituto de Energías Renovables IER for the support given to conduct my doctoral studies

To the Consejo Nacional de Ciencia y Tecnología CONACyT for the support given through the postgraduate scholarship program (grant number 299692)

To my supervisory committee, Dr. Jorge Rojas, Dr. Luis Miguel De la Cruz, and Dr. Abel Hernández, for their advice and assessment in the development of my research project

To my family for their love and support, they are an essential part of my life

To my friends and fellows for their companionship

Resumen

El sector de edificios es uno de los mayores consumidores de energía a nivel mundial. El empleo de combustibles fósiles como la principal fuente de producción de energía y la demanda de energía prevista para el uso del aire acondicionado en el sector de edificios llevará a un recrudecimiento de los efectos del cambio climático. Por lo tanto, es muy importante trabajar en el desarrollo de tecnologías sustentables en las edificaciones para reducir el consumo de energía y las emisiones de CO_2. Recientemente el uso de materiales de cambio de fase (MCF) colocados en la envolvente de las edificaciones se ha convertido en una alternativa atractiva para alcanzar estos objetivos. El diseño adecuado de las envolventes de edificaciones que incorporen MCF debe tener en cuenta las propiedades termofísicas de la envolvente, las condiciones climáticas, y las cargas internas de calor con el fin de seleccionar valores óptimos de las propiedades clave de los materiales de cambio de fase (temperatura pico de fusión, cantidad y ubicación dentro del sistema constructivo). De particular relevancia es el estudio de los efectos de la histéresis (la existencia de diferentes curvas de entalpía para los procesos de fusión y congelación) en el desempeño térmico de los MCF y la selección de valores óptimos de las propiedades termofísicas para diferentes condiciones de uso. El objetivo principal de esta tesis es avanzar en el estudio del desempeño térmico de MCF colocados en la envolvente de las edificaciones, considerando diferentes condiciones de uso, diferentes climas y teniendo en cuenta la histéresis. El segundo objetivo es desarrollar las bases de una metodología para seleccionar valores óptimos de las propiedades termofísicas de los MCF para su uso en diferentes climas mexicanos y condiciones de uso. Para lograr estos objetivos se desarrolló un cÃşdigo numérico que resuelve la transferencia de calor unidimensional dependiente del tiempo a través de sistemas constructivos que incorporan MCF colocados en la envolvente de las edificaciones considerando tres modelos diferentes de histéresis, y se analizó su desempeño térmico. Una comparación del desempeño térmico de una pared MCF (nombre comercial Energain) con una pared de placa de cemento (nombre comercial Durock) mostró la superioridad de la pared MCF: ésta reduce la carga de enfriamiento en la condición de aire acondicionado en hasta 41% para una pared MCF de 50 mm de espesor y las horas grado de disconfort cálido en la condición de no aire acondicionado en hasta 52% para una pared MCF de 40 mm de espesor. Se realizaron varios estudios paramétricos del desempeño térmico de una pared con MCF variando sus propiedades termofísicas (temperatura pico de fusión, espesor y diferencia de temperatura de histéresis). Se encontró que la temperatura pico de fusión óptima es cercana a la temperatura de confort térmico, en concordancia con investigaciones previas reportadas en la literatura; y como resultado novedoso se encontró que la histéresis mejora el desempeño térmico y que la selección del espesor debe hacerse caso por caso considerando aspectos técnicos, económicos, y ambientales. Asimismo, al estudiar el desempeño térmico de una pared MCF considerando los tres modelos diferentes de histéresis, se encontraron diferencias importantes entre cada uno, evidenciando el complejo comportamiento térmico de los sistemas constructivos MCF y la dificultad para estudiar la transferencia de calor a través de ellos. Los casos de estudio mostrados en esta tesis, tanto

los que consideraron y los que no consideraron la histéresis, demostraron que no es posible derivar una regla general que permita seleccionar valores óptimos de las propiedades termofísicas de los MCF, en lugar de ello se debe realizar un análisis holístico antes de optar por los MCF como parte de los sistemas constructivos de la envolvente de las edificaciones.

Palabras clave: materiales de cambio de fase; desempeño térmico; dependiente del tiempo; optimización; histéresis

Abstract

The buildings sector is one of the largest energy-consuming sectors globally. The utilization of fossil fuels as the main source of energy production and the expected energy demand in the buildings sector for air-conditioning use, will led to a worsening of climate change effects. Therefore it is very important to work in the development of sustainable building technologies to reduce energy consumption and CO_2 emissions. Recently, the use of phase change materials (PCMs) placed in the building envelope has become an attractive alternative to achieve these goals. Proper design of building envelopes incorporating PCMs must take into account thermophysical properties of the envelope, climate conditions, and internal heating loads in order to select optimal values of the key properties of phase change materials (peak melting temperature, quantity, and location within the constructive system). Of particular relevance is the study of the effects of the hysteresis phenomenon (the existence of different enthalpy curves for the melting and freezing processes) on the thermal performance of PCMs and the selection of the PCM optimal thermophysical properties for different use conditions. The main objective of this thesis is to advance in the study the thermal performance of PCMs placed in the building envelope, considering different use conditions, different climates, and taking into account the hysteresis phenomenon. Also, the second main objective is to develop the basis of a methodology to select optimal values of the thermophysical properties of PCMs for use in different Mexican climates and use conditions. To achieve these objectives it was developed a numerical code that solves the time-dependent one-dimensional heat transfer through PCM-constructive-systems in the building envelope considering three different hysteresis models, and the PCM thermal performance was analyzed. A comparison of the thermal performance of a PCM-wall (commercial name Energain) with a cement board wall (commercial name Durock) showed the superiority of the PCM-wall: it reduces the cooling load in the air-conditioning condition in up to 41% for a PCM-wall 50 mm-thick and the hot discomfort degree hours in the non-air-conditioning condition in up to 52% for a PCM-wall 40 mm-thick. Several parametric studies of the PCM thermal performance varying their thermophysical properties (peak melting temperature, thickness and hysteresis temperature difference) were carried out. It was found that the optimal peak melting temperature is close to the thermal comfort temperature, in agreement with previous research reported in literature; and as a novel result it was found that hysteresis improves the thermal performance and that the thickness selection should be made on a case-by-case basis considering technical, economic, and environmental issues. Also, when studying the thermal performance of a PCM-wall considering the three different hysteresis models there were found important differences between each one, evidencing the complex behavior of PCM-constructive-systems and the difficulty to study the heat transfer through them. The study cases shown in this thesis, cases in which the hysteresis phenomenon was and was not considered, demonstrated that it is not possible to derive a general rule that allows selecting optimal thermophysical

properties of PCMs, instead a holistic analysis should be done before opting for PCMs as a part of the building envelope constructive systems.

Keywords: phase change materials; thermal performance; time-dependent; optimization; hysteresis

Contents

List of Figures

List of Tables

Chapter 1

Introduction

Nowadays, energy and environment are two of the most important challenges for mankind (Glenn et al., 2015). Industrial development and population growth have led to a huge increase in global energy demand, in which the main source of energy production is fossil fuels. In 2014 there was an increase of 1.1% in global energy demand with respect to 2013, with fossil fuels accounting for 81.2% of the world energy production (IEA, 2016a). Overuse of fossil fuels has led to a progressive increase in atmospheric CO_2 and a worsening of global warming, which has been documented in recent years (IPCC, 2013). Of the energy-consuming sectors (buildings, industry, transport, and others), the buildings sector (comprising the residential, commerce, and public services sub-sectors) accounts for 31% of global final energy consumption (Figure 1.1) (IEA, 2016a), contributes about one-third of global CO_2 emissions, and it is expected a 50% increase in energy demand in this sector by 2050 (IEA, 2013).

In 2014 Mexico ranked 15th worldwide in energy consumption, with 1.3% of total world consumption. By 2015 the final energy consumption showed an increase of 3.0% with respect to 2014, being of 5283 PJ[1]. Figure 1.2 shows the final energy consumption by sector in Mexico in 2015. In Mexico during 2015 18.7% (952 PJ) of the final energy consumption was used in buildings (residential, commerce, and public services sub-sectors) (SENER, 2016).

As global temperatures increase and incomes rise worldwide, energy demand in the buildings sector over the next decades is expected to grow dramatically due to the needs of heating and cooling air-conditioning associated with thermal comfort (Davis and Gertler, 2015). Therefore, reductions of energy consumption and CO_2 emissions through the decarbonisation and implementation of technologies in buildings are very important to reach global energy targets and to achieve a sustainable growth (IEA, 2016b).

A key component in buildings to reduce their energy consumption and improve their thermal performance is the envelope (IEA, 2013; Kośny, 2015; Akeiber et al., 2016; Long and Ye, 2016). According to IEA (2013), worldwide heating and cooling energy savings of more than 40% (about 6 EJ by 2050) can be directly attributable to a high performance building envelope. Recently, the use of thermal energy storage systems in the building envelope

[1]The joule (J) is a derived unit of energy in the International System of Units. The petajoule (PJ) is equal to 10^{15} J.

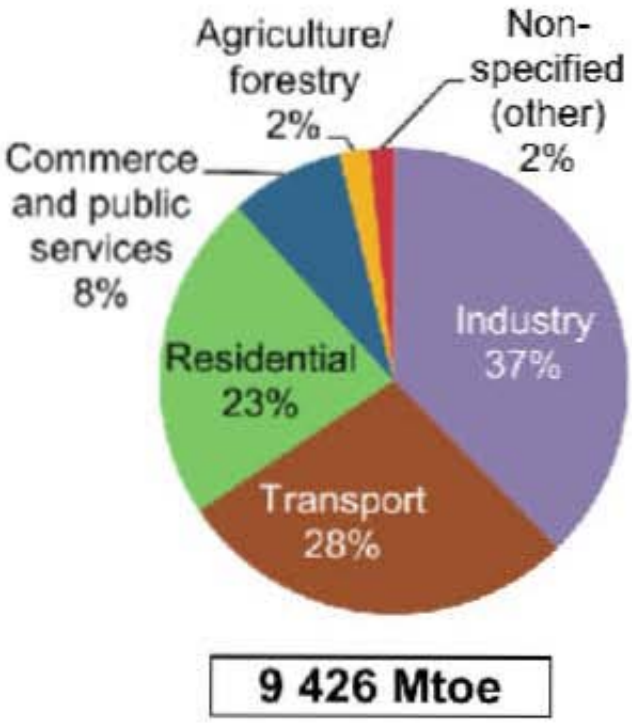

Figure 1.1: Global final energy consumption by sector in 2014. Image taken from IEA (2016a).

has become an attractive alternative contributing to achieve a high performance building envelope, particularly through the use of phase change materials, PCMs. Kośny (2015), Lee et al. (2015), Akeiber et al. (2016), Lei et al. (2016), Ramakrishnan et al. (2017), and Soares et al. (2017) have studied the potential of PCMs placed in the building envelope to reduce energy consumption in buildings and improve the thermal comfort of people.

For building applications, sensible and latent heat storage are the two main ways of thermal energy storage. In sensible heat storage the heat is stored or released accompanied with temperature change of the storage media, whereas in latent heat storage the heat is stored or released as heat of fusion/solidification during phase change processes of the storage media. Compared to sensible heat storage, latent heat storage provides a large energy storage density with a nearly isothermal condition during the phase change processes of the media, so this type of thermal energy storage is preferred (Zhou et al., 2012).

The utilization of PCMs in the building envelope allows to increase the thermal mass of the latter without increase its thickness and they are particularly useful in climates with large diurnal temperature variations. PCMs use energy from the sun continuously, storing energy during the day (through the melting process), and releasing that energy during the night (through the solidification process). In this way the energy demand for heating and cooling is reduced if air-conditioning is used; whereas if air-conditioning is not used the daily indoor air temperature swings are reduced, improving the thermal comfort of people. Figure 1.3 shows a representation of how PCMs work.

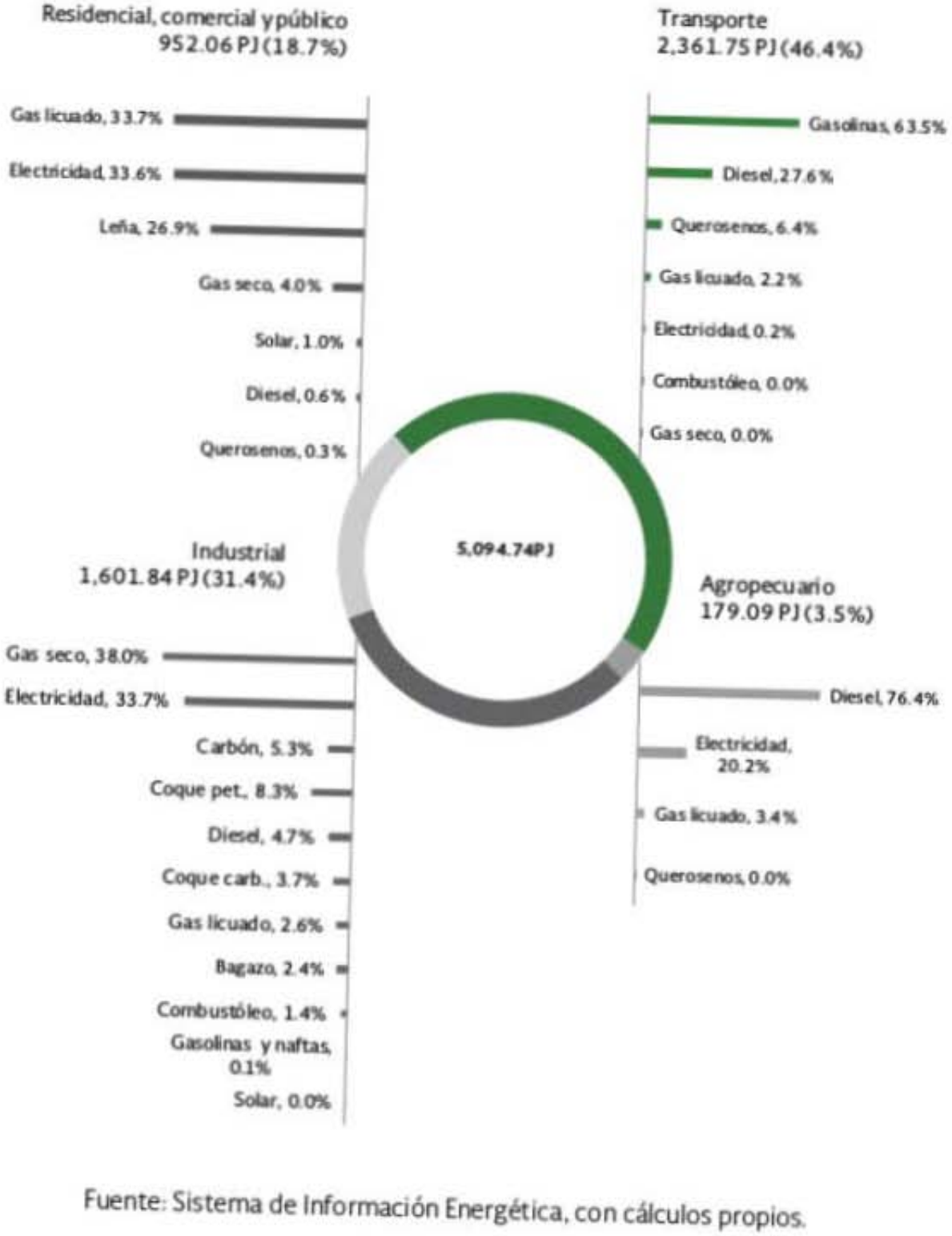

Figure 1.2: Final energy consumption by sector in Mexico in 2015. Image taken from SENER (2016).

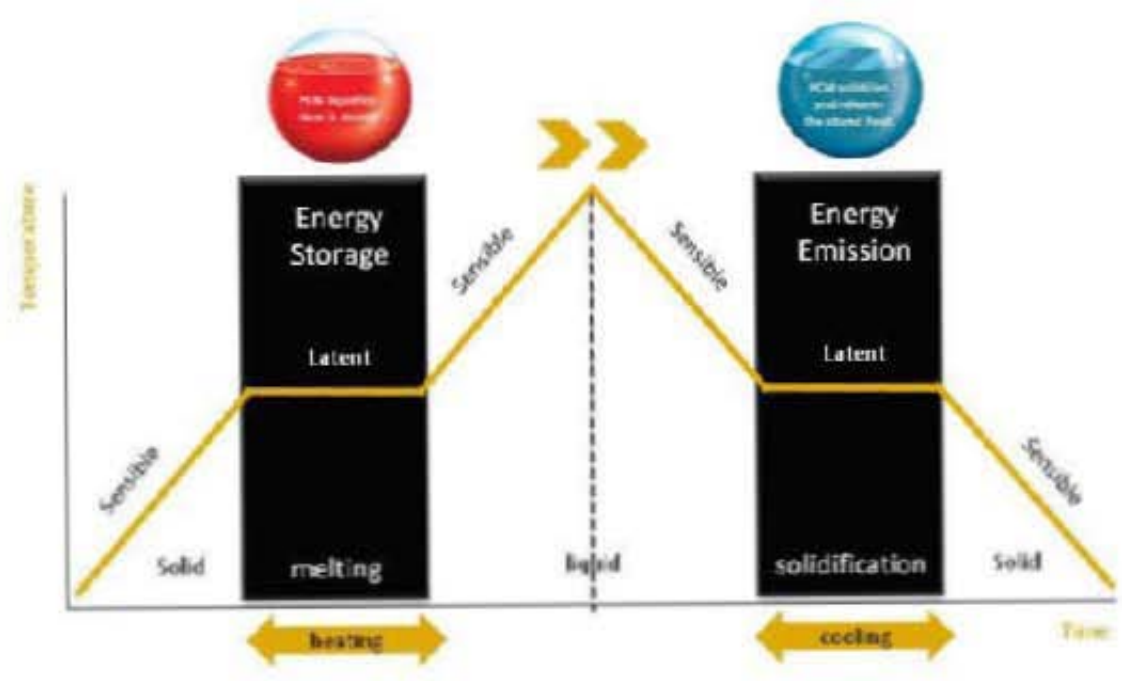

Figure 1.3: A representation of how the phase change materials work. Image by Pazrev - Own work, distributed under a CC BY-SA 4.0 license via Wikimedia Commons, retrieved from https://commons.wikimedia.org/wiki/File:Phase_Change_Materials.png.

Proper design of building envelopes incorporating PCMs is necessary to take full advantage of them as well as to spread their use in the market. The thermal performance of the building envelope is determined by a range of factors: thermophysical properties of the envelope (thermal conductivity, specific heat, density, thickness, outdoor surface solar absorptivity, and infrared emissivity), climate conditions (solar radiation, outdoor temperature, wind velocity, and humidity), and internal heating loads (people, electronic devices, and furniture) (Zhang et al., 2007; Zhou et al., 2012). For PCMs their key properties are peak melting temperature, quantity, and location within the constructive system (Kośny, 2015). Of particular relevance is the selection of the PCM thermophysical properties according to the use condition (air-conditioning, non-air-conditioning, or a combined use of them) in different climates (hot, cold, or climates with a large seasonal temperature range).

Another important property of PCMs is the hysteresis, i.e., the existence of different enthalpy curves for the melting and freezing processes (Mehling and Cabeza, 2008). Lack of knowledge of these both enthalpy curves can leads to a bad estimation of the thermal performance and potential benefits of PCMs. Some studies have shown the importance of considering hysteresis in the numerical simulations to describe the PCM temperature evolution accurately (Kuznik and Virgone, 2009; Gowreesunker et al., 2012; Gowreesunker and Tassou, 2013; Moreles and Huelsz, 2015a), however, no conclusive research has been

done of a physical model of the hysteresis phenomenon in PCMs (Chandrasekharan et al., 2013; Bony and Citherlet, 2007; Jaworski et al., 2014; Delcroix et al., 2015a). Furthermore, there are no research concerning the effects of the hysteresis on the thermal performance of PCMs placed in the building envelope, nor how it modifies the selection of the PCM optimal thermophysical properties for different use conditions.

Based on the above background, the main objective of this thesis is to advance in the study the thermal performance of PCMs placed in the building envelope, considering different use conditions, different climates, and taking into account the hysteresis phenomenon. Also, the second main objective is to develop the basis of a methodology to select optimal values of the thermophysical properties of a PCM for different climates and use conditions. These objectives are addressed using numerical modeling through the following specific objectives:

1. Develop a validated numerical code to simulate the heat transfer through a PCM, that considers the hysteresis phenomenon.

2. Investigate the thermal performance of PCMs in air-conditioning and non-air-conditioning conditions for different climates and compare the optimal thermophysical properties of PCMs for each case.

3. Study the effects of the hysteresis of a building envelope PCM-wall on its thermal performance in conjunction with the peak melting temperature and thickness for different use conditions.

4. Advance in the understanding of the hysteresis phenomenon in PCM-walls through an analysis of their behavior in partial melting-freezing cycles, considering different approaches to simulate them.

The thesis is organized as follows. Chapter 2 presents a review of the phase change materials (properties, classification, and impregnation methods) in building envelope applications. Chapter 3 presents the development and validation of a numerical code used to solve the one-dimensional unsteady heat conduction equation, which is the basis for the development of more complex models solving phase change materials. Chapter 4 presents the mathematical theory of phase change (the Stefan problem) and several numerical methods to simulate it. In Chapter 5 the development, validation, and a sensitivity analysis of a numerical code to simulate the heat transfer through PCMs are presented. An analysis of the thermal performance of a PCM-wall in different climates and use conditions, along with the thermal performance comparison of the PCM-wall with a cement board wall are shown in Chapter 6. The study of the combined effects of hysteresis, peak melting temperature, and thickness of a building envelope PCM-wall on its thermal performance is shown in Chapter 7. The numerical analysis of different approaches to simulate the behavior of a PCM-wall in partial melting-freezing cycles and their effect on the thermal performance of the PCM-wall is shown in Chapter 8. Finally, conclusions are given in Chapter 9.

Chapter 2

Phase change materials for building envelope applications

This chapter presents a review of the phase change materials used in building envelopes, their properties, classification, and the most common incorporation techniques into construction materials.

2.1 Properties of PCMs for use in building envelopes

The process of selecting a suitable PCM is crucial for thermal energy storage. Some obvious requirements are: a suitable melting temperature, large heat of fusion (also called melting enthalpy), and a suitable thermal conductivity specified by the practical application. Another desirable property is congruent melting, i.e., the process in which PCMs melt and freeze repeatedly without phase segregation and consequent degradation of their latent heat of fusion; in contrast with incongruent melting, in which PCMs do not melt uniformly, decomposing into another solid and a liquid with different compositions (Sharma et al., 2009). For their employment as latent heat storage materials in building envelope PCMs must exhibit certain desirable physical, chemical, and economic requirements, which are listed in Table 2.1.

2.1.1 Measurement of thermal properties of PCMs

To correctly analyze a latent heat storage system using PCMs it is necessary to know the thermophysical properties of them. Measurement methods have been developed in order to get the thermophysical properties of PCMs: latent heat of fusion, specific heat, and melting-solidification temperature (Kuznik et al., 2011). The techniques most commonly used for this purpose are described below.

Table 2.1: Selection criteria of PCMs. Table built up from Abhat (1983)) and Mehling and Cabeza (2008).

Requirement		Property	Purpose
Physical	1.	Melting temperature in desired range	To assure storage and release of heat in an application with given temperatures for heat source and heat sink.
	2.	High latent heat of fusion per unit volume	To achieve high storage density compared to sensible heat storage.
	3.	High thermal conductivity	To store or release the latent heat in a given volume of the storage material in a short time.
	4.	High specific heat	To provide for additional significant sensible heat storage.
	5.	High density	To use a smaller volume of the material.
	6.	Small volume changes on phase change	To reduce the containment problems, i.e., to use nearly the same containment volume in both phases of the PCM.
	7.	Small vapor pressure at operating temperatures	To reduce the containment problems, i.e., to use nearly the same containment volume in both phases of the PCM.
	8.	Cycling stability	To use the storage material as many times for storage and release of heat as required by an application.
	9.	Congruent melting	To assure that the liquid and solid phases are identical in composition when a composite material melts.
	10.	High nucleation rate	To avoid supercooling[a].
	11.	High rate of crystal growth	For an efficient heat recovery from the storage system.
Chemical	1.	Chemical stability	To assure long lifetime of the PCM if it is exposed to higher temperatures, radiation, gases, etc.
	2.	Compatibility with materials of construction	To assure long lifetime of the PCM container or of the surrounding materials (e.g., no corrosiveness).
	3.	Safety constraints	To ensure the integrity of the people and the building (e.g., no toxic, no flammable, and no explosive).
Economic	1.	Large-scale availabilities	For a large-scale industrial production.
	2.	Low price	To be competitive with other options for reducing the heat transfer through the building envelope.
	3.	Good recyclability	For environmental and economic reasons.

[a]A PCM is supercooled when it remains in liquid phase when cooled below the freezing temperature.

Differential scanning calorimetry (DSC)

Differential scanning calorimetry (DSC) is a technique for the thermal characterization of materials using small samples of these (with a typical size of 6.3 mm in diameter and 6.3 mm high). This technique provides local values of different properties and is not useful to characterize actual scale PCM composites incorporated in buildings (Kuznik et al., 2014).

This technique characterizes the melting and fusion processes. A differential scanning calorimeter measures the heat flux between the test sample and a reference sample (commonly alumina, Al_2O_3), while both samples are maintained at nearly the same temperature and the reference sample is heated or cooled at a constant rate. The heat flux is recorded as function of temperature or time (Whiffen and Riffat, 2013). In a heat flux versus temperature curve, the latent heat of fusion is calculated as the area under the peak for the melting process, whereas the melting temperature is calculated by the tangent at the greatest slope point on the first portion of the peak (Sharma and Sagara, 2005).

Figure 2.1 shows the freezing and melting curves for a paraffin mixture obtained with a DSC, with a heating and cooling rate of 0.05 $K \cdot min^{-1}$. The calculated latent heats of melting and freezing are, respectively, 107.5 $J \cdot g^{-1}$ and 104.5 $J \cdot g^{-1}$ for the interval [−20°C, 35°C]; and 72.4 $J \cdot g^{-1}$ and 71 $J \cdot g^{-1}$ for the interval [5°C, 30°C] (Kuznik et al., 2011).

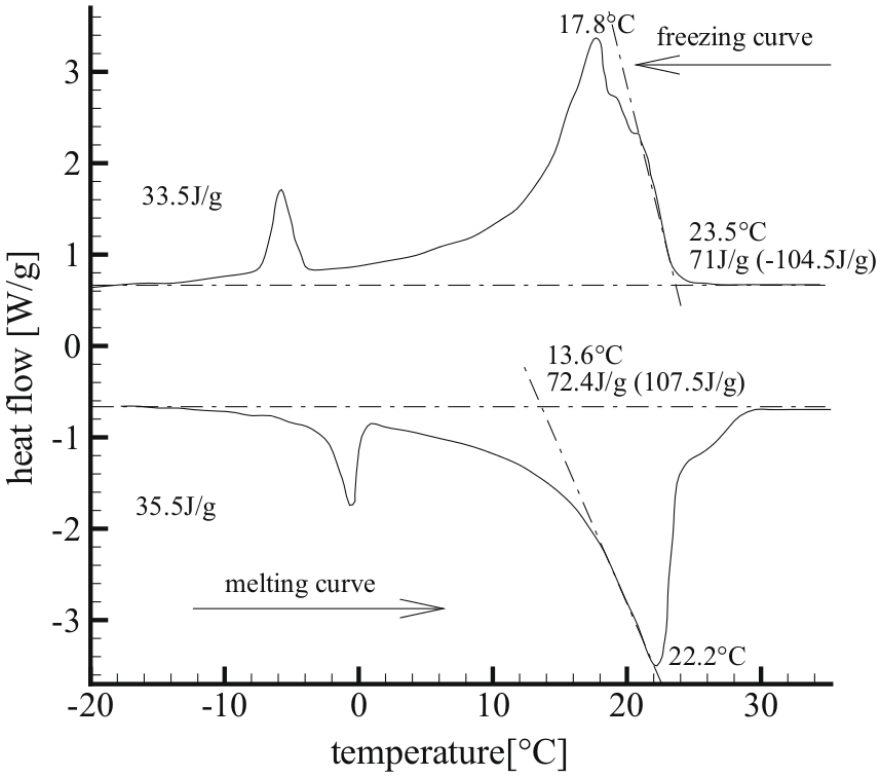

Figure 2.1: Differential scanning calorimeter melting and freezing curves for a paraffin mixture. Image taken from Kuznik et al. (2011).

Soares et al. (2013) indicated that the omission of certain phenomena in a DSC test (convection, non-uniformity in the temperature profile of the sample, thermal inertia of the sample, and the small sample size) results in an inappropriate calculation of the equivalent heat capacity. These drawbacks, in addition to the costly and complexity of the test, are the main limitations of the DSC technique.

Differential thermal analysis (DTA)

DTA technique is an alternative technique to DSC. In this technique the heat flux applied to the test sample and the reference sample remains the same and the temperature differences between them are recorded. From this, the test sample can be characterized and several thermal properties can be calculated (e.g., heat capacity and thermal conductivity). (Soares et al., 2013; Zhou et al., 2012).

The T-history method

Zhang et al. (1999) proposed a new calorimetric method, the T-history method, which solves some of the limitations of the DSC and DTA techniques. The T-history method is useful to determine the heat of fusion, specific heat, and thermal conductivity of large samples of PCMs with a simple experimental configuration. Through a group of tests it can analyze lots of PCM samples and then calculate values for different thermophysical properties of each sample, with an acceptable precision for engineering applications; also, the phase change processes can be clearly observed. Zhang et al. (1999) used the T-history method to measure the thermophysical properties of several PCMs and found a difference of 10% between their results with data reported in literature.

In this method the test samples and the reference sample are put in vertical tubes, and the temperature of them is recorded with thermocouples located inside each tube. The test starts with all of the samples in liquid phase, then they are inmersed into a monitored and controlled ambient (usually cold water) where the temperature is maintained below the PCM fusion temperature (Kuznik et al., 2011).

The PCM temperature is recorded as function of time, then the PCM thermophysical properties can be obtained by comparison of this curve with the corresponding curve of a reference material (commonly pure water) (Zhang et al., 2007). An example of the curve obtained is shown in Figure 2.2, in which it is possible to observe three different processes: cooling of the liquid phase, the solidification of the PCM, and the cooling of the solid phase. The heat capacity in the solid state is calculated as the area between the temperature curve of the test sample and the temperature curve of the ambient (A_1 area) during the cooling of the liquid phase, the latent heat of solidification is calculated as the area between the temperature curve of the test sample and the temperature curve of the ambient (A_2 area) during the solidification process, and the heat capacity in the liquid state is calculated as the area between the temperature curve of the test sample and the temperature curve of the ambient (A_3 area) during the cooling of the solid phase. Using the total solidification time

and an inverse method, the thermal conductivity of the sample can be obtained (Kuznik et al., 2011).

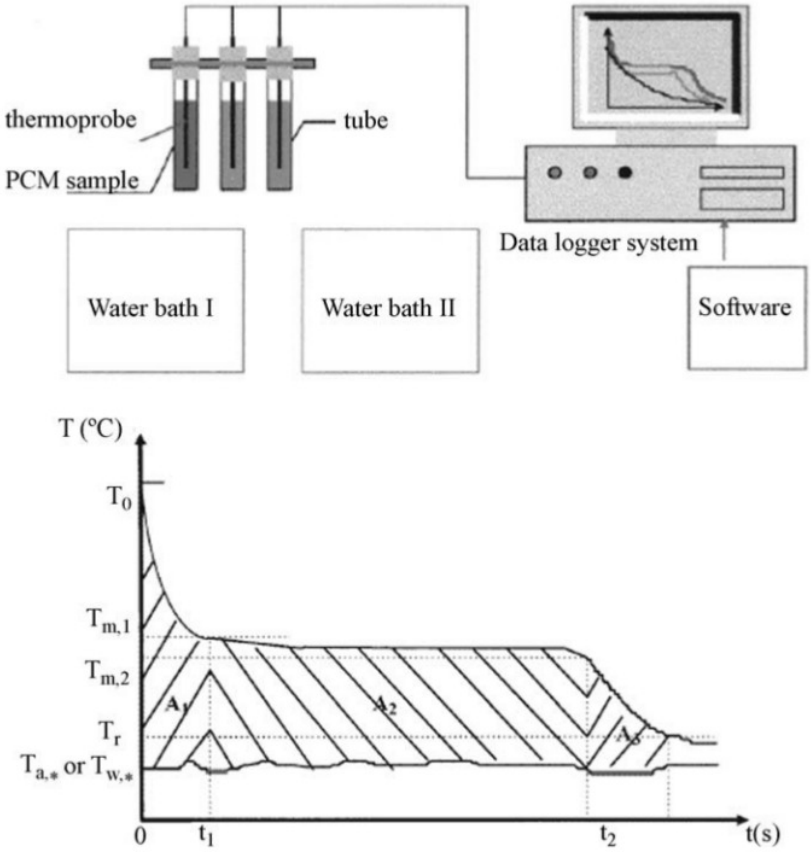

Figure 2.2: T-history experimental setup (top figure) and T-history temperature curves (lower figure). Image taken from Kuznik et al. (2011). T is temperature, t is time, T_o is the initial temperature record in the test, T_f is the final temperature record in the test, $T_{m,1}$ is the onset solidification temperature, $T_{m,2}$ is the ending solidification temperature, $T_{a,*}$ is the ambient temperature, and $T_{w,*}$ is the water temperature.

Despite the simplicity and usefulness of the T-history method, the most used methods to characterize the thermal performance of PCMs are the DSC and DTA techniques (Whiffen and Riffat, 2013).

2.2 Classification of PCMs

There are a large number of phase change materials in a wide range of melting temperatures. Figure 2.3 shows the classification of PCMs and Table 2.2 summarizes the advantages and disadvantages of the different PCMs for use in heat storage.

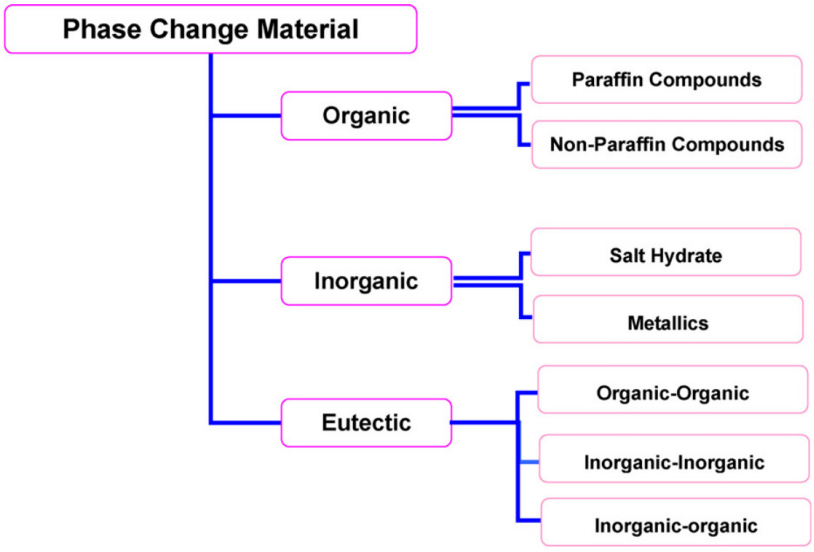

Figure 2.3: Classification of PCMs. Image taken from Sharma et al. (2009).

Table 2.2: Comparison of different kinds of PCMs. Table taken from Zhou et al. (2012).

Classification	Advantages	Disadvantages
Organic	1. Availability in a large temperature range 2. High heat of fusion 3. No supercooling 4. Chemically stable and recyclable 5. Good compatibility with other materials	1. Low thermal conductivity (around 0.2 $W \cdot m^{-1} \cdot K^{-1}$) 2. Relative large volume change 3. Flammability
Inorganic	1. High heat of fusion 2. High thermal conductivity (around 0.5 $W \cdot m^{-1} \cdot K^{-1}$) 3. Low volume change 4. Availability in low cost	1. Supercooling 2. Corrosion
Eutectics	1. Sharp melting temperature 2. High volumetric thermal storage density	1. Lack of currently available test data of thermo-physical properties

The melting enthalpy and melting temperature for the different groups of PCMs are shown in Figure 2.4. Figure 2.5 presents the melting temperature and heat of fusion graphically for the different groups of PCMs. On the chart, each marker type represents a different PCM category:

- $\times$ Organics (e.g., paraffins).
- $\diamondsuit$ Organic eutectics (e.g., fatty acid mixtures).
- $-$ Inorganics (e.g., salt hydrates).
- $\circ$ Inorganic eutectics (e.g., salt mixtures).

Figure 2.5 shows that the salt hydrates have the highest values of heat of fusion. However, within the range of human comfort temperature ($[18°C, 28°C]$), paraffin-based organics have the highest values of heat of fusion (Whiffen and Riffat, 2013).

The following section describes the main characteristics, as well as their advantages and disadvantages, of the different phase change materials for their application in building envelope.

2.2.1 Organic phase change materials

Organic PCMs can be subdivided in two groups: paraffins and non-paraffins.

Paraffins

Paraffins are mixtures composed mainly of straight chain n-alkanes, $CH_3 - (CH_2)_n - CH_3$. Due to their molecular constitution, it is possible to increase their melting temperature and latent heat of fusion by increasing their chain length. Laboratory grade paraffin waxes (tetradecane, hexadecane, and their binary mixtures) have been tested for cool storage applications and it has been found that they are excellent PCM candidates; however technical grade paraffin waxes are still quite used due to excessive prices of the laboratory grade materials. Paraffins have several advantages: they are safe, reliable, predictable, non-corrosive, chemically inert, and stable below 500°C. Also, they have little volume changes on melting, low vapor pressure in the melt form, congruent melting, and good nucleating properties. On the other hand they have some disadvantages (low thermal conductivity, non-compatible with the plastic container, and moderately flammable); however, these disadvantages can be partly eliminated by slightly modifying the wax and the storage unit (Sharma et al., 2009).

Non-paraffins

The non-paraffin organic compounds are the largest group of PCMs for heat storage systems in building applications. They include fatty acids, esters, alcohols, and glycols, which can be subdivided as fatty acids and other non-paraffin organic. Each of these materials

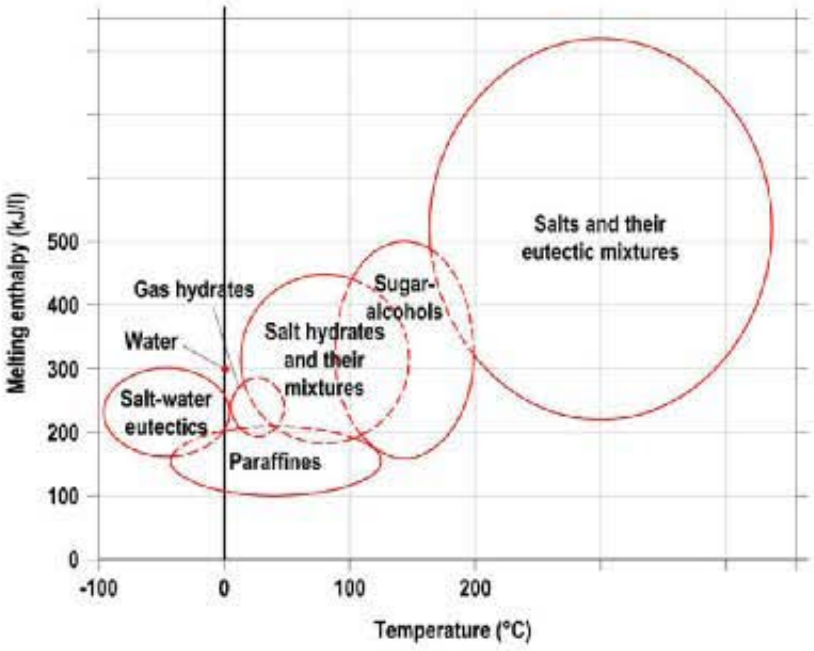

Figure 2.4: The melting enthalpy and melting temperature for the different groups of phase change materials. Image taken from Baetens et al. (2010).

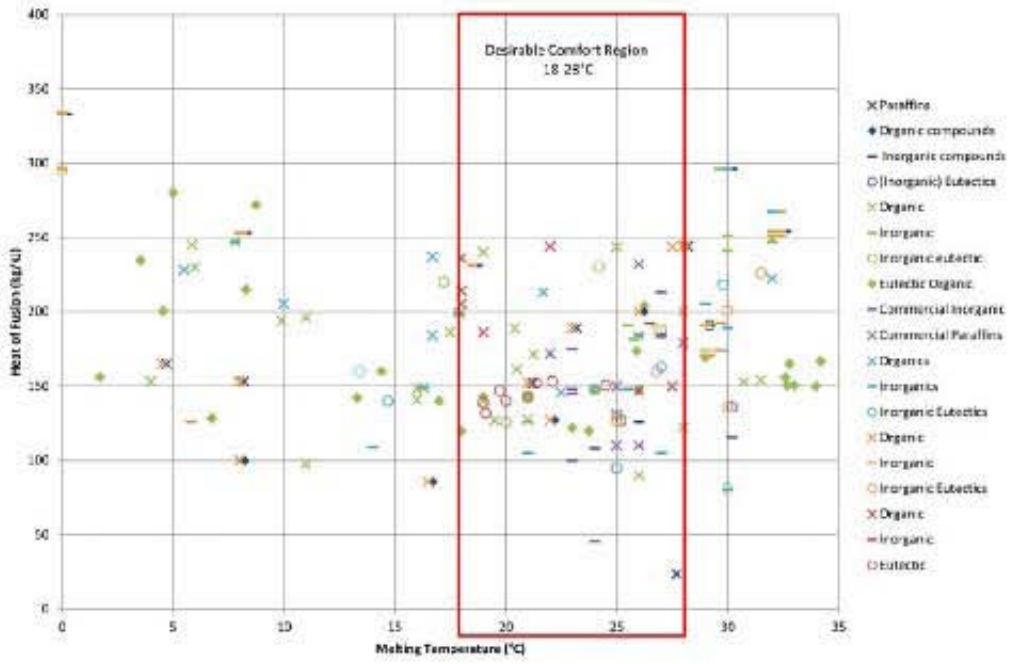

Figure 2.5: Melting temperature and heat of fusion for known PCMs with melting temperatures between 0°C and 35°C. The red rectangle indicates the desirable comfort region. Different colors of markers represent each of the sources from which data are taken. Image taken from Whiffen and Riffat (2013).

have particular properties and different form each other. These materials exhibit the following properties: high heat of fusion, inflammability, low thermal conductivity, low flash temperature, varying level of toxicity, and instability at high temperatures (Sharma et al., 2009).

Fatty acids, whose general molecular formula is $CH_3(CH_2)_{2n} \cdot COOH$, have high values of heat of fusion compared to that of paraffins. They have reproducible melting and freezing behavior and do not exhibit supercooling. However, they are expensive and mild corrosive (Sharma et al., 2009).

2.2.2 Inorganic phase change materials

Inorganic materials can be subdivided in hydrated salts and metallics. Relevant properties of these materials are that they do not exhibit an appreciable supercooling and that their heat of fusion do not degrade with cycling (Sharma et al., 2009).

Salt hydrates

Salt hydrates are alloys of inorganic salts and water, whose general molecular formula is $AB \cdot nH_2O$. The advantages of these compounds are: high latent heat of fusion per unit volume, relatively high thermal conductivity (almost double of the paraffins), small volume changes on melting, not very corrosive, compatible with plastics, slightly toxic, and not so expensive.

The main drawback of these compounds is that they melt incongruently. Sharma et al. (2009) mentioned that "this disadvantage can be solved by mechanical stirring, by encapsulating the PCM to reduce separation, by adding of the thickening agents which prevent setting of the solid salts by holding it in suspension, by use of excess of water so that melted crystals do not produce supersaturated solution, or by modifying the chemical composition of the system and making incongruent material congruent". Other disadvantages of salt hydrates are poor nucleating properties and supercooling, which can be solved by adding a nucleating agent (Sharma et al., 2009).

Metallics

These group includes the low melting metals and metal eutectics. These materials change phase in a sharp temperature interval, have high values of density and thermal conductivity, and low values of heat of fusion and vapor pressure. However, due to their heavy weight they are not considered for use in building applications (Sharma et al., 2009).

2.2.3 Eutectics

Eutectics are mixtures made of two or more organic, inorganic or organic-inorganic compounds, designed to change phase at a specific temperature in a sharp interval (Whiffen and

Riffat, 2013). An eutectic has a lower melting temperature than that of each individual component, which melts and freezes congruently and without phase segregation (Sharma et al., 2009). These materials have high volumetric storage densities, but to date there is no enough data of their properties, which has limited their use (Whiffen and Riffat, 2013).

2.2.4 Commercial PCMs

Most PCMs designed to be used as latent heat storage system in buildings do not satisfy the desirable requirements listed in Table 2.1. Then, one should select the PCM with the better properties and design the system according to the particular PCM application (Sharma et al., 2009).

Table 2.3 shows several commercial PCMs with a melting temperature between 18°C and 28°C (the commonly accepted comfort temperature range), along with their thermal properties.

Table 2.3: Commercially available PCMs with melting temperature range between 18°C and 28°C. Table taken from Whiffen and Riffat (2013).

Material	Type	Melting temperature (°C)	Heat of fusion ($kJ \cdot kg^{-1}$)	Thermal conductivity ($W \cdot m^{-1} \cdot K^{-1}$)	Company source
RT 20	Paraffin	22	172	0.88	Rubitherm GmbH
Climsel C 23	Salt hydrate	23	148		Climator
E 23	Salt hydrate	23	155	0.43	EPS Ltd.
Climsel C 24	Salt hydrate	24	108	1.48	Climator
TH 24	Salt hydrate	24	45.5	0.8	TEAP
RT 26	Paraffin	25	131	0.88	Rubitherm GmbH
RT 25	Paraffin	26	232		Rubitherm GmbH
STL 27	Salt hydrate	27	213	1.09	Mitsubishi Chemical
S27	Salt hydrate	27	207		Cristopia
AC 27	Salt hydrate	27	207	1.47	Cristopia
RT 27	Paraffin	28	179	0.87	Rubitherm GmbH

2.3 Incorporation of PCMs into construction materials

This section describes the principal mechanisms for the incorporation of PCMs into construction materials: incorporation methods and containers.

2.3.1 Incorporation methods

The three most commonly used methods to incorporate PCMs into construction materials are direct incorporation, immersion, and encapsulation. After the incorporation the melting and freezing temperatures of PCMs may vary slightly. Another methods include shape-stabilised PCMs and laminated PCM boards (Zhang et al., 2007).

Direct incorporation

In this method melted or powdered PCMs are added directly into construction materials (e.g., gypsum, concrete, or plaster) during their phase of production. This method has the advantage of not requiring additional equipment, but has the disadvantage that problems of leakage and incompatibility with construction materials can occur (Zhou et al., 2012).

Immersion

In this method construction materials (e.g., gypsum, brick, or concrete) are immersed into melted PCMs such that PCMs can be absorbed into the internal pores of the construction materials by capillarity. Then the construction materials are cooled to keep the PCM inside the pores. This method is very easy and practical, but may has the problem of leakage for long-term use (Zhang et al., 2007; Zhou et al., 2012).

Macroencapsulation

In this method PCMs are encapsulated in a container (e.g., tubes, spheres, or panels) before incorporating them into the construction materials. This method prevents leakage, but has the following disadvantages: reduces the PCM thermal conductivity, may cause solidification at the edges, requires more work than the previous methods, and is expensive (Zhang et al., 2007; Zhou et al., 2012).

Microencapsulation

In this method small PCM particles are enclosed in a thin, sealed, and high molecular weight polymeric film. This method is easy, practical, and economic. Also it provides good heat transfer rates and prevents leakage, but may affect the mechanical strength of structures (Zhang et al., 2007; Zhou et al., 2012).

Shape-stabilised PCMs

In this method the PCM is dispersed on a supporting material (e.g. high density polyethylene) to form a composite material. The resulting material is stable (keep its shape during the phase change processes), has a large apparent specific heat, a high thermal conductivity, and a good cycling performance for the long-term use. Shape-stabilised PCMs can be used as

linings in interior walls, ceilings, and floors (Zhou et al., 2012). Figure 2.6 shows a shape-stabilised PCM. The attractive properties of this kind of PCMs have motivated the attention of many researchers, which have analyzed their thermal performance in different conditions (e.g., Zhang et al. (2006) and Zhou et al. (2008)).

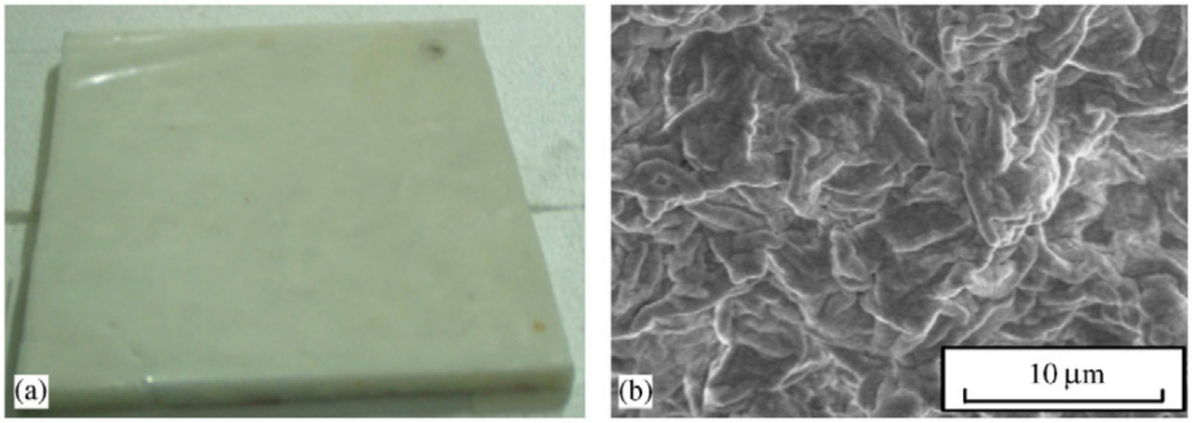

Figure 2.6: The photos of the shape-stabilized PCM. (a) Photo of the plate and (b) electronic microscopic picture by scanning electric microscope (SEM) HITACHI S-450. Image taken from Zhang et al. (2007).

Laminated PCM board

Another incorporation method is the laminate. In this method PCMs are laminated into a single layer of the building envelope (e.g., an inside lining wall) (Zhang et al., 2007). The thermal performance of this kind of PCM is better than that of the randomly mixed PCM drywalls[1], as was shown in the studies carried out by Darkwa and Kim (2004, 2005).

2.3.2 Containers

In this method PCM are held in conventional construction materials (e.g., gypsum board, concrete, brick, and plaster). Also, PCMs can be encapsulated into other panels such as PVC panels, CSM panels, plastic and aluminum foils (Zhou et al., 2012).

[1]The randomly-mixed PCM drywall is made up of one layer of PCM and gypsum mixed together.

Chapter 3

Model of heat conduction through a constructive system without phase change

This chapter presents the description of the physical problem of heat conduction through a constructive system placed in the building envelope, the mathematical model used to represent it, and the numerical method to solve it. From the numerical method a numerical code was written to evaluate the thermal performance of different constructive systems of the building envelope. Finally, the validation of the numerical code is presented. The validation was made by comparing an analytical solution for a specific case and by comparing the results obtained with a numerical program named Ener-Habitat.

3.1 Physical problem

The problem to solve considers the time-dependent one-dimensional heat transfer through a constructive system placed in the building envelope (Figure 3.1). T_{sa} is the sol-air temperature (ASHRAE, 2005), which represents the outdoor conditions, T_i is the indoor air temperature, T_{os} is the temperature at the outdoor surface, T_{is} is the temperature at the indoor surface, and d is a distance measured from the indoor surface to the indoor space at which the heat transfer is supposed to be zero (a distance at which an adiabatic or a symmetry condition is assumed) (Barrios et al., 2016). In this work the indoor air was supposed perfectly mixed, so T_i is homogeneous. Also, internal heat gains and infiltration were not considered.

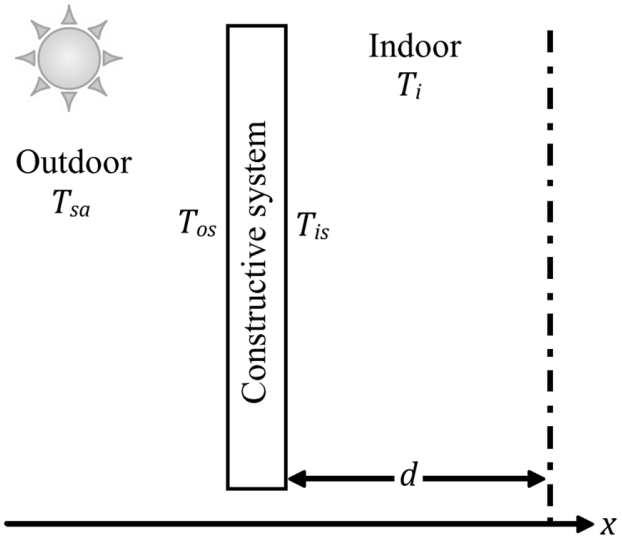

Figure 3.1: Scheme of heat transfer through a constructive system of the building envelope. T_{sa} is the sol-air temperature, T_i is the indoor air temperature, T_{os} is the temperature at the outdoor surface, T_{is} is the temperature at the indoor surface, x is the spatial coordinate, and d is a distance measured from the indoor surface to the indoor space at which the heat transfer is supposed to be zero.

3.2 Mathematical model

In order to solve the physical problem described above, the time-dependent one-dimensional heat conduction equation for the constructive system was considered (Farlow, 1993),

$$\rho c \frac{\partial T}{\partial t} = \frac{\partial}{\partial x}\left(k \frac{\partial T}{\partial x}\right). \tag{3.1}$$

Equation (3.1) expresses the principle of conservation of energy (thermal energy) considering heat flows only in one dimension. T is the temperature as function of time, t, and space, x, ρ is the density, c is the specific heat, and k is the thermal conductivity. For temperature dependent properties ($c = c(T)$, $\rho = \rho(T)$, and $k = k(T)$) the heat equation becomes quasi-linear, for non-uniform material ($k = k(x)$) the heat equation becomes nonlinear, and for homogeneous material (k constant) the heat equation becomes parabolic (Farlow, 1993).

The solution of this partial differential equation (PDE) requires two types of additional equations (Farlow, 1993):

1. The initial condition (IC) describing the physical phenomenon at the start of the experiment: $T(x, 0) = f(x)$.

2. Two boundary conditions (BCs) describing the physical condition of the problem on

the boundaries. The three most common types of boundary conditions are:

1. $T = g(t)$ temperature specified on the boundary by a function $g(t)$.
2. $-k\dfrac{\partial T}{\partial x} = g(t)$ heat flux across the boundary specified by a function $g(t)$.
3. $-k\dfrac{\partial T}{\partial x}\Big|_B = \mu\left(T_{sm} - T_B\right)$ heat flux across the boundary B, specified via a heat transfer coefficient, μ, the temperature of the surrounding medium, T_{sm}, and the temperature at the boundary, T_B. T_{sm} can represent T_{sa} or T_i.

With the IC and BCs specified, there is only one function $T(x,t)$ that satisfies the PDE.

In this work the boundary conditions were specified via the heat flux across the outdoor surface, q_{os}, and the heat flux across the indoor surface, q_{is}. At the outdoor surface, os, and at the indoor surface, is, these conditions are:

$$q_{os} = -k\frac{\partial T}{\partial x}\Big|_{os} = \mu_o\left(T_{sa} - T_{os}\right), \tag{3.2}$$

$$q_{is} = -k\frac{\partial T}{\partial x}\Big|_{is} = \mu_i\left(T_{is} - T_i\right), \tag{3.3}$$

where $\mu_o = 13.0\,\mathrm{W{\cdot}m^{-2}{\cdot}K^{-1}}$ and $\mu_i = 8.1\,\mathrm{W{\cdot}m^{-2}{\cdot}K^{-1}}$ are the outdoor and indoor film coefficients, respectively, which were taken from the Mexican official standard NOM-ENER-020-2011 (SENER, 2011).

Two conditions on the indoor air temperature, T_i, were considered: the non-air-conditioning (nAC) condition and the air-conditioning (AC) condition. For the nAC condition it was considered that the rate of change of the energy of the indoor air is equal to the heat flux across the indoor surface. Using Equation (3.3) this is expressed as

$$d\rho_a c_a\frac{dT_i}{dt} = \mu_i\left(T_{is} - T_i\right), \tag{3.4}$$

where ρ_a is the density of the air and c_a is the specific heat of the air. In this work, according to Barrios et al. (2016) a value of 2.5 m for the distance d was considered. When evaluating a wall, d is the distance at which an adiabatic or a symmetry condition is assumed, the center of the room (Barrios et al., 2016). For the AC condition there are two choices:

- The simplest type. T_i is constant and fixed to the comfort temperature, T_c.
- An energy saving type. When T_i is within the thermal comfort zone (TCZ) the air-conditioning is turned off and T_i is calculated according to Equation (3.4). If T_i is greater than the upper limit of the TCZ the air-conditioning cools the space with the upper limit of the TCZ as the setpoint. If T_i is below the lower limit of the TCZ then the air-conditioning heats the space with the lower limit of the TCZ as the setpoint.

An air-conditioning system that can supply any amount of cooling or heating load was considered.

3.3 Numerical model

This section presents the numerical solution of Equation (3.1) using the control-volume formulation to deriving the discretization equations. In this formulation the domain is discretized using several grid points, with nonoverlapping control volumes surrounding the grid points, and with the temperature recorded at each grid point. Alike the space discretization, the temperature is recorded in discrete time intervals. Then, the heat conduction equation (Equation (3.1)) is integrated over each control volume and the discretization equations are obtained. The most attractive attribute of this formulation is that the energy conservation principle holds for every control volume and for any number of grid points (Patankar, 1980).

In the evaluation of the thermal performance of constructive systems in the envelope of buildings is appropriate to assume ρc constant for each material. Then, the solution is obtained by moving forward in time (with a time step Δt) from a given initial distribution of temperature, and finding the values of the temperature in successive time steps, given the boundary conditions.

The grid considered for the constructive system is shown in Figure 3.2. The constructive system was discretized in $Nx - 1$ control volumes and two half control volumes adjacent to the boundaries, which are denoted by the points 0 and Nx. Each control volume i has a length $(\delta x_l)_i + (\delta x_r)_i$ and the interfaces between the control volumes are specified by s_i.

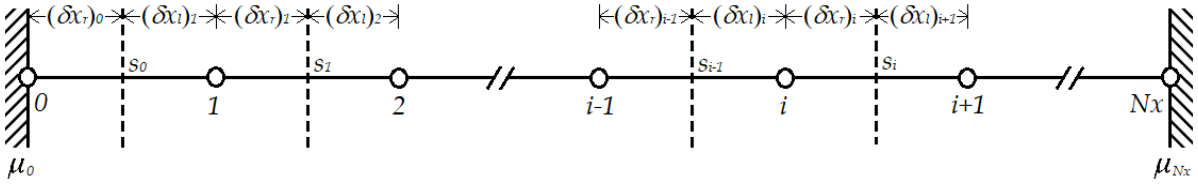

Figure 3.2: Grid considered for the constructive system. Control volumes for the internal and boundary points are shown.

The procedure to solve Equation (3.1) was taken from Patankar (1980). However, the notation for the grid considered is different from that considered by Patankar (1980), so the notation for the discretization equation is also different.

The discretization equation is derived by integrating Equation (3.1) over a control volume and over a time interval (t to $t + \Delta t$). Thus

$$(\rho c)_i^{n+1} \int_{s_{i-1}}^{s_i} \int_t^{t+\Delta t} \frac{\partial T}{\partial t} dt dx = \int_t^{t+\Delta t} \int_{s_{i-1}}^{s_i} \frac{\partial}{\partial x} \left(k \frac{\partial T}{\partial x} \right) dx dt, \tag{3.5}$$

where the order of the integrations is chosen according to the nature of the term. For the representation of the term $\partial T/\partial t$, it will be assumed that the grid-point value of T prevails

throughout the control volume. Then

$$(\rho c)_i^{n+1} \int_{s_{i-1}}^{s_i} \int_t^{t+\Delta t} \frac{\partial T}{\partial t} dt dx = (\rho c)_i^{n+1} \left(\delta x_l + \delta x_r\right)_i \left(T_i^{n+1} - T_i^n\right), \tag{3.6}$$

where the subscript corresponds to the spatial coordinate and the superscript corresponds to the time coordinate.

For a good representation of the heat flux at the interface (e.g., s_i) the expression for the conductivity at the interface must be (e.g., s_i)

$$k_{s_i} = \left[\frac{1 - f_{s_i}}{k_i} + \frac{f_{s_i}}{k_{i+1}}\right]^{-1}, \tag{3.7}$$

where

$$f_{s_i} = \frac{(\delta x_l)_{i+1}}{(\delta x_r)_i + (\delta x_l)_{i+1}}. \tag{3.8}$$

For the spatial integration of Equation (3.6) it is obtained

$$(\rho c)_i^{n+1} \left(\delta x_l + \delta x_r\right)_i \left(T_i^{n+1} - T_i^n\right) = \int_t^{t+\Delta t} \left[\frac{k_{s_i}\left(T_{i+1} - T_i\right)}{(\delta x_r)_i + (\delta x_l)_{i+1}} - \frac{k_{s_{i-1}}\left(T_i - T_{i-1}\right)}{(\delta x_r)_{i-1} + (\delta x_l)_i}\right] dt. \tag{3.9}$$

Now, it is needed an assumption about how T_i, T_{i+1} and T_{i-1} vary with time from t to $t + \Delta t$. The usual approach is

$$\int_t^{t+\Delta t} T_i dt = \left[f T_i^{n+1} + (1 - f) T_i^n\right] \Delta t, \tag{3.10}$$

where f is a weighting factor between 0 and 1. Using similar formulas for the integrals of T_{i+1} and T_{i-1}, it is derived from Equation (3.9),

$$\begin{aligned}(\rho c)_i^{n+1} \frac{\left(\delta x_l + \delta x_r\right)_i}{\Delta t} \left(T_i^{n+1} - T_i^n\right) =& f \left[\frac{k_{s_i}^{n+1}\left(T_{i+1}^{n+1} - T_i^{n+1}\right)}{(\delta x_r)_i + (\delta x_l)_{i+1}} - \frac{k_{s_{i-1}}^{n+1}\left(T_i^{n+1} - T_{i-1}^{n+1}\right)}{(\delta x_r)_{i-1} + (\delta x_l)_i}\right] \\ &+ (1 - f) \left[\frac{k_{s_i}^{n+1}\left(T_{i+1}^n - T_i^n\right)}{(\delta x_r)_i + (\delta x_l)_{i+1}} - \frac{k_{s_{i-1}}^{n+1}\left(T_i^n - T_{i-1}^n\right)}{(\delta x_r)_{i-1} + (\delta x_l)_i}\right].\end{aligned} \tag{3.11}$$

Rearranging this, it is obtained

$$\begin{aligned}a_i^{n+1} T_i^{n+1} =& b_i^{n+1} \left[f T_{i+1}^{n+1} + (1 - f) T_{i+1}^n\right] + c_i^{n+1} \left[f T_{i-1}^{n+1} + (1 - f) T_{i-1}^n\right] \\ &+ \left[\beta_i^{n+1} - (1 - f) b_i^{n+1} - (1 - f) c_i^{n+1}\right] T_i^n,\end{aligned} \tag{3.12}$$

where

$$b_i^{n+1} = \frac{k_{s_i}^{n+1}}{(\delta x_r)_i + (\delta x_l)_{i+1}}, \tag{3.13}$$

$$c_i^{n+1} = \frac{k_{s_{i-1}}^{n+1}}{(\delta x_r)_{i-1} + (\delta x_l)_i}, \tag{3.14}$$

$$\beta_i^{n+1} = (\rho c)_i^{n+1} \frac{(\delta x_l)_i + (\delta x_r)_i}{\Delta t}, \tag{3.15}$$

$$a_i^{n+1} = f b_i^{n+1} + f c_i^{n+1} + \beta_i^{n+1}. \tag{3.16}$$

Specific values of the weighting factor f lead to different schemes: $f = 0$ leads to the explicit scheme, $f = 0.5$ to the Crank-Nicolson scheme, and $f = 1$ to the fully implicit scheme. The explicit scheme requires a very small time step to obtain physically realistic results, whereas the fully implicit scheme produces physically realistic results regardless of the time step size, although the accuracy of the results improves as the time step is reduced. The Crank-Nicolson scheme also requires small time steps to obtain physically realistic results and it is more accurate than the fully implicit scheme. Finally, the Crank-Nicolson scheme provides a more representative description of the temperature in a time step than the other two schemes, because the integral value of the temperature over a time interval depends on the temperatures values at the beginning and at the end of the time interval (Equation (3.10)) (Patankar, 1980).

In this work the fully implicit scheme was chosen due to its characteristics of simplicity and realistic physical behavior. The fully implicit form of Equation (3.12) is

$$a_i^{n+1} T_i^{n+1} = b_i^{n+1} T_{i+1}^{n+1} + c_i^{n+1} T_{i-1}^{n+1} + d_i^{n+1}, \tag{3.17}$$

where

$$b_i^{n+1} = \frac{k_{s_i}^{n+1}}{(\delta x_r)_i + (\delta x_l)_{i+1}}, \tag{3.18a}$$

$$c_i^{n+1} = \frac{k_{s_{i-1}}^{n+1}}{(\delta x_r)_{i-1} + (\delta x_l)_i}, \tag{3.18b}$$

$$d_i^{n+1} = \beta_i^{n+1} T_i^n = (\rho c)_i^{n+1} \frac{(\delta x_l)_i + (\delta x_r)_i}{\Delta t} T_i^n, \tag{3.18c}$$

$$a_i^{n+1} = b_i^{n+1} + c_i^{n+1} + \beta_i^{n+1}. \tag{3.18d}$$

The equation system (3.17) represents the discretization equations of Equation (3.1) considering a fully implicit scheme.

3.3.1 Boundary conditions

To derive the equations for the boundary points, consider the left-hand boundary point 0, which is adjacent to the first internal point 1 (Figure 3.2).

If the boundary temperature is given (T_0 is known), no particular difficulty arises and no additional equations are required. When the boundary temperature is not given, it is needed to construct and additional equation for T_0. This is done by integrating the differential equation over the half control volume adjacent to the boundary.

- Temperature specified on the boundaries (T_0^{n+1} and T_{Nx}^{n+1} $\forall$ $n = 1, 2, \ldots, Nt$), the equations are:

  For the node $i = 0$:

$$\begin{aligned} a_0^{n+1} &= 1, \\ b_0^{n+1} &= 0, \\ c_0^{n+1} &= 0, \\ d_0^{n+1} &= T_0^{n+1}. \end{aligned}$$

  For the node $i = Nx$:

$$\begin{aligned} a_{Nx}^{n+1} &= 1, \\ b_{Nx}^{n+1} &= 0, \\ c_{Nx}^{n+1} &= 0, \\ d_{Nx}^{n+1} &= T_{Nx}^{n+1}. \end{aligned}$$

- Heat flux across the boundaries specified (q_0^{n+1} y q_{Nx}^{n+1} $\forall$ $n = 1, 2, \ldots, Nt$), the equations are:

  For the node $i = 0$:

$$\left[(\rho c)_0^{n+1}(\delta x_r)_0 + \frac{k_{s_0}^{n+1}\Delta t}{(\delta x_r)_0 + (\delta x_l)_1}\right] T_0^{n+1} = \frac{k_{s_0}^{n+1}\Delta t}{(\delta x_r)_0 + (\delta x_l)_1} T_1^{n+1} + q_0^{n+1}\Delta t + (\rho c)_0^{n+1}(\delta x_r)_0 T_0^n, \tag{3.19}$$

  where

$$\begin{aligned} a_0^{n+1} &\equiv \left[(\rho c)_0^{n+1}(\delta x_r)_0 + \frac{k_{s_0}^{n+1}\Delta t}{(\delta x_r)_0 + (\delta x_l)_1}\right], \\ b_0^{n+1} &\equiv \frac{k_{s_0}^{n+1}\Delta t}{(\delta x_r)_0 + (\delta x_l)_1}, \\ d_0^{n+1} &\equiv q_0^{n+1}\Delta t + (\rho c)_0^{n+1}(\delta x_r)_0 T_0^n. \end{aligned}$$

  For the node $i = Nx$:

$$\left[(\rho c)_{Nx}^{n+1}(\delta x_l)_{Nx} + \frac{k_{s_{Nx-1}}^{n+1}\Delta t}{(\delta x_r)_{Nx-1} + (\delta x_l)_{Nx}}\right] T_{Nx}^{n+1} = \frac{k_{s_{Nx-1}}^{n+1}\Delta t}{(\delta x_r)_{Nx-1} + (\delta x_l)_{Nx}} T_{Nx-1}^{n+1} - q_{Nx}^{n+1}\Delta t + (\rho c)_{Nx}^{n+1}(\delta x_l)_{Nx} T_{Nx}^n, \tag{3.20}$$

where

$$a_{Nx}^{n+1} \equiv \left[(\rho c)_{Nx}^{n+1} (\delta x_l)_{Nx} + \frac{k_{s_{Nx-1}}^{n+1} \Delta t}{(\delta x_r)_{Nx-1} + (\delta x_l)_{Nx}} \right],$$
$$c_{Nx}^{n+1} \equiv \frac{k_{s_{Nx-1}}^{n+1} \Delta t}{(\delta x_r)_{Nx-1} + (\delta x_l)_{Nx}},$$
$$d_{Nx}^{n+1} \equiv -q_{Nx}^{n+1} \Delta t + (\rho c)_{Nx}^{n+1} (\delta x_l)_{Nx} T_{Nx}^{n}.$$

- Heat flux across the boundaries specified via a heat transfer coefficient (μ_0 and μ_{Nx}) and the temperature of the surrounding medium ($(T_{sm})_0^{n+1}$ and $(T_{sm})_{Nx}^{n+1} \; \forall \, n = 1, 2, \ldots, Nt$), the equations are:

  If the temperature of the surrounding medium is not function of the heat flux across the boundary

  For the node $i = 0$:

$$\left[(\rho c)_0^{n+1} (\delta x_r)_0 + \frac{k_{s_0}^{n+1} \Delta t}{(\delta x_r)_0 + (\delta x_l)_1} + \mu_0^{n+1} \Delta t \right] T_0^{n+1} = \frac{k_{s_0}^{n+1} \Delta t}{(\delta x_r)_0 + (\delta x_l)_1} T_1^{n+1} + \mu_0^{n+1} (T_{sm})_0^{n+1} \Delta t + (\rho c)_0^{n+1} (\delta x_r)_0 T_0^{n}, \quad (3.21)$$

  where

$$a_0^{n+1} \equiv \left[(\rho c)_0^{n+1} (\delta x_r)_0 + \frac{k_{s_0}^{n+1} \Delta t}{(\delta x_r)_0 + (\delta x_l)_1} + \mu_0^{n+1} \Delta t \right],$$
$$b_0^{n+1} \equiv \frac{k_{s_0}^{n+1} \Delta t}{(\delta x_r)_0 + (\delta x_l)_1},$$
$$d_0^{n+1} \equiv \mu_0^{n+1} (T_{sm})_0^{n+1} \Delta t + (\rho c)_0^{n+1} (\delta x_r)_0 T_0^{n}.$$

  For the node $i = Nx$:

$$\left[(\rho c)_{Nx}^{n+1} (\delta x_l)_{Nx} + \frac{k_{s_{Nx-1}}^{n+1} \Delta t}{(\delta x_r)_{Nx-1} + (\delta x_l)_{Nx}} + \mu_{Nx}^{n+1} \Delta t \right] T_{Nx}^{n+1} = \frac{k_{s_{Nx-1}}^{n+1} \Delta t}{(\delta x_r)_{Nx-1} + (\delta x_l)_{Nx}} T_{Nx-1}^{n+1} + \mu_{Nx}^{n+1} (T_{sm})_{Nx}^{n+1} \Delta t + (\rho c)_{Nx}^{n+1} (\delta x_l)_{Nx} T_{Nx}^{n}, \quad (3.22)$$

  where

$$a_{Nx}^{n+1} \equiv \left[(\rho c)_{Nx}^{n+1} (\delta x_l)_{Nx} + \frac{k_{s_{Nx-1}}^{n+1} \Delta t}{(\delta x_r)_{Nx-1} + (\delta x_l)_{Nx}} + \mu_{Nx}^{n+1} \Delta t \right],$$
$$c_{Nx}^{n+1} \equiv \frac{k_{s_{Nx-1}}^{n+1} \Delta t}{(\delta x_r)_{Nx-1} + (\delta x_l)_{Nx}},$$
$$d_{Nx}^{n+1} \equiv \mu_{Nx}^{n+1} (T_{sm})_{Nx}^{n+1} \Delta t + (\rho c)_{Nx}^{n+1} (\delta x_l)_{Nx} T_{Nx}^{n}.$$

If the temperature of the surrounding medium is function of the heat flux across the boundary (right boundary)

For the node $i = 0$:

$$\left[(\rho c)_0^{n+1}(\delta x_r)_0 + \frac{k_{s_0}^{n+1}\Delta t}{(\delta x_r)_0 + (\delta x_l)_1} + \mu_0^{n+1}\Delta t\right] T_0^{n+1} = \frac{k_{s_0}^{n+1}\Delta t}{(\delta x_r)_0 + (\delta x_l)_1} T_1^{n+1} + \mu_0^{n+1}(T_{sm})_0^{n+1}\Delta t + (\rho c)_0^{n+1}(\delta x_r)_0 T_0^n, \tag{3.23}$$

where

$$\begin{aligned} a_0^{n+1} &\equiv \left[(\rho c)_0^{n+1}(\delta x_r)_0 + \frac{k_{s_0}^{n+1}\Delta t}{(\delta x_r)_0 + (\delta x_l)_1} + \mu_0^{n+1}\Delta t\right], \\ b_0^{n+1} &\equiv \frac{k_{s_0}^{n+1}\Delta t}{(\delta x_r)_0 + (\delta x_l)_1}, \\ d_0^{n+1} &\equiv \mu_0^{n+1}(T_{sm})_0^{n+1}\Delta t + (\rho c)_0^{n+1}(\delta x_r)_0 T_0^n. \end{aligned}$$

For the node $i = Nx$:

$$\left[(\rho c)_{Nx}^{n+1}(\delta x_l)_{Nx} + \frac{k_{s_{Nx-1}}^{n+1}\Delta t}{(\delta x_r)_{Nx-1} + (\delta x_l)_{Nx}} + \mu_{Nx}^{n+1}\Delta t - \frac{\left(\mu_{Nx}^{n+1}\Delta t\right)^2}{d\rho_{sm}c_{sm} + \mu_{Nx}^{n+1}\Delta t}\right] T_{Nx}^{n+1} = \frac{k_{s_{Nx-1}}^{n+1}\Delta t}{(\delta x_r)_{Nx-1} + (\delta x_l)_{Nx}} T_{Nx-1}^{n+1} + \mu_{Nx}^{n+1}\Delta t \frac{d\rho_{sm}c_{sm}}{d\rho_{sm}c_{sm} + \mu_{Nx}^{n+1}\Delta t}(T_{sm})_{Nx}^n + (\rho c)_{Nx}^{n+1}(\delta x_l)_{Nx} T_{Nx}^n, \tag{3.24}$$

where

$$\begin{aligned} a_{Nx}^{n+1} &\equiv (\rho c)_{Nx}^{n+1}(\delta x_l)_{Nx} + \frac{k_{s_{Nx-1}}^{n+1}\Delta t}{(\delta x_r)_{Nx-1} + (\delta x_l)_{Nx}} + \mu_{Nx}^{n+1}\Delta t - \frac{\left(\mu_{Nx}^{n+1}\Delta t\right)^2}{d\rho_{sm}c_{sm} + \mu_{Nx}^{n+1}\Delta t}, \\ c_{Nx}^{n+1} &\equiv \frac{k_{s_{Nx-1}}^{n+1}\Delta t}{(\delta x_r)_{Nx-1} + (\delta x_l)_{Nx}}, \\ d_{Nx}^{n+1} &\equiv \mu_{Nx}^{n+1}\Delta t \frac{d\rho_{sm}c_{sm}}{d\rho_{sm}c_{sm} + \mu_{Nx}^{n+1}\Delta t}(T_{sm})_{Nx}^n + (\rho c)_{Nx}^{n+1}(\delta x_l)_{Nx} T_{Nx}^n. \end{aligned}$$

3.3.2 Solution of the linear algebraic equations

The equation system (3.17) can be arranged as a matrix system with a tridiagonal matrix of coefficients. Such a system can be solved using a particular Gaussian-elimination method, the Thomas algorithm or the TDMA (TriDiagonal-Matrix Algorithm) (Patankar, 1980).

For a specific time step, the discretization equations are written as

$$a_i T_i = b_i T_{i+1} + c_i T_{i-1} + d_i, \qquad \forall\ i = 0, 1, 2, \ldots, Nx. \tag{3.25}$$

From Equation (3.25) the boundary-point equations are

$$a_0 T_0 = b_0 T_1 + c_0 T_{-1} + d_0, \tag{3.26}$$

$$a_{Nx} T_{Nx} = b_{Nx} T_{Nx+1} + c_{Nx} T_{Nx-1} + d_{Nx}, \tag{3.27}$$

in which the temperatures T_{-1} and T_{Nx+1} must not have any physical meaning. To account for these requirements the following conditions must be met,

$$c_0 = 0 \qquad \text{and} \qquad b_{Nx} = 0. \tag{3.28}$$

It can be shown that the discretization equation for $i = 1$ is a relation between T_1 and T_2, for $i = 2$ is a relation between T_2 and T_3, for $i = 3$ is a relation between T_3 and T_4, ..., for $i = Nx$ is a relation between T_{Nx} and T_{Nx+1}. But since T_{Nx+1} has no physical meaning, from the discretization equation for $i = Nx$ the T_{Nx} value can be obtained directly. This enables to begin a back-substitution process in which T_{Nx-1} can be obtained from the discretization equation for $i = Nx-1$, T_{Nx-2} can be obtained from the discretization equation for $i = Nx - 2$, and so on until the discretization equation for $i = 0$ is reached. In this way the temperature values at all of the grid points are obtained (Patankar, 1980).

Suppose, in the forward-substitution process, it is sought a relation

$$T_i = P_i T_{i+1} + Q_i, \tag{3.29}$$

after it has been just obtained

$$T_{i-1} = P_{i-1} T_i + Q_{i-1}. \tag{3.30}$$

Substitution of Equation (3.30) into Equation (3.25) leads to

$$a_i T_i = b_i T_{i+1} + c_i \left(P_{i-1} T_i + Q_{i-1} \right) + d_i, \tag{3.31}$$

which can be rearranged to look like Equation (3.29). In other words, the coefficients P_i and Q_i then stand for

$$P_i = \frac{b_i}{a_i - c_i P_{i-1}}, \tag{3.32}$$

$$Q_i = \frac{d_i + c_i Q_{i-1}}{a_i - c_i P_{i-1}}. \tag{3.33}$$

These are recurrence relations. To start the recurrence process it is noted that the values of P_1 and Q_1 are

$$P_1 = \frac{b_1}{a_1} \qquad \text{and} \qquad Q_1 = \frac{d_1}{a_1}. \tag{3.34}$$

At the other end of the P_i, Q_i sequence, it is noted that $b_{Nx} = 0$. This leads to $P_{Nx} = 0$, and hence from Equation (3.29) it is obtained

$$T_{Nx} = Q_{Nx}. \tag{3.35}$$

In this work a periodic T_{sa} function was used and the numerical code was iterated until obtaining periodic solutions of T and T_i. Simulations were made for a day and the numerical code was iterated until the difference in the temperature values of each node of the constructive system for $t = 0$ h and $t = 24$ h was less than a tolerance value, ζ. The periodicity of the solutions implies the following: *i*) the energy absorbed by the indoor air is equal to the energy released by it for the 24 hours period; *ii*) the energy absorbed by each of the control volumes of the PCM-wall (see Figure 3.2) is equal to the energy released by them for the 24 hours period, thus, the daily energy flux at each of the interfaces of the control volumes and at the outdoor and indoor surfaces is equal to zero.

3.4 Validation of the numerical code

This section shows the validation of the numerical code developed: (i) an analytical validation made by comparing an analytical solution for a specific case, and (ii) a validation made by comparing the results obtained with the program Ener-Habitat.

3.4.1 Analytical validation

In this thesis, the following system was solved analytically in order to perform the analytical validation,

$$\text{PDE}: \quad \frac{\partial T(x,t)}{\partial t} = \alpha \frac{\partial^2 T(x,t)}{\partial x^2}, \qquad 0 < x < 1, \quad 0 < t < \infty, \tag{3.36a}$$

$$\text{IC}: \quad T(x,0) = \sigma(x), \qquad 0 \leq x \leq 1, \tag{3.36b}$$

$$\text{BC}_1: \quad -k\frac{\partial T(0,t)}{\partial x} = \mu_o \left[T_{sm}(t) - T(0,t)\right], \qquad 0 < t < \infty, \tag{3.36c}$$

$$-k\frac{\partial T(0,t)}{\partial x} + \mu_o T(0,t) = g_1(t), \tag{3.36d}$$

$$\text{BC}_2: \quad T(1,t) = g_2, \qquad 0 < t < \infty, \tag{3.36e}$$

where $\alpha = k/(\rho c)$ is the thermal diffusivity, μ_o is the outside heat transfer coefficient, and $g_1(t) \equiv \mu_o T_{sm}(t)$. For the analytical validation two different functions (two study cases) for the temperature of the surrounding medium, T_{sm}, were considered: a constant value and a periodic function.

The procedure to solve Equation (3.36) was taken from Farlow (1993), but the solution of the eigenvalue equation (3.43) and the validation analysis are an own derivation.

Because the boundary conditions are nonhomegeneous, it is necessary to change them to homogeneous ones to solve Equation (3.36) by using the eigenfunction expansion method.

This can be addressed by considering the following ansatz[1] for Equation (3.36),

$$T(x,t) = S(x,t) + U(x,t), \tag{3.37}$$

where $S(x,t)$ satisfies the BCs of the problem,

$$S(x,t) = (1-x)\frac{-kg_2 - g_1(t)}{-k-\mu_o} + xg_2, \tag{3.38}$$

and the transformed problem in $U(x,t)$ is

$$\text{PDE}: \quad \frac{\partial U(x,t)}{\partial t} = \alpha\frac{\partial^2 U(x,t)}{\partial x^2} + f(x,t), \qquad 0<x<1, \quad 0<t<\infty, \tag{3.39a}$$

$$\text{IC}: \quad U(x,0) = \phi(x), \qquad 0 \le x \le 1, \tag{3.39b}$$

$$\text{BC}_1: \quad -k\frac{\partial U(0,t)}{\partial x} + \mu_o U(0,t) = 0, \qquad 0<t<\infty, \tag{3.39c}$$

$$\text{BC}_2: \quad U(1,t) = 0, \qquad 0<t<\infty, \tag{3.39d}$$

where $f(x,t) = -\partial S(x,t)/\partial t$ and $\phi(x) = \sigma(x) - S(x,0)$.

The basic idea in the eigenfunction expansion method is to decompose the heat source $f(x,t)$ into simples components,

$$f(x,t) = f_1(t)X_1(x) + f_2(t)X_2(x) + \ldots + f_n(t)X_n(x) + \ldots$$

and find the response $U_n(x,t)$ to each of these individual components $f_n(t)X_n(x)$, so the solution of the transformed problem (3.39) can be written as

$$U(x,t) = \sum_{n=0}^{\infty} U_n(x,t) = \sum_{n=0}^{\infty} X_n(x)M_n(t), \tag{3.40}$$

where $X_n(x)$ are the eigenfuntions of the transformed problem.

The eigenfunctions are found by solving the Sturm-Liouville problem for $0<x<1$,

$$\text{ODE}: \quad \frac{\partial^2 X_n(x)}{\partial x^2} + \lambda_n^2 X_n(x) = 0, \tag{3.41a}$$

$$\text{BC}_1: \quad -k\frac{\partial X_n(0)}{\partial x} + \mu_o X_n(0) = 0, \tag{3.41b}$$

$$\text{BC}_2: \quad X_n(1) = 0, \tag{3.41c}$$

whose solution is

$$X_n(x) = \sin(\lambda_n x) + \lambda_n \cos(\lambda_n x), \tag{3.42}$$

[1] An ansatz is a proposal for the functional form (a trial answer) of the solution of a differential equation (Gershenfeld, 1999, p. 10).

where the eigenvalues λ_n satisfy the eigenvalue equation

$$\tan \lambda_n = -\lambda_n. \tag{3.43}$$

The norm of the problem, $N(\lambda_n)$, is defined by the ortogonality property of the eigenfunctions $X_n(x)$,

$$\int_0^1 X_m(x) X_n(x)\, dx = N(\lambda_m)\, \delta_{mn}. \tag{3.44}$$

Using this property it is possible to find the functions $f_n(t)$,

$$f_n(t) = \frac{1}{N(\lambda_n)} \int_0^1 f(x,t) \left[\sin(\lambda_n x) + \lambda_n \cos(\lambda_n x)\right] dx. \tag{3.45}$$

The functions $M_n(t)$ are found by solving the system

$$\text{ODE}: \quad \frac{dM_n(t)}{dt} + \lambda_n^2 \alpha M_n(t) = f_n(t), \qquad 0 < t < \infty, \tag{3.46a}$$

$$\text{IC}: \quad M_n(0) = \frac{1}{N(\lambda_n)} \int_0^1 \phi(\xi) X_n(\xi)\, d\xi, \tag{3.46b}$$

whose solution is

$$M_n(t) = e^{-\lambda_n^2 \alpha t} \left[G_n + \int e^{\lambda_n^2 \alpha t} f_n(t)\, dt \right], \tag{3.47}$$

where

$$G_n = M_n(0) - \left| \int e^{\lambda_n^2 \alpha t} f_n(t)\, dt \right|_{t=0}. \tag{3.48}$$

To find analytical expressions of $M_n(t)$ must be possible to perform the indicated integral in Equation (3.47), which is only possible if $f_n(t)$ is a simple function, i.e., if $T_{sm}(t)$ is a constant, linear, or simple periodic function.

To complete the solution of the system (3.36) it is neccesary to solve the eigenvalue equation (3.43). From the graphical solution (Figure 3.3) it is noted that

$$\lambda_n = \frac{(2n+1)\pi}{2} + \epsilon_n, \qquad n \in \mathbb{N}, \tag{3.49}$$

where ϵ_n is a correction term to be calculated, which tends to zero for $n \gg 1$. The eigenvalues λ_n can be calculated by the following expression,

$$\lambda_n = -\tan \lambda_n = -\frac{\sin \lambda_n}{\cos \lambda_n} = -\frac{\sin\left[\frac{(2n+1)\pi}{2} + \epsilon_n\right]}{\cos\left[\frac{(2n+1)\pi}{2} + \epsilon_n\right]} = \frac{\cos \epsilon_n}{\sin \epsilon_n} \approx \frac{1}{\epsilon_n},$$

i.e.,

$$\lambda_n = \frac{(2n+1)\,\pi}{2} + \epsilon_n \approx \frac{1}{\epsilon_n},$$

then the correction term is given by

$$\epsilon_n \approx \frac{(2n+1)\,\pi}{4}\left[\sqrt{1+\left[\frac{4}{(2n+1)\,\pi}\right]^2} - 1\right]. \tag{3.50}$$

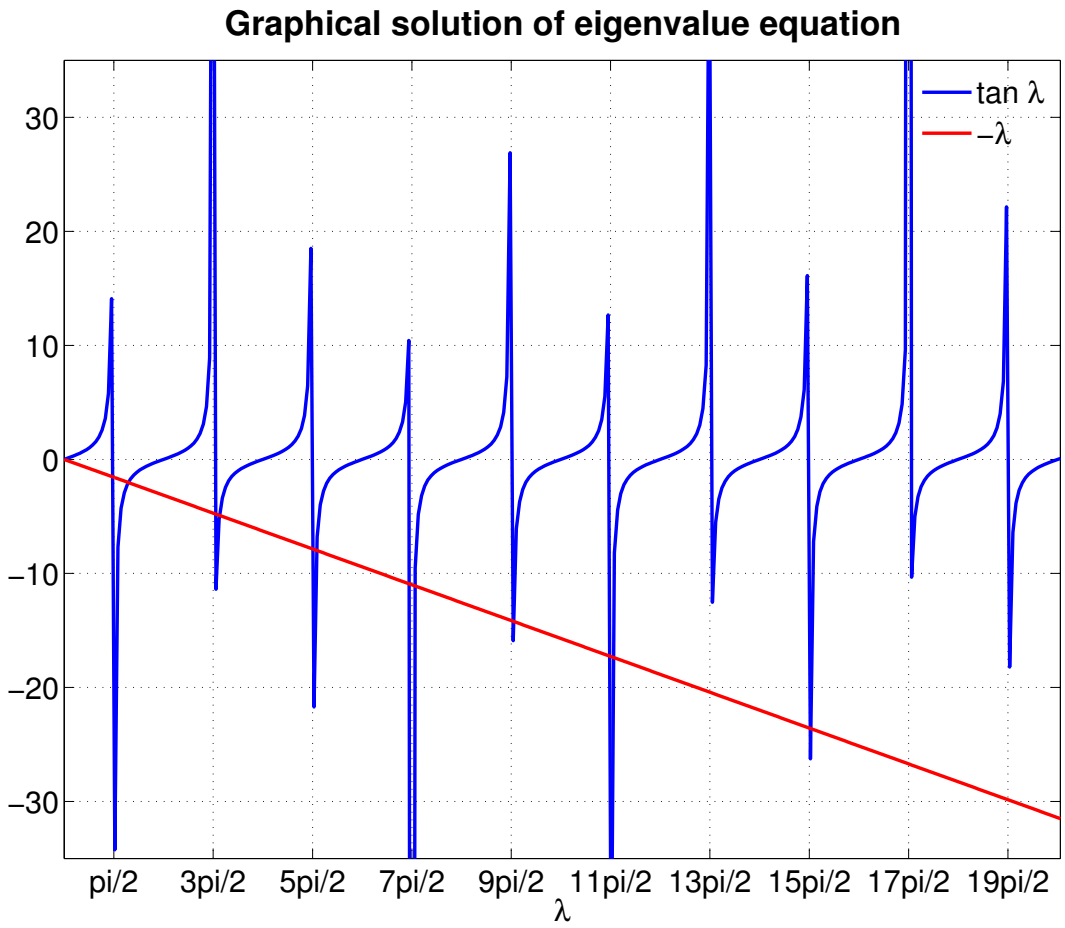

Figure 3.3: Graphical solution of the eigenvalue equation (Equation (3.49)).

Table 3.1 shows the exact values of λ_n (obtained with MATLAB R2010a), those obtained with Equations (3.49) and (3.50), and the difference between these two values. For $n > 5$ the approximate values are equal to the exact values up to the fourth decimal position.

Table 3.1: Exact values (obtained with MATLAB R2010a) and approximate values (obtained with Equations (3.49) and (3.50)) of λ_n.

n	λ_n exact	λ_n approximate	Difference |exact-approx|
0	2.0288	2.0570	0.0282
1	4.9132	4.9158	0.0026
2	7.9787	7.9793	0.0006
3	11.0855	11.0858	0.0003
4	14.2077	14.2076	0.0001
5	17.3364	17.3364	0.0000
6	20.4692	20.4692	0.0000

The first case analyzed for the analytical validation considered $T_{sm}(t) = 35.0°\text{C}$. The results for the first case are shown in Figure 3.4, which compares the stationary solution obtained analytically and numerically. The second case analyzed considered $T_{sm}(t) = 25.0°\text{C} + 8.0°\text{C}\sin(2\pi t/P - \pi)$, where P is 24 h. The results for the second case are shown in Figure 3.5, which compares the periodic-state solution[2] at the beginning of the day ($t = 0$ h) obtained analytically and numerically. For both cases analyzed, the analytical solutions were obtained by replacing the first two eigenvalues for their exact values. From Figures 3.4 and 3.5 it is observed that both solutions coincide up to the fourth decimal, which gives the order of accuracy of the numerical solution.

3.4.2 Validation with a numerical program

This validation was made by comparing the results of the numerical code developed with the results of the numerical program Ener-Habitat, which is a wall/roof envelope thermal performance simulator (Barrios et al., 2014). The validation of Ener-Habitat is reported in Barrios et al. (2016).

The first part of the validation (AC case) consisted on simulating the periodic-state solution of the temperature considering a fixed indoor air temperature, equal to the value of the comfort temperature, for various constructive systems, C.S. (Table 3.2), and compare the obtained results with those of Ener-Habitat for a typical day of some month. To do this, the heating and cooling loads (Barrios et al., 2012) were compared.

The second part of the validation (nAC case) consisted on simulating the periodic-state solution of the temperature considering that the indoor air temperature evolves according to the heat flux across the indoor surface, for various constructive systems (Table 3.2), and compare the obtained results with those of Ener-Habitat for the typical day of some month. To do

[2]The periodic-state solution refers to the periodic solution obtained after a long enough time period, which no longer depends on the initial condition. The periodic-state solution was obtained considering a tolerance value $\zeta = 0.0001°\text{C}$.

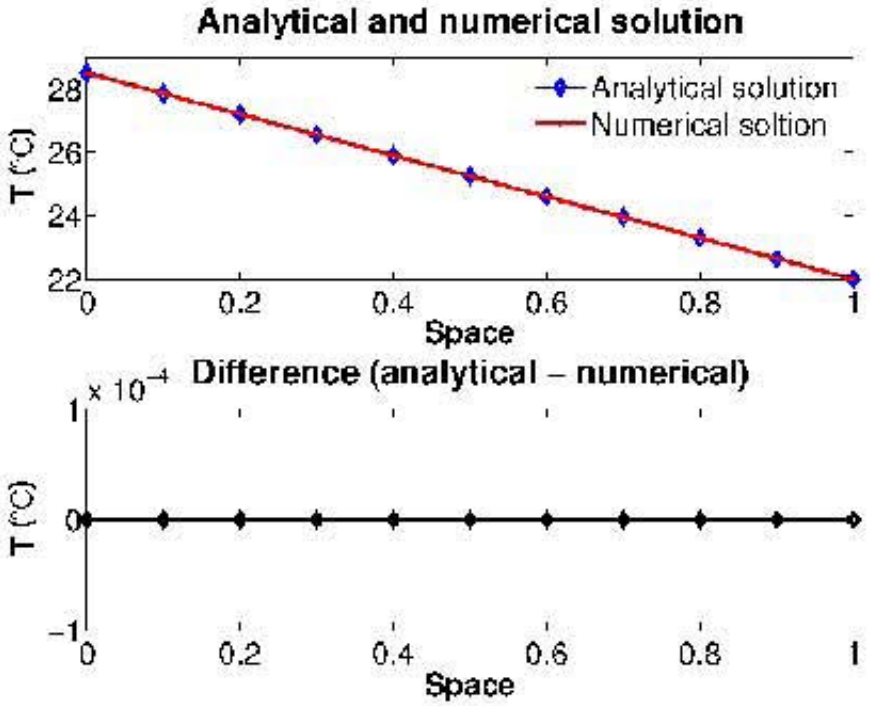

Figure 3.4: Comparison of the analytical and numerical solution for constant T_{sm}.

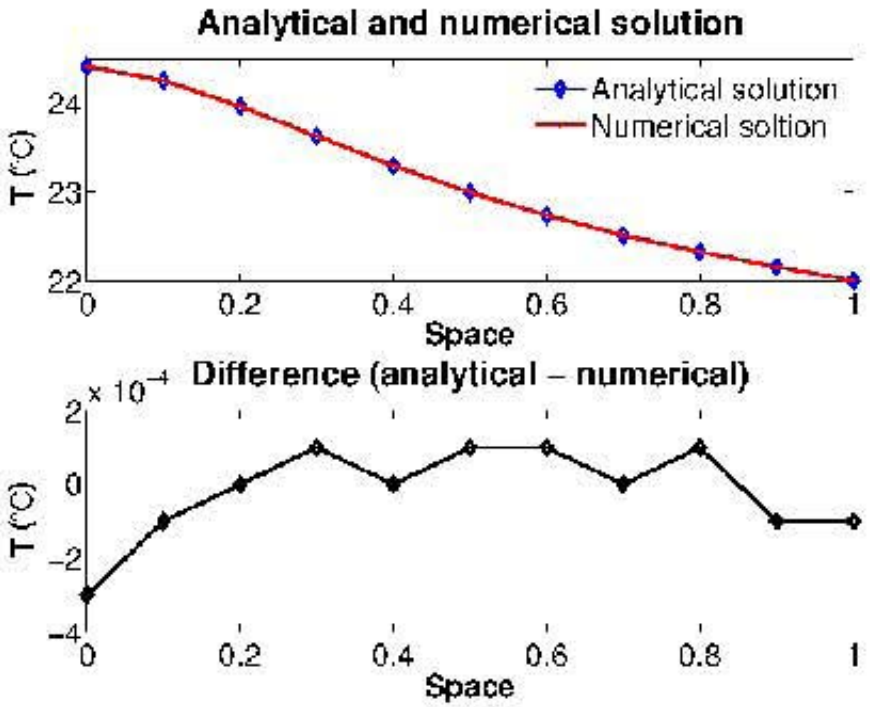

Figure 3.5: Comparison of the analytical and numerical solution for periodic T_{sm}.

this, the following parameters were compared: transmitted energy per day, TE [W·h·m^{-2}], sol-air decrement factor, DF_{sa} [-], sol-air lag time, LT_{sa} [h], average indoor air temperature, $\bar{T}_i$ [°C], minimum indoor air temperature, $T_{i,min}$ [°C], maximum indoor air temperature, $T_{i,max}$ [°C], hot discomfort degree hours per day, DDH_{hot} [°C·h], and cold discomfort degree hours per day, DDH_{cold} [°C·h] (Barrios et al., 2012). Simulations for both cases were performed for the city of Aguascalientes, Mexico, for the typical day of May[3].

Table 3.2: Constructive systems used for the comparative validation. C.S. is the constructive system, HDC is high density concrete, and EPS is expanded polystyrene.

C. S. Roof	Material (outside to inside)	Solar absorptivity [-]	Thermal conductivity [W·m^{-1}·K^{-1}]	Density [kg·m^{-3}]	Specific heat [J·kg^{-1}·°C^{-1}]
1	10 cm HDC	0.7	2.00	2400	1000
2	10 cm EPS	0.2	0.04	15	1400
3	2 cm EPS + 8 cm HDC	0.2			
4	8 cm HDC + 2 cm EPS	0.7			

All of the parameters mentioned above are calculated using the surface temperatures of the constructive system and/or the indoor air temperature. Then, the deviation of the results of the developed numerical code with respect to Ener-Habitat depends on the difference of the values of corresponding temperatures.

Table 3.3 shows the results for the AC case. This table presents, for each C.S., the values of cooling load per day, CL [W·h·m^{-2}], and heating load per day, HL [W·h·m^{-2}], obtained with Ener-Habitat (EH) and with the developed numerical code (NC), and the difference, Dif, of the results of the developed numerical code with respect to the results of Ener-Habitat. Percentage differences of up to 3.4% for CL and of up to 4.8% for HL were found. In the simulation 20 control volumes and a time step of 60 s were used.

Table 3.3: Results of Ener-Habitat (EH) and the developed numerical code (NC) considering AC case.

C. S. Roof	CL - EH [W·h·m^{-2}]	CL - NC [W·h·m^{-2}]	Dif - CL [W·h·m^{-2}]	HL - EH [W·h·m^{-2}]	HL - NC [W·h·m^{-2}]	Dif - HL [W·h·m^{-2}]
1	999.283	996.701	2.582	222.830	220.987	1.843
2	26.609	26.362	0.247	43.650	43.282	0.368
3	39.466	39.439	0.027	102.965	102.487	0.478
4	362.863	350.483	12.380	62.834	59.809	3.025

[3]The weather variables and monthly comfort temperature for the city were obtained from Ener-Habitat.

Table 3.4 shows the results for the nAC case. Differences of up to three decimals in all the calculated parameters were found.

The validation carried out indicates that the results obtained with the developed numerical code are accurate.

Table 3.4: Results of Ener-Habitat (EH) and the developed numerical code (NC) considering nAC case.

Parameter	C.S. 1			C.S. 2			C.S. 3			C.S. 4		
	EH	NC	Dif	EH	NC	Dif	EH	NC	Dif	EH	NC	Dif
TE [W·h·m^{-2}]	25.001	24.922	0.079	17.300	17.252	0.048	2.350	2.347	0.003	29.392	29.281	0.111
DF_{sa} [-]	0.52	0.52	0.00	0.80	0.79	0.01	0.11	0.11	0.00	0.61	0.61	0.00
LT_{sa} [h]	4.2	4.2	0.0	2.5	2.5	0.0	5.9	5.9	0.0	4.0	4.1	-0.1
$\bar{T}_i$ [°C]	35.9	35.9	0.0	24.6	24.6	0.0	24.7	24.7	0.0	35.8	35.8	0.0
$T_{i,min}$ [°C]	21.2	21.3	-0.1	14.2	14.2	0.0	23.1	23.1	0.0	19.0	19.1	-0.1
$T_{i,max}$ [°C]	51.6	51.5	0.1	35.2	35.2	0.0	25.9	25.9	0.0	54.7	54.6	0.1
DDH_{hot} [°C·h]	244.6	244.5	0.1	53.8	53.6	0.2	0.0	0.0	0.0	257.7	257.4	0.3
DDH_{cold} [°C·h]	19.8	19.6	0.2	98.7	98.5	0.2	44.2	44.0	0.2	33.1	32.8	0.3

Chapter 4

Numerical modeling of solid-liquid phase changes

This chapter presents a literature review of solid-liquid phase change theory through the Stefan problem and the numerical methods used to simulate heat transfer through phase change materials embedded in building envelopes.

4.1 Solid-liquid phase changes

Problems dealing with solid-liquid phase changes of single component systems (pure substances) and multicomponent systems (mixture of several pure substances) are described by the Stefan problem. The mathematical models of these processes contain free boundaries, i.e., moving surfaces of phase change that are unknown beforehand (Samarskii and Vabishchevich, 1995). This section describes the three-dimensional theory for solid-liquid phase changes in single component and multicomponent systems. The description was taken from Samarskii and Vabishchevich (1995).

4.1.1 Phase changes in single component systems

When dealing with solid-liquid phase changes in single component systems it is assumed that the phase change occurs at a given, fixed temperature T^*. It is considered that the interface between the two phases, $S(t)$, divides the domain Ω into two subdomains: the domain $\Omega_l(t) = \{(x,y,z)|(x,y,z) \in \Omega, T(x,y,z,t) > T^*\}$ filled with the liquid, in which the temperature is greater than the phase change temperature, and the domain $\Omega_s(t) = \{(x,y,z)|(x,y,z) \in \Omega, T(x,y,z,t) < T^*\}$ filled with the solid phase. Subscripts l and s refer to liquid and solid phases, respectively.

The heat equation for each phase should be considered. In the solid phase the heat

equation is

$$c_s \rho_s \frac{\partial T_s}{\partial t} = \operatorname{div}\left(k_s \operatorname{grad} T_s\right), \qquad (x, y, z, t) \in Q_s, \tag{4.1}$$

where $Q_s = \{(x, y, z, t) | (x, y, z) \in \Omega_s, t > 0\}$. In the liquid phase the heat equation is

$$c_l \rho_l \left(\frac{\partial T_l}{\partial t} + \vec{v} \operatorname{grad} T_l \right) = \operatorname{div}\left(k_l \operatorname{grad} T_l\right), \qquad (x, y, z, t) \in Q_l, \tag{4.2}$$

where $Q_l = \{(x, y, z, t) | (x, y, z) \in \Omega_l, t > 0\}$. In Equation (4.2) $\vec{v}$ is the local velocity of the medium and the term with $\vec{v} \operatorname{grad} T$ defines temperature change due to convection.

There are two boundary conditions at the interface S in the phase change. The first boundary condition considers the continuity of the temperature,

$$[T] = T_s - T_l = 0, \qquad (x, y, z) \in S, \tag{4.3}$$

where the brackets denote the jump of a quantity through $S(t)$ from the solid phase to the liquid one. The second boundary condition considers that the phase change is accompanied by a release/absorption of a certain amount of heat. Therefore the heat flow is discontinuous on the phase change boundary and is defined by the equation

$$\left[k \frac{\partial T}{\partial n} \right] = -L \, V_n, \qquad (x, y, z) \in S, \tag{4.4}$$

where L is the phase change enthalpy per volume and V_n is the normal velocity of the phase change boundary.

For single component systems, the interface is determined at each moment in time as follows: $S = S(t) = \{(x, y, z, t) | (x, y, z) \in \Omega, T(x, y, z, t) = T^*\}$, or in other words, the first-kind conditions,

$$T(x, y, z, t) = T^*, \qquad (x, y, z) \in S(t). \tag{4.5}$$

Conditions (4.3), (4.4), and (4.5) are called the Stefan conditions and the corresponding problem for Equations (4.1) and (4.2) is referred to as the Stefan problem. In this problem, processes in both phases are studied, and the problem is also called the two-phase Stefan problem; in contrast with the monophase Stefan problem, which the temperature field in one phase is known and it is only needed to find the temperature field for one phase.

In the case there is a surface heat source with capacity q_S on the interface S, the temperature continuity assumption holds, i.e., Equation (4.3) is satisfied, while the heat flow has a discontinuity and it must be replaced by a nonhomogeneous condition,

$$\left[k \frac{\partial T}{\partial n} \right] = q_S, \qquad (x, y, z, t) \in S(t). \tag{4.6}$$

The conjunction condition (4.3) can be included in the heat equation written in the whole computational domain without separating the contact boundary S. The surface heat source is taken into account by introducing an additional term in Equation (4.2), namely

$$\rho c \frac{dT}{dt} = \operatorname{div}(k \operatorname{grad} T) + \delta_S q_S, \tag{4.7}$$

where δ_S is a surface Dirac delta-function such that for a given function $P(x, y, z)$, δ_S satisfies

$$\int_\Omega \delta_S P(x, y, z)\, dxdydz = \int_S P(x, y, z)\, ds.$$

The formulation of the Stefan problem can be generalized so that conditions (4.3), (4.4), and (4.5) are included in the heat equation itself. This is very important from the viewpoint of constructing efficient computational algorithms.

To pass from Equations (4.1) and (4.2) equipped with conditions (4.3)-(4.5) to a single heat equation, Equations (4.1) and (4.2) are rewritten, using Equations (4.6) and (4.7), as

$$c(T)\rho(T)\left(\frac{\partial T}{\partial t} + \vec{v} \operatorname{grad} T\right) = \operatorname{div}(k \operatorname{grad} T) - \delta_S L V_n, \qquad (x, y, z, t) \in Q, \tag{4.8}$$

where $Q = Q_s \cup Q_l$.

Near the boundary of the phase change the local orthogonal coordinates (x', y', z') are introduced with unit metric coefficients. The surface delta-function δ_S in these coordinates becomes $\delta_S = \delta(x' - x'_0)$, where the equation $x' = x'_0$ defines the boundary S. Similarly, the velocity of the free surface is $V_n = dx'/dt$. The Stefan condition in Equation (4.5) correspond to $T = T(x', t)$ and $T(x'_0, t) = T^*$ in the new coordinates. Taking this into account, the following result is obtained

$$\delta_S V_n = \delta(x' - x'_0)\frac{dx'}{dt} = \delta(T - T^*)\frac{dT}{dt}. \tag{4.9}$$

Substitution of Equation (4.9) into Equation (4.8) yields the desired equation

$$\rho(T)c_{eff(ps)}(T)\left(\frac{\partial T}{\partial t} + \vec{v} \operatorname{grad} T\right) = \operatorname{div}(k \operatorname{grad} T), \qquad (x, y, z, t) \in Q, \tag{4.10}$$

where the effective specific heat for single component systems, $c_{eff(ss)}$, is defined as

$$c_{eff(ss)}(T) = c(T) + \rho^{-1}(T) L\, \delta(T - T^*). \tag{4.11}$$

The quasi-linear heat equation (4.10) is remarkable because it does not include the unknown boundary of the phase change explicitly. The procedures for approximate solution of the Stefan problem are based on this equation.

4.1.2 Phase changes in multicomponent systems

To address the solidification and melting processes of multicomponent systems, which solidify in a temperature interval, it is sufficient to consider the fraction of the liquid phase Ψ at temperature T. In this case, it exists a spatial mushy (solid and liquid) region between solid and liquid phases. Then the Stefan problem is expressed as a single heat equation,

$$\rho(T)c_{eff(is)}(T)\left(\frac{\partial T}{\partial t}+\vec{v}\,\mathrm{grad}\,T\right)=\mathrm{div}\,(k\,\mathrm{grad}\,T)\,,\qquad (x,y,z,t)\in Q, \tag{4.12}$$

where the effective specific heat for multicomponent systems, $c_{eff(ms)}$, is defined as

$$c_{eff(ms)}(T)=c(T)+\rho^{-1}(T)L\frac{d\Psi}{dT}. \tag{4.13}$$

Equation (4.12) is the basis for the simplest quasi-equilibrium model for the two-phase zone. Evidently, Equation (4.12) yields Equation (4.10) for a single component system.

Hereinafter it will be considered conduction-dominated heat transfer, i.e., convection effects due to density change at the phase interface or density variations in the liquid phase are neglected. That is, the velocity of the medium in liquid phase $\vec{v}$ in Equations (4.10) and (4.12) is approximated to zero.

4.2 Numerical methods for phase changes

Problems with phase changes deal with nonlinearity, which is, first of all, accounted for by the presence of an unknown (free) phase interface. Nonlinearities can also be due to the dependence of thermal parameters on temperature. There are two groups of methods to solve phase change problems: variable domain methods and fixed domain methods. In the variable domain methods the position of the interface is calculated in each time step using specific grid points (the interface is explicitly separated), which is achieved by using variable time steps and grid sizes. In the fixed domain methods a fixed grid is used and the interface is not explicitly separated, however it can be tracked using auxiliary functions (Idelsohn et al., 1994; Samarskii and Vabishchevich, 1995).

The variable domain methods require some degree of regularity of the interface as well as of its evolution. They have a good numerical behavior in one-dimensional problems, nevertheless, in multidimensional problems they are difficult to implement and have large computational costs. On the other hand, the fixed domain methods are simple compared to the variable domain methods, most versatile, convenient, adaptable, easily-programmable in multidimensional problems, and can handle complex topologycal evolutions of the interface. However, since they represent temperature gradients as a smooth function the temperature profile resolution is not good enough (Idelsohn et al., 1994; Samarskii and Vabishchevich, 1995).

Table 4.1 shows the most common variable and fixed domain methods to simulate PCMs in building envelopes. Table 4.2 shows the main features, advantages and disadvantages of the most common fixed domain methods to simulate PCMs, which are described in the following subsections.

Table 4.1: The most common methods to simulate PCMs in building envelopes. Table constructed from Idelsohn et al. (1994) and AL-Saadi and Zhai (2013).

Variable domain methods	**Fixed domain methods**
Fixed mesh, finite differences	Effective specific heat
Variable mesh, finite differences	Enthalpy
Moving mesh, finite elements	Latent heat source
Moving boundary element	Temperature-transforming

4.2.1 The effective specific heat method

Equation (4.12) is often referred to as the effective specific heat equation,

$$\rho(T)c_{eff}(T)\frac{\partial T}{\partial t} = \operatorname{div}\left(k \operatorname{grad} T\right), \qquad (x, y, z, t) \in Q, \tag{4.14}$$

where for simplicity the term $c_{eff(is)}$ has been written as c_{eff},

$$c_{eff}(T) = c(T) + \rho^{-1}(T)L\frac{d\Psi}{dT}. \tag{4.15}$$

Equation (4.14) is written in terms of a single variable, the temperature T, with the non-linear latent and specific heat effects grouped in the effective specific heat c_{eff}. The temperature is the only variable that needs to be solved in the discretization form (Samarskii and Vabishchevich, 1995).

For the numerical implementation of this method two points should be considered when evaluating c_{eff} (Voller et al., 1990):

i c_{eff} can not be evaluated using Equation (4.15) if $\Psi(T)$ contains jump discontinuities. However, this problem can be addressed by introducing small artificial temperature ranges at the jumps, such that $\Psi(T)$ is piecewise continuous.

ii An effective numerical approximation must be used to take into account the high dependence of c_{eff} on both space and time.

The key in this method lies in the function c_{eff}, which can be obtained from testing data with calorimetric methods or using analytical or numerical approximations.

Table 4.2: Main features, advantages, and disadvantages of the most common fixed domain methods to simulate PCMs. Table taken from AL-Saadi and Zhai (2013).

Method	**Main feature**	**Advantages**	**Disadvantages**
Effective specific heat	Specific heat accounts for sensible and latent heat	1. Intuitive since dealing with one dependent variable (temperature) 2. Easy to program 3. Suitable for gradual phase change	1. Lack of computational efficiency 2. Small time step and fine grids are required for accuracy 3. Difficult to handle cases with small phase change temperature range 4. Difficult to obtain convergence, it could be underestimated the latent heat 5. Not applicable for cases where phase change occurs at fixed temperature
Enthalpy	Enthalpy accounts for sensible and latent heat	1. Fast if proper scheme is selected 2. Deal with sharp as well as gradual phase change	1. Difficult to handle supercooling problems 2. The temperature at a typical grid point may oscillate with time
Latent heat source	Latent heat is treated as a source term	1. Intuitive due to separating the latent and sensible heat 2. Deal with sharp as well as gradual phase change	1. Requires under-relaxation 2. Lack of computational efficiency 3. Problems with round-off errors if melting occurs over range temperature
Temperature-transforming	Heat coefficient and source term are used to account for sensible and latent heat	1. Deal with sharp and gradual phase change 2. Handle large time step and coarse grids	1.Not a common method and therefore not tested to evaluate the pros and cons

Analytical approximations are useful when only limited data of the PCM are available (usually data provided by manufacturers such that density, ρ, melting temperature, T_m, phase change enthalpy per volume, L, and specific heats at solid and liquid states, c_s and c_l, respectively). In this situation a simple expression for c_{eff} can be constructed considering a fictitious melting temperature range, 2ϵ. The expression has the following form (AL-Saadi and Zhai, 2013):

$$c_{eff}(T) = \begin{cases} c_s, & T \leq T_m - \epsilon \quad \text{(Solid region)}, \\ \frac{c_s + c_l}{2} + \frac{L}{2\epsilon\rho}, & T_m - \epsilon < T < T_m + \epsilon \quad \text{(Mushy region)}, \\ c_l, & T \geq T_m + \epsilon \quad \text{(Liquid region)}. \end{cases} \tag{4.16}$$

Appropriate values of ϵ, time step, and grid size should be selected in order to avoid convergence issues and to have an adequate representation of the phase change phenomenon.

On the other hand, numerical approximations are used when the specific enthalpy curve, $h\,(T)$, is available. These approximations are based on temporal or space averaging of the enthalpy (AL-Saadi and Zhai, 2013).

A temporal averaging approximation commonly used in iterative schemes is given by Morgan et al. (1978),

$$c_{eff} = \frac{h\,(T^{new}) - h\left(T^{old}\right)}{T^{new} - T^{old}}, \tag{4.17}$$

where *new* represents the actual time step and *old* represents the previous time step. The calculation of c_{eff} using Equation (4.17) assures an accurate evaluation of it in each time step (Voller et al., 1990).

Space averaging approximations consider gradients of enthalpy and temperature, e.g., the method proposed by Lemmon (1979),

$$c_{eff} = \left(\frac{\text{grad } h \cdot \text{grad } h}{\text{grad } T \cdot \text{grad } T}\right)^{0.5}. \tag{4.18}$$

In this kind of approximations grad h and grad T must be approximated in the same way. A disadvantage of using Equation (4.18) is that the calculated c_{eff} value can be discontinuous at a given node point (Voller et al., 1990).

4.2.2 The enthalpy method

In the enthalpy method there are two unknown variables, the enthalpy and the temperature. For multicomponent systems (Equation (4.12)) the specific enthalpy is calculated using the following equation (Samarskii and Vabishchevich, 1995),

$$\frac{dh(T)}{dT} = c_{eff}(T) = c(T) + \rho^{-1}(T)L\,\frac{d\Psi}{dT}. \tag{4.19}$$

Using this relation, Equation (4.12) takes the form

$$\rho(T)\frac{\partial h(T)}{\partial t} = \text{div}\,(k\ \text{grad}\ T)\,, \qquad (x, y, z, t) \in Q, \tag{4.20}$$

where the specific enthalpy has the following expression

$$h(T) = \int_{T_{ref}}^{T} \left[c(\theta) + \rho^{-1}(\theta) L \, \frac{d\Psi}{d\theta} \right] d\theta. \tag{4.21}$$

Equation (4.20) represents the enthalpy approach to model phase changes.

For single component systems the specific enthalpy h has a discontinuity on the interface (for $T = T^*$). To overcome this problem a mushy zone must be introduced to smooth the discontinuous function $h(T)$ (Samarskii and Vabishchevich, 1995).

4.2.3 The latent heat source method

In the latent heat source method the temperature and the liquid fraction are the two unknown variables. In this method the specific enthalpy is split into the specific heat and the latent heat, which the latent heat acts as a source term (Voller et al., 1990),

$$\rho(T)c(T)\frac{\partial T}{\partial t} = \operatorname{div}(k \operatorname{grad} T) - L\frac{\partial \Psi}{\partial t}, \qquad (x, y, z, t) \in Q. \tag{4.22}$$

Unlike the effective specific heat method, the latent heat source method can deal with a general function of the liquid fraction, Ψ, since the derivative of Ψ is with respect to time, not with respect to temperature (Voller et al., 1990).

4.2.4 The temperature-transforming method

The temperature-transforming method can be considered as a combination of the effective specific heat method and the latent heat source method, when the problem considers solid-liquid phase changes in binary systems (two component systems) (Zeng and Faghri, 1994). In this case the liquid volume fraction depends on the temperature and mass concentration[1], η, i.e., $\Psi = \Psi(T, \eta)$. The temperature-transforming equation is (Zeng and Faghri, 1994)

$$A(T, \eta)\frac{\partial T}{\partial t} = \operatorname{div}(k \operatorname{grad} T) + B(T, \eta), \qquad (x, y, z, t) \in Q, \tag{4.23}$$

where

$$A(T, \eta) = \rho(T)c(T) + L\frac{\partial \Psi}{\partial T}, \tag{4.24}$$

$$B(T, \eta) = -L\frac{\partial \Psi}{\partial \eta}\frac{\partial \eta}{\partial t}. \tag{4.25}$$

The latent heat evolution with reference to temperature evolution is accounted for the effective heat coefficient $A(T, \eta)$, whereas the latent heat evolution with reference to concentration variation is described by the source term $B(T, \eta)$. For the case of $\partial\Psi/\partial\eta = 0$, Equation (4.23) reduces to the effective specific heat method, whereas for the case of $\partial\Psi/\partial T = 0$, Equation (4.23) reduces to the latent heat source method (Zeng and Faghri, 1994).

[1]The mass concentration is defined as the mass of a component divided by the volume of the mixture.

A key feature in the development of fixed domain methods is the definition of the liquid phase fraction Ψ. In general the liquid phase fraction depends on the solidification process. However, to simplify, commonly the liquid phase fraction is taken to be a function of temperature alone, i.e., $\Psi = \Psi(T)$.

Chapter 5

Model of heat conduction through a constructive system with phase change

This chapter describes the numerical model used to develop a numerical code that simulates the heat transfer through a building envelope constructive system made of a phase change material. The physical problem is similar to that presented in Section 3.1, except that the constructive system is made of a material that presents solid-liquid phase changes. The validation of the numerical code was carried out using a numerical benchmark proposed by the International Energy Agency. Finally, a sensitivity analysis considering the time step and grid size is included.

5.1 Numerical model

This section describes the one-dimensional time-dependent heat conduction model used to simulate the heat transfer through a PCM-constructive-system in the building envelope. In order to increase the capacity of certain building energy simulation programs (e.g., EnerHabitat) to simulate PCMs, the numerical code was developed considering a one-dimensional approach such that it can be easily integrated into that simulation program. The numerical code uses the effective specific heat method presented in Section 4.2.1, which expresses the heat transfer only as a function of the PCM temperature (Samarskii and Vabishchevich, 1995). This method addresses the solidification and melting processes of multicomponent systems, which solidify in a temperature interval leading to a spatial mushy region between solid and liquid phases. The non-linear latent and specific heat effects are grouped in a single term, the effective specific heat, c_{eff}. Its formulation is

$$\rho\, c_{eff} \frac{\partial T}{\partial t} = \operatorname{div}\left(k \operatorname{grad} T\right), \tag{5.1}$$

$$c_{eff} = c + \rho^{-1} L \frac{d\Psi}{dT}, \tag{5.2}$$

where T is the temperature as function of time, t, and space, x, ρ is the density, c is the specific heat, k is the thermal conductivity, L is the phase change enthalpy per volume, and Ψ is the fraction of the liquid phase that can be a function of T and x. It was considered that each phase of the PCM is homogeneous and isotropic and that the thermophysical properties of each phase are constant.

The value of c_{eff} can be obtained from testing data with calorimetric methods or using numerical approximations based on space or temporal averaging of the enthalpy (AL-Saadi and Zhai, 2013). In this work a numerical approximation for c_{eff} was used. From a provided specific enthalpy curve, h, c_{eff} was calculated using a temporal averaging (Morgan et al., 1978),

$$c_{eff} = \frac{h\left(T^{new}\right) - h\left(T^{old}\right)}{T^{new} - T^{old}}, \tag{5.3}$$

where *new* represents the actual time step and *old* represents the previous time step in iterative schemes.

The boundary conditions were specified via a film coefficient and the temperature of the surrounding medium (Equations (3.2) and (3.3)). Internal heat gains and infiltration were not considered.

For the nAC condition T_i was calculated using Equation (3.4). For the AC condition there are two choices:

- The simplest type. T_i is constant and fixed to the comfort temperature, T_c.
- An energy saving type. When T_i is within the thermal comfort zone (TCZ) the air-conditioning is turned off and T_i is calculated according to Equation (3.4). If T_i is greater than the upper limit of the TCZ the air-conditioning cools the space with the upper limit of the TCZ as the setpoint. If T_i is below the lower limit of the TCZ then the air-conditioning heats the space with the lower limit of the TCZ as the setpoint.

An air-conditioning system that can supply any amount of cooling or heating load was considered.

A periodic T_{sa} function was used and the numerical code was iterated until obtaining periodic solutions of T and T_i. Simulations were made for a day and the numerical code was iterated until the difference in the temperature values of each node of the constructive system for $t = 0$ h and $t = 24$ h was less than a tolerance value, ζ[1]. By considering only one enthalpy curve, i.e., no hysteresis, and the periodicity of the solutions, the following is implied: *i*) the energy absorbed by the indoor air is equal to the energy released by it for the 24 hours period; *ii*) the energy absorbed by each of the control volumes of the PCM-wall (see Figure 3.2) is equal to the energy released by them for the 24 hours period, thus, the daily

[1]In this work a tolerance value $\zeta = 0.0001$°C was considered.

energy flux at each of the interfaces of the control volumes and at the outdoor and indoor surfaces is equal to zero.

The model discretization was made using a control-volume formulation. The solution of the discretization equations were obtained using a fully implicit scheme and the TriDiagonal-Matrix Algorithm (see Section 3.3).

According to the above description, for this model the input data for the properties of PCMs are the enthalpy curves, density, specific heat in solid and liquid phases, thermal conductivity, and thickness.

5.2 Validation of the numerical code

The validation of the numerical code was made using a one-dimensional numerical benchmark (Johannes et al., 2011) proposed by the International Energy Agency. In this benchmark the one-dimensional thermal behavior of a building wall containing PCM in time-dependent conditions was simulated by different working groups (groups of France, Norway, and China). Each working group developed a numerical code to this end: the group of France developed a code under TRNSYS software using the effective specific heat method, the group of Norway did not provide details concerning the model they used, whereas the group of China developed a code using the enthalpy method written in FORTRAN.

Nine cases (Table 5.1) were analyzed by all the working groups. The thermal properties of the materials which undergo no phase change are presented in Table 5.2. For the PCM, $\rho = 1100.0\,\mathrm{kg{\cdot}m^{-3}}$, whereas its values of c_{eff} and k are functions of T (Figure 5.1). In this benchmark the radiative heat transfer was not considered, the indoor and outdoor convection heat transfer coefficients were equal to $2.5\,\mathrm{W{\cdot}m^{-2}{\cdot}K^{-1}}$ and $8.0\,\mathrm{W{\cdot}m^{-2}{\cdot}K^{-1}}$, respectively, and the indoor air temperature was supposed constant and equal to 20.0°C. The outdoor air temperature varied according to $12.0^{\circ}\mathrm{C} + 20.0^{\circ}\mathrm{C/h} \times t$ for $t \leq 1\,\mathrm{h}$ and 32°C for $t > 1\,\mathrm{h}$.

Table 5.1: Cases analyzed in the benchmark carried out by Johannes et al. (2011).

Case	Outdoor layer	Indoor layer
1	5 mm PCM	
2	10 mm PCM	
3	50 mm PCM	
4	30 mm concrete	10 mm PCM
5	10 mm PCM	30 mm concrete
6	200 mm concrete	10 mm PCM
7	10 mm PCM	200 mm concrete
8	100 mm insulation	10 mm PCM
9	10 mm PCM	100 mm insulation

Table 5.2: Thermal properties of the materials with no no phase change used in the benchmark carried out by Johannes et al. (2011). k is the thermal conductivity, ρ is the density, and c is the specific heat.

Material	k [W·m^{-1}·K^{-1}]	ρ [kg·m^{-3}]	c [J·kg^{-1}·°C^{-1}]
Concrete	1.2	2000.0	1000.0
Insulation	0.04	50.0	1000.0

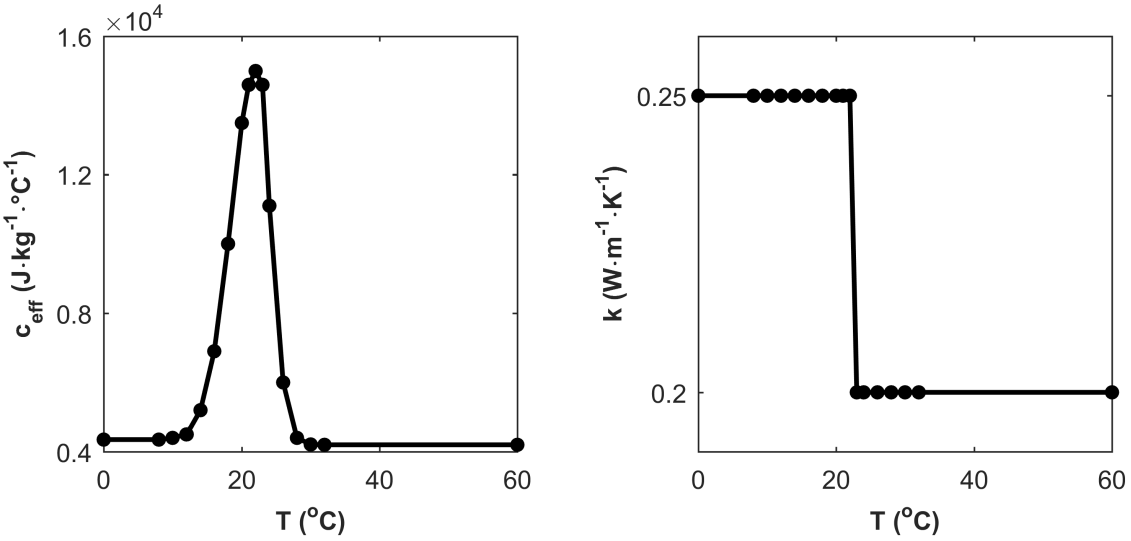

Figure 5.1: Effective specific heat, c_{eff}, and thermal conductivity, k, of the PCM used in the benchmark carried out by Johannes et al. (2011), as functions of temperature, T.

All the cases analyzed in the benchmark were simulated using the numerical code developed in this work[2] and the results were compared with those obtained by the different working groups. Figure 5.2 shows the indoor surface temperature T_{is} as function of time t of the wall for each case obtained with the numerical code developed in this work, by the group of France, and by the group of Norway (the comparison with the group of China was not possible because the temperature values at the indoor surface for different times were not reported in Johannes et al. (2011)). Figure 5.2 shows that the results of the numerical code developed in this work are in good agreement with those of the benchmark.

In addition to the qualitative comparison, a quantitative comparison was made in terms of the absolute value of the maximum percentage error, MPE, and the mean absolute percentage error, MAPE. Table 5.3 shows that the maximum differences with the group of France are 10% in the MPE for case 2 and 2% in the MAPE for cases 2 and 3; whereas with the group of Norway the maximum differences are 4% in the MPE for case 4 and 2% in the MAPE for

[2]A time-step of 1 min and a grid-size of 0.5 mm were used.

cases 3, 4, 6, and 7.

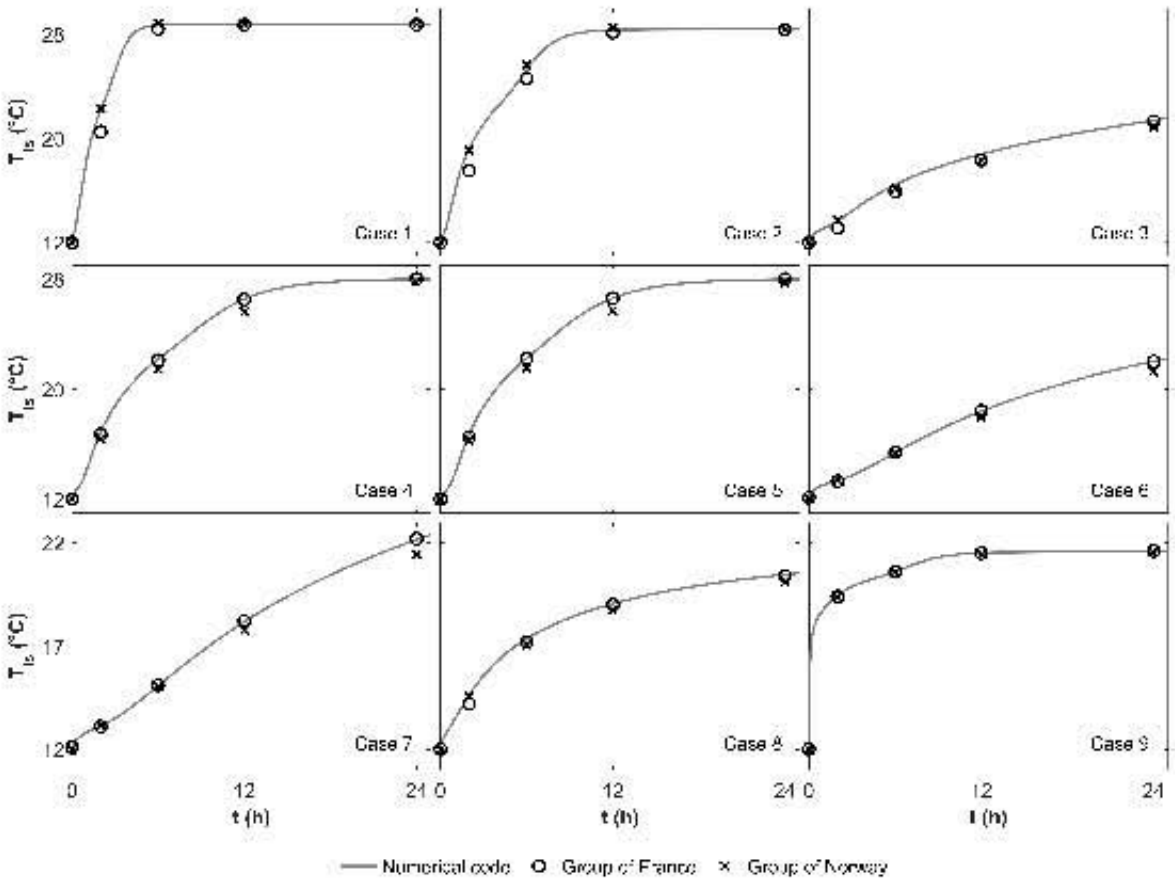

Figure 5.2: Graphical comparison of the results of the numerical code developed in this work with those of the benchmark carried out by Johannes et al. (2011). It is shown the indoor surface temperature, T_{is}, as function of time, t, of the wall for each case obtained with the numerical code developed in this work, by the group of France, and by the group of Norway.

Table 5.3: Quantitative comparison of the results of the numerical code developed in this work with those of the benchmark carried out by Johannes et al. (2011). MPE is the absolute value of the maximum percentage error and MAPE is the mean absolute percentage error.

	France		**Norway**	
Case	**MPE (%)**	**MAPE (%)**	**MPE (%)**	**MAPE (%)**
1	8	1	1	1
2	10	2	1	1
3	4	2	3	2
4	1	1	4	2
5	1	1	3	1
6	1	1	3	2
7	1	1	3	2
8	3	1	2	1
9	1	1	1	1

5.3 Grid sensitivity analysis

The grid sensitivity analysis consisted of analyzing the sensitivity of different calculated parameters of the thermal performance of a constructive system, when variations in the time step and grid size are considered. To do this, the periodic-state solution of the temperature of a PCM roof under nAC condition in the city of Aguascalientes, Mexico, over a typical day of May[3] was simulated.

In order to analyze the grid sensitivity when the phase change of the PCM occurs in a wide and a narrow temperature interval, two different functions of effective specific heat were considered. Yet, to be able to observe the effect of the phase change in the indoor surface temperature, an appropriate thickness should be selected for each case (Figures 5.3 and 5.4). For the wide phase change interval a 5 mm-thick roof was chosen, whereas for the narrow phase change interval a 50 mm-thick roof was chosen. Also, the corresponding thermal conductivity functions were adjusted to each case (Figures 5.3 and 5.4). The density of the PCM was considered constant and equal to 1100.0 $kg \cdot m^{-3}$.

Figures 5.5 and 5.6 show the indoor surface temperature for the two PCM roofs considering different time steps and grid sizes, for different times of the day. In both cases a convergent pattern is observed, which indicates a convergent solution is obtained when the time step and grid size are reduced. These figures show that for the 5 mm-thick PCM roof the simulated indoor surface temperature is almost independent of the grid size, but is highly dependent of the time step; whereas for the 50 mm-thick PCM roof the simulated indoor surface temperature exhibits high variations whit the time step and small variations with the grid size. For a given time step and the different grid sizes tested, differences in indoor

[3]The weather variables and monthly comfort temperature for the city were obtained from Ener-Habitat.

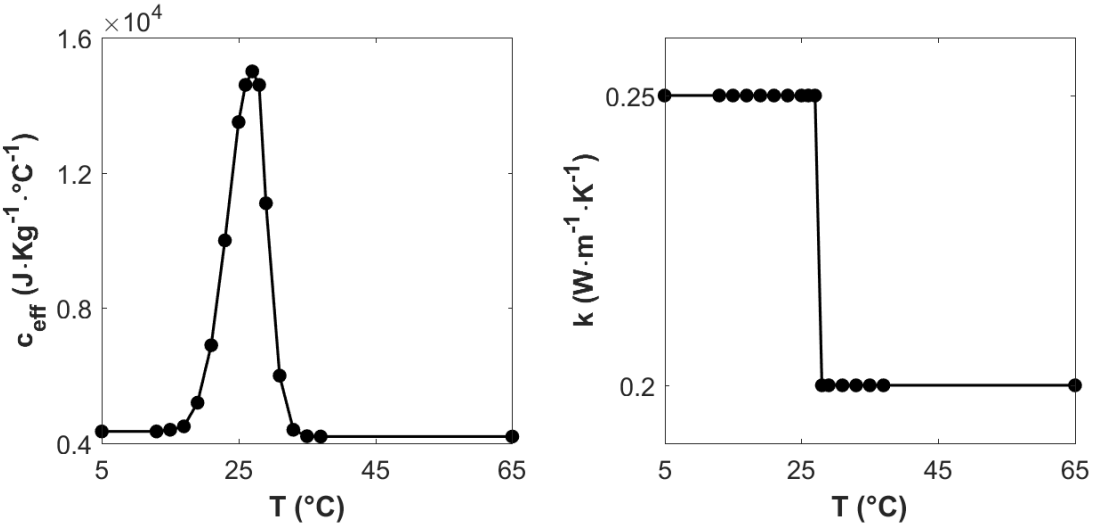

Figure 5.3: Effective specific heat, c_{eff}, and thermal conductivity, k, of the 5 mm-thick PCM roof as functions of temperature, T.

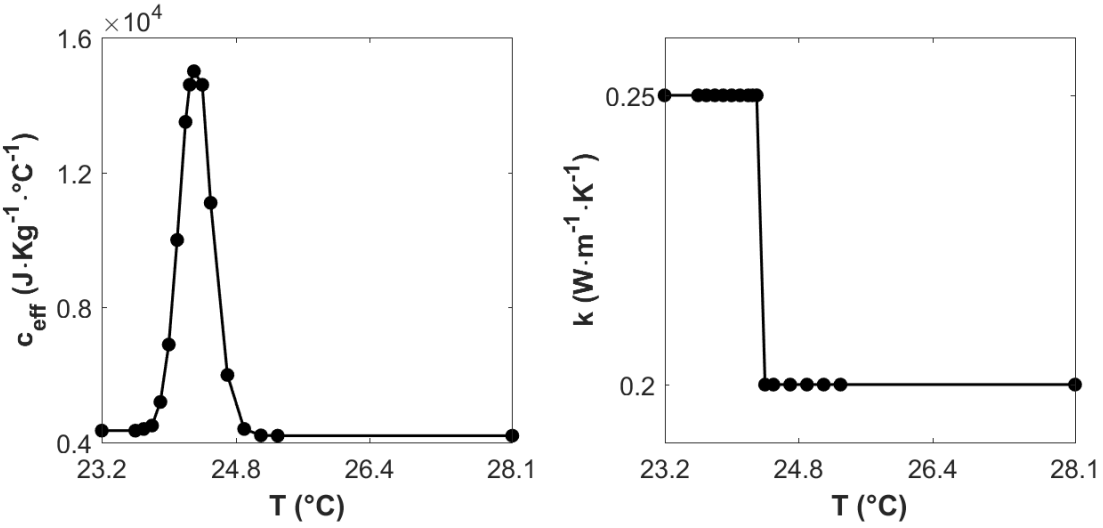

Figure 5.4: Effective specific heat, c_{eff}, and thermal conductivity, k, of the 50 mm-thick PCM roof as functions of temperature, T.

surface temperature of up to 0.001°C for the 5 mm-thick roof and of up to 0.17°C for the 50 mm-thick roof were obtained, which suggest that the differences could be associated to the thermal inertia of the constructive system. These results indicate that for the analyzed cases a PCM layer can be well simulated using only five control volumes.

To select the longest time step that adequately describes the thermal performance of the constructive system under nAC condition, it is necessary to select an appropriate parameter. According to Barrios et al. (2012), the transmitted energy, TE, through the wall/roof during a day is a reliable parameter to do this, particularly for periodic conditions. Figure 5.7 shows the TE parameter for the two cases. It shows that there is a maximum variation of 1.8% and 3.6% between the value of TE obtained with $\Delta t = 10$ min, and the value obtained using the most refined grid, for the cases 1 and 2, respectively. According to these results, a PCM layer represented by five control volumes and a time step of 10 min are suitable to simulate the thermal performance of a constructive system under nAC condition. Figure 5.8 shows the indoor surface temperature for the two cases considering the most refined grid and the proposed grid.

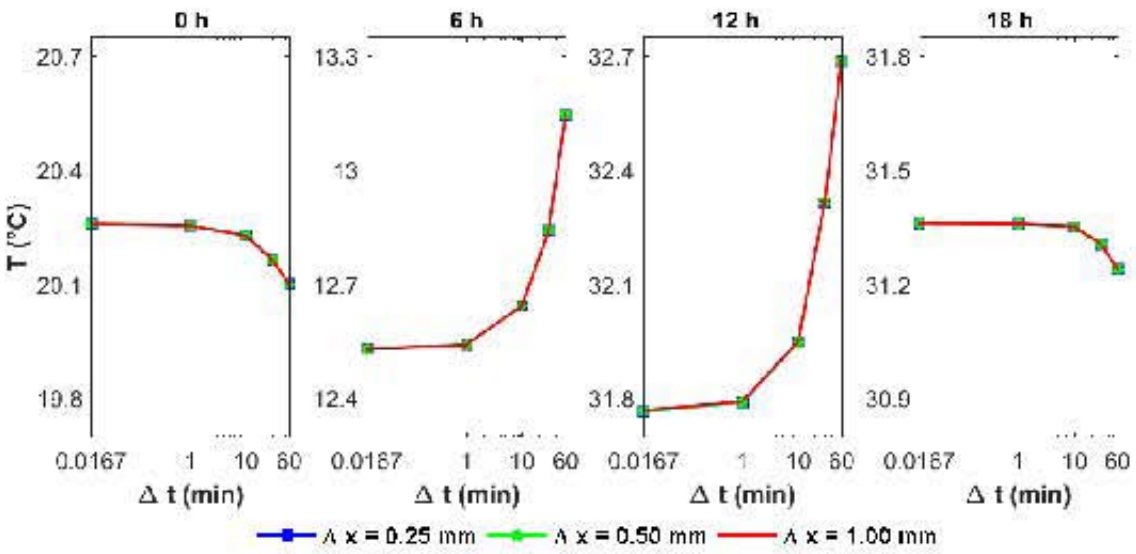

Figure 5.5: Indoor surface temperature variations for the 5 mm-thick PCM roof considering different time steps and grid sizes.

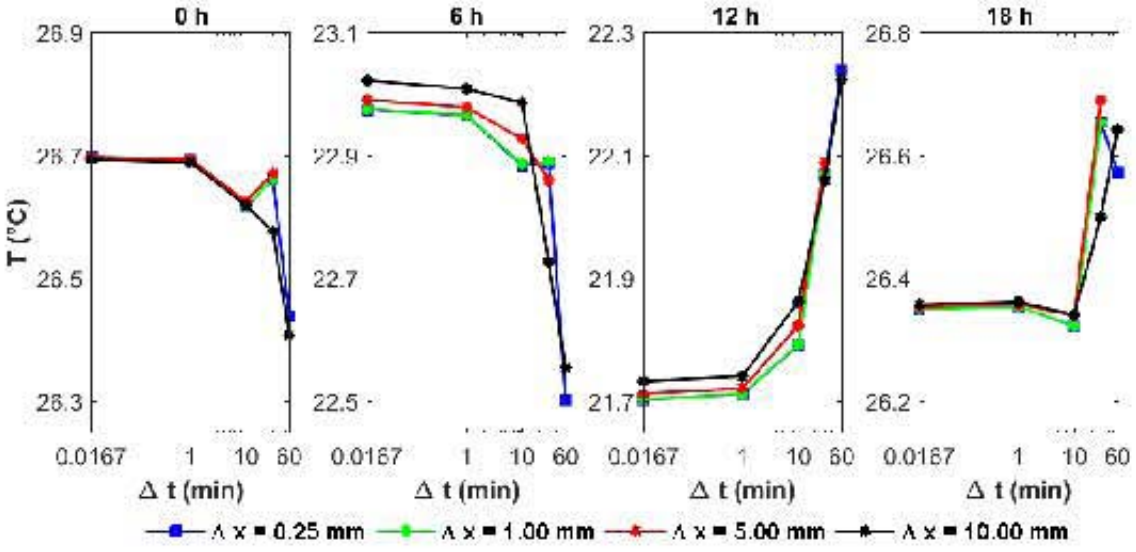

Figure 5.6: Indoor surface temperature variations for the 50 mm-thick PCM roof considering different time steps and grid sizes.

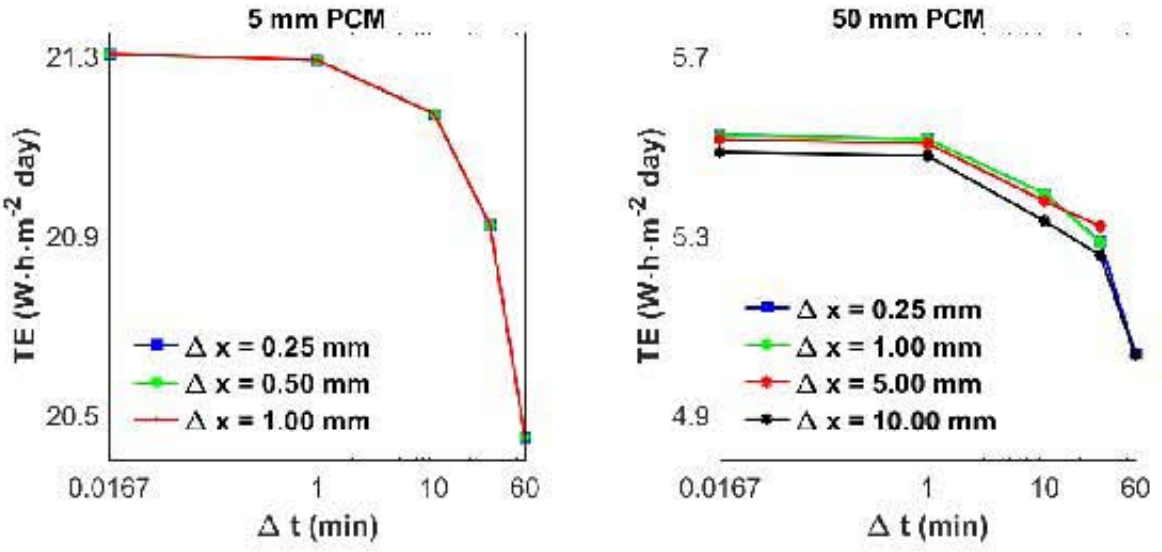

Figure 5.7: Transmitted energy, TE, variations for the two PCM roofs considering different time steps and grid sizes.

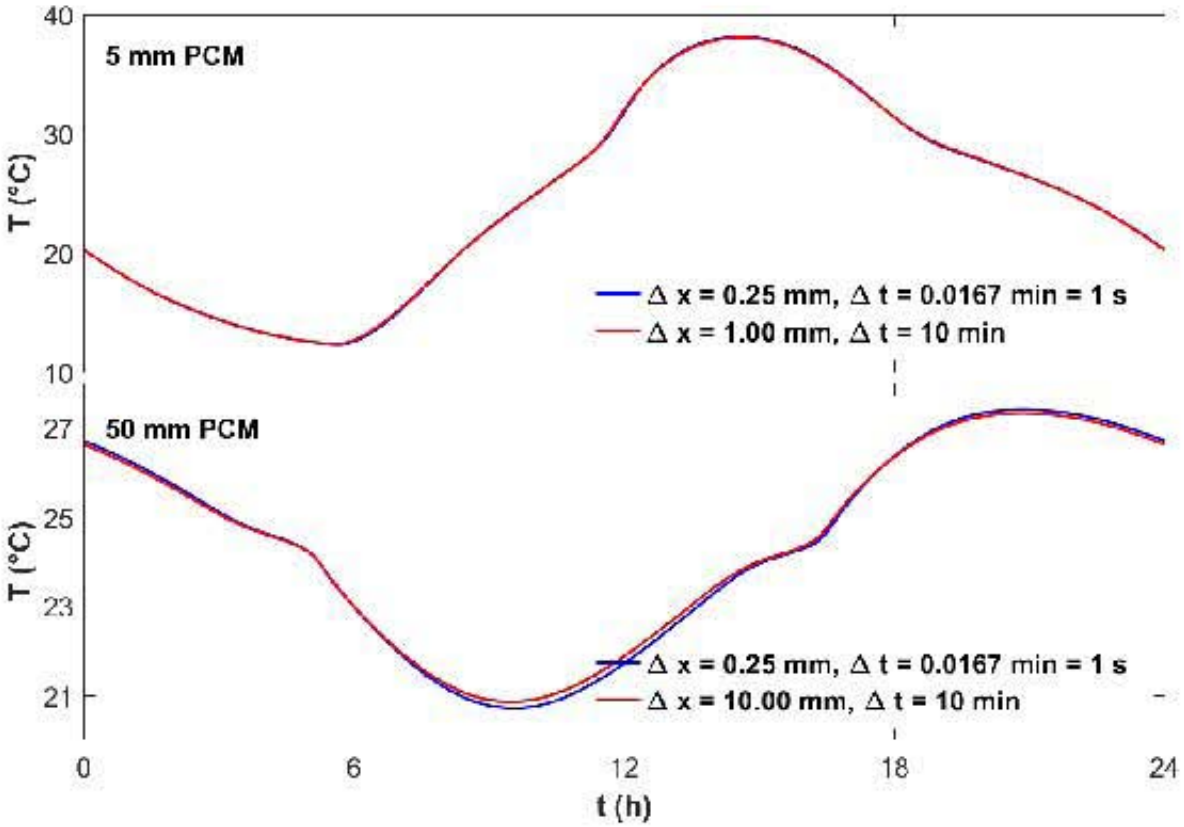

Figure 5.8: Indoor surface temperature of the two PCM roofs for the most refined (blue line) and proposed (red line) grids.

Chapter 6

Thermal performance of lightweight walls with phase change materials

A short version of this chapter was published as:
E. Moreles and G. Huelsz. Thermal performance of lightweight walls with phase change materials. In *Proceedings of the 10th Conference on Advanced Building Skins*, pages 47 - 56, Bern, Switzerland, Nov. 3 - 4 2015. Economic Forum.

Abstract

This work presents numerical simulations of the thermal performance of lightweight walls of the building envelope with phase change materials (PCMs), using a time dependent one-dimensional heat conduction model. The considered constructive system is a PCM-wall composed by microencapsulated paraffin within a copolymer laminated on both sides with a 100 μm aluminum sheet. The simulations considered variations in melting temperature and thickness of the PCM for air-conditioned (AC) and non-air-conditioned (nAC) conditions in a hot and a cold climate in Mexico, using the typical day of a month for the analysis. The evaluation parameter for AC condition is the heating or cooling load, whereas for nAC condition is the heat or cold discomfort degree hours. The differences of thermal performance under AC and nAC conditions were investigated and values of melting temperature and thickness that minimize the evaluation parameters were found. Finally, a comparison of the thermal performance of the PCM-wall with a lightweight wall constructive system without PCM (a cement board wall) was carried out.

Keywords: thermal performance; PCM-wall; time dependent heat conduction model; melting temperature; thickness; air conditioning; non-air conditioning

6.1 Literature review

The energy and the environment are two of the most important issues at the present time. The industrial development and the population boom have led an enormous increase in energy

demand to an annual rate of 2.3% (Zhou et al., 2012). In 2012 Mexico occupied the sixteenth place in the world energy consumption, with 1.3% of total world consumption. In 2013 the national energy consumption increased 2.3% compared to 2012, being the fossil fuels the main source of energy production (SENER, 2014), which have led a progressive increase in the levels of atmospheric CO_2, leading to intensification of climate change, which has been documented in recent years (IPCC, 2013). In Mexico the use of energy in buildings (which comprises use in residential, commercial, and public buildings) covers a high percentage of the total consumption. In 2013, 18% (909 PJ) of the national energy consumption was used in buildings (SENER, 2014), and it is expected that the demand grows due to the needs of heating and cooling air-conditioning associated with the thermal comfort, particularly in lightweight buildings. Nowadays, lightweight construction has become popular, since it has several advantages: speed of construction, low weight, architectural flexibility for retrofitting purposes, and economy of mass production due to a superior quality and high standards achieved by off-site manufacture control (Soares et al., 2014). However, due to the low thermal mass of these construction materials, it is very difficult to achieve thermal comfort in the case of non-air-conditioning; and if the air-conditioning is used, an extra good insulation is required in order to reduce energy consumption. Options that increase the thermal mass of the construction materials without increasing their thickness are desirable. Recently, the latent heat energy storage through the use of phase change materials (PCMs) has become an interesting alternative to solve the problem of low thermal mass in the lightweight building envelope (Zhang et al., 2007; Sadineni et al., 2011). In the last decades a lot of research in the use of PCMs in the building envelope, considering AC and nAC conditions, has been done. These studies analyze either the thermal performance of a single component or the thermal performance of a whole building, considering one-dimensional heat transfer.

The studies that analyze a single component in AC condition are the following. Ahmad et al. (2006) studied via experiments and computer simulations (using the software Heating) three types of wallboards containing a PCM (a polycarbonate panel filled with paraffin granulates; a polycarbonate panel filled with polyethylene glycol PEG 600; and a PVC panel filled with PEG 600 and coupled to a VIP), in order to select wallboards for the light envelope of buildings with thickness less than 5 cm. They found that the third wallboard showed the best thermal performance. Halford and Boehm (2007), using an explicit finite difference model, evaluated numerically the ability of a PCM layer placed between 2 layers of insulation to reduce the peak air-conditioning load for the summer season. They defined two baseline cases (a "mass but no phase-change" and a "insulation only"). They found maximum reductions in peak load of 11% - 25% when compared to the "mass but no phase change" case, and a 19% - 57% decrease over the "insulation only" case.

Also, there is one study on the thermal performance of a single component in both AC and nAC conditions (Diaconu and Cruceru, 2010) and one in nAC conditions (Silva et al., 2012). Diaconu and Cruceru (2010) evaluated numerically, using the enthalpy method, a new type of a composite PCM wallboard wall system, for the heating and cooling season in Béchar, Algeria. The wall system was composed by a layer of insulation located between two different PCM wallboards: an exterior PCM active during the cooling season (set point temperature of

25°C) and an interior PCM active during the heating season (set point temperature of 20°C). A reference wall with constant values of the specific heat for both PCMs was considered. For the nAC condition a reduction of 0.5°C in the peak indoor temperature, with reference to the reference wall, was found. For the AC condition, annual energy savings for the cooling load of 1% (with a PCM melting temperature of 20.0°C) and 12.8% for the heating load (with a PCM melting temperature of 24.4°C) were found. Silva et al. (2012) studied experimentally and numerically (using ANSYS FLUENT) the effect of the incorporation of PCM macro encapsulated inside the hollows of a typical Portuguese clay brick masonry envelope wall. Two walls, one composed by bricks with PCM and the other composed by bricks without PCM, were built and placed between a climatic chamber (representing the outdoor) an another chamber (representing the indoor). Decreases of about 2°C in the indoor temperature and time delays of 2.5 h between the two walls were found.

Concerning the studies in a whole building considering the AC condition, there are the following studies. Peippo et al. (1991), using a shoebox model[1] and the enthalpy method, studied a PCM panel attached to all indoor surfaces of a room in two climatic zones (Helsinki, Finland and Madison, Wisconsin) for the heating season. They found an optimum melting temperature of about 1°C to 3°C above the average room temperature and an optimum thickness of 10 mm to 15 mm. Also they found annual energy savings of 15% in Madison and 6% in Helsinki. Heim and Clarke (2004) through numerical simulations with ESP-r of a building in Warsaw, with large glazing areas, showed that the application of an indoor layer made of 1.2 cm of PCM-gypsum composite wallboard on the envelope walls (made of 25 cm of concrete with a 12 cm polystyrene layer at the outdoor), can reduce the heating energy demand by up to 90% during the heating season, compared to the wall without the PCM layer. Chan (2011) assessed the thermal and energy performance of a residential flat in Hong Kong for the cooling season, using EnergyPlus, without and with a PMC. The baseline case has envelope walls composed by layers, from outdoor to indoor, of a 5 mm mosaic tile, 10 mm cement, 100 mm heavy concrete and 10 mm gypsum plaster. The walls with the PCM are the same, but enhanced with a 5 mm layer of Energain placed between the cement and the concrete layers. Through the comparison with the baseline case, he found decreases of up to 1.5°C in the maximum indoor surface temperatures and an annual saving in cooling energy of 2.9%. Zhu et al. (2011) presented numerical studies, using a Capacitor-Resistance (RC) model, on the energy performance of a commercial building with envelope walls made of concrete with a thickness of 115 mm, enhanced by 10 mm shape-stabilized PCM (SSPCM) placed at the indoor surface, in a subtropical climate (Hong Kong) and a dry continental climate (Beijing), for the summer season. They found energy savings in the SSPCM building of 10.61% in Hong Kong and 12.76% in Beijing, with reference to the building without the PCM layer. Soares et al. (2014), using EnergyPlus and GenOpt, made an annual evaluation of the impact of indoor PCM-drywalls in a glazed lightweight steel-framed building, along with an optimization analysis (thickness, melting peak temperature, and solar absortance)

[1]Shoebox modeling is one of the complexity scales of building energy simulation. It analyzes a single floor or space within a floor for energy performance (Anderson, 2014).

for several European climates. Six PCM-drywalls melting peak temperatures of 18°C, 20°C, 22°C, 26°C and 28°C were considered. An optimum thickness of 4.0 cm for all the case studies was found; optimum melting temperatures between 22°C and 26°C for the warmer climates and between 18°C and 24°C for the colder climates were found; and indoor surfaces with optimum solar absortances of 0.9 and 0.3 for colder and warmer climates were found. Also, annual heating and cooling energy savings of 10% to 62% were found.

On the other hand, the following studies analyze a whole building in nAC condition. Athienitis et al. (1997) shown that the utilization of gypsum boards impregnated with PCM 13 mm-thick attached on the walls as indoor layer of an experimental outdoor test room in Montreal, may reduce the maximum room temperature by 4°C during the daytime in the winter season, compared to a gypsum drywall 13 mm-thick. Zhou et al. (2007), using the enthalpy method, performed a numerical study on the thermal performance of two PCM composites attached to the indoor surfaces of walls and the ceiling of a direct gain passive solar house in winter in Beijing, China. A PCM composite was a 30 mm-thick mixed type PCM-gypsum, and the other consisted of separate layers of 19 mm-thick gypsum and 11 mm-thick shape-stabilized PCM (SSPCM). They showed that both PCM composites reduce the indoor temperature swing in 3.2°C and 3.6°C, respectively, compared to a 30 mm-thick gypsum drywall.

Finally, there are two studies on the use of PCM in a whole building in AC and nAC condition. Kong et al. (2014), via experiments and using FLUENT, studied two PCM system panels installed on the outdoor and on the indoor surface of walls and roof located in Tianjin, China, during the summer session. The reference room was composed by walls 240 mm-thick of perforated bricks and a roof made of a polystyrene board placed between two cement boards reinforced with glass-fiber. They found reductions in the maximum indoor wall and roof surface temperatures of up to 2.4°C in the nAC condition and reductions in the heating load of 80% for the AC condition. Using EnergyPlus, Alam et al. (2014) investigated the potential of BioPCM placed in the indoor surface of the roof in a single room house to reduce the energy consumption in different Australian cities. For the nAC condition they found reductions from 1°C to 3°C in the mean air temperature. For the AC condition they found annual energy savings from 17% to 23% for heating and cooling.

The diversity of results obtained with the use of PCM-constructive-systems involves a variety of causes, such as: sol-air temperature, level of insulation of the room, use of night ventilation, type of constructive systems used (hollow or solid bricks), thermophysical properties of PCMs, and the way the thermal performance is evaluated. This is why it is not possible to derive a general rule to forecast the thermal performance of PCM-constructive-systems, each case must be evaluated independently.

In the design of buildings, the thermal performance of the envelope plays a main role in its operation, which is determined by a range of factors: thermophysical properties of the envelope (thermal conductivity, specific heat, density, thickness, outdoor surface solar absorptivity, and infrared emissivity), climate conditions (solar radiation, outdoor temperature, wind velocity, and humidity), and internal heating loads (people, electronic devices, and

furniture) (Zhang et al., 2007; Zhou et al., 2012). The successful application of PCMs in the building envelope requires that its thermophysical properties have to be selected according to the climate. One of the most important aspects to maximize the thermal energy storage and achieve thermal comfort inside buildings using PCMs in the envelope, is to optimize the phase change temperature of the PCM for each particular application. There are much research in this direction (Peippo et al., 1991; Stritih and Novak, 1996; Neeper, 2000; Onishi et al., 2001; Nikolić et al., 2003; Heim and Clarke, 2004), in which the general conclusion is that the maximum diurnal energy storage occurs at a PCM melting temperature that is close to the comfort temperature (from 1.0°C to 3.0°C above the comfort temperature).

It is therefore of interest to do research about the thermal performance of PCMs in nAC buildings and contrast it with that of AC buildings, as well as identify the differences in the thermal performance of the PCM in two different climates. This chapter reports on the results on a numerical simulation of a single component of the thermal performance of PCM-walls in two different climates in Mexico (a hot and a cold climate) considering AC and nAC conditions. So as to do the analysis, variations in melting temperature and thickness of the PCM were considered. The specific goals of this work are: to find the differences between the thermal performance of a PCM-wall for AC and nAC conditions; to find optimum values of melting temperature and thickness of the PCM for each case and each condition; and to compare the thermal performance of a PCM-wall with a cement board wall (one of the most commonly used lightweight walls worldwide (Amy Saunders and Emma Davidson, 2014). The question to be answered is, from the perspective of thermal comfort and energy saving, is it worth using PCMs in the lightweight buildings envelope?

6.2 Numerical model

The numerical model is described in Section 5.1. For the AC condition, the indoor temperature, T_i, was set to the comfort temperature, T_c. T_c was calculated using the methodology proposed by Humphreys and Nicol (2000).

6.3 Study cases and evaluation parameters

All simulations were performed for an east wall, considering two constructive systems: a cement board manufactured by USG (commercial name Durock) with a thickness of 12.7 mm and a composite phase change material produced by Dupont (commercial name Energain). The composite PCM is made of 60% microencapsulated paraffin within an ethylene based copolymer (40%). It is produced in a form of panel (1.2 m × 1 m × 5 mm) laminated on both sides with a 130 μm aluminum sheet. The edges are closed with a 75 μm aluminum tape. It has an area weight of 4.5 $\mathrm{kg \cdot m^{-2}}$ and the melting temperature, T_m, is 21.7°C. The thermal conductivity is 0.22 $\mathrm{W \cdot m^{-1} \cdot K^{-1}}$ in liquid phase and decreases to 0.18 $\mathrm{W \cdot m^{-1} \cdot K^{-1}}$ in solid phase. The thermophysical properties of both constructive systems are presented in

Table 6.1. The experimental effective specific heat of the composite PCM for the melting curve is shown in Figure 6.1.

Table 6.1: Thermal properties of the constructive systems.

Constructive system	k [W·m^{-1}·K^{-1}]	ρ [kg·m^{-3}]	c_p [J·kg^{-1}·°C^{-1}]	Solar absorptivity [–]
Cement board	0.25	1042.20	1090.00	0.4
Composite PCM	0.22-0.18	900.00	Variable	0.4

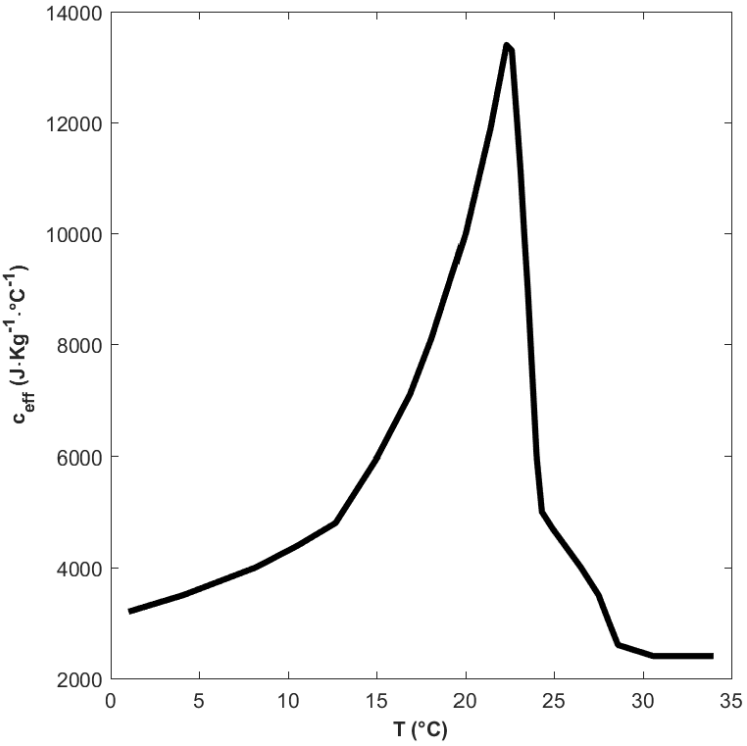

Figure 6.1: Experimental effective specific heat, c_{eff}, of the composite PCM for the melting process, as function of temperature, T. Data taken from Kuznik and Virgone (2009).

Two climates were considered. As example of a hot climate, the typical day of May in Temixco, Morelos, Mexico (18°85′N, 99°23′W, 1280 m altitude) was considered; and for a cold climate, the typical day of January in Toluca, Estado de México, Mexico (19°20′N, 99°40′W, 2667 m altitude) was considered[2]. The typical day for each month was constructed using the methodology proposed by Chow and Levermore (2007). This methodology uses the averages

[2]The month of May corresponds to the hottest month of the year in Temixco and the month of January corresponds to the coldest month of the year in Toluca

of the daily values of the maximum solar radiation, the maximum and minimum outdoor temperatures, and the time when they occur. These values were obtained from a typical year using Meteonorm. The sol-air temperature, T_{sa}, the comfort temperature, T_c, the upper limit of the thermal comfort zone, $T_c + \Delta T_c$, and the lower limit of the thermal comfort zone, $T_c - \Delta T_c$, for both cities are shown in Figure 6.2. The thermal comfort zone amplitude was calculated as proposed by Morillón-Gálvez et al. (2004). For Temixco $T_c = 28.1$°C and $\Delta T_c = 1.25$°C; whereas for Toluca $T_c = 17.6$°C and $\Delta T_c = 2.0$°C. As it can be seen, high temperatures are the main issue in Temixco, whereas in Toluca the main issue are low temperatures.

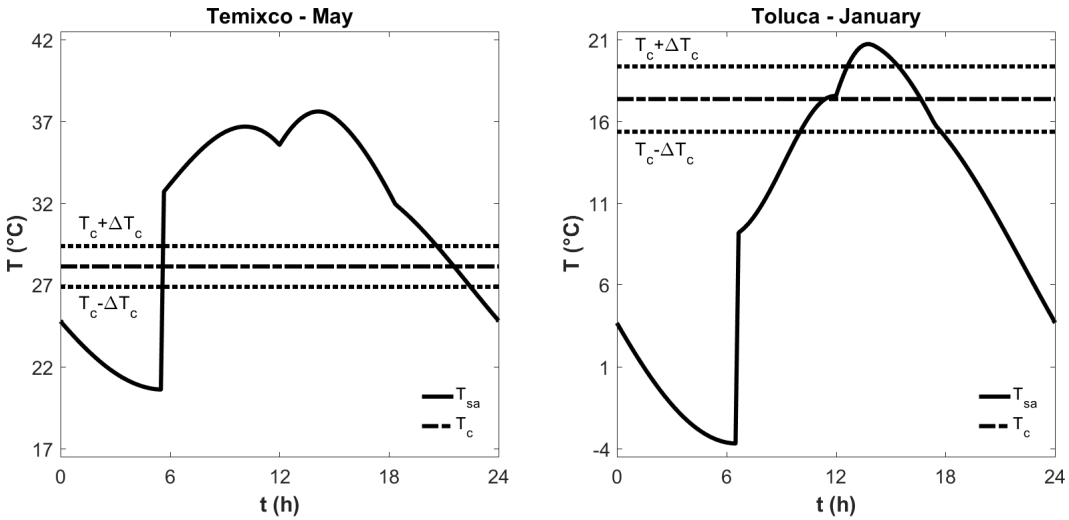

Figure 6.2: Temperature variables (the sol-air temperature, T_{sa}, the outdoor air temperature, T_a, the comfort temperature, T_c, the upper limit of the thermal comfort zone, $T_c + \Delta T_c$, and the lower limit of the thermal comfort zone, $T_c - \Delta T_c$) as functions of time, t, for Temixco in May and for Toluca in January considering a east facing wall with a solar absorptivity of 0.4.

According to several results in the literature concerning the optimal melting temperature of PCMs for use in buildings (Peippo et al., 1991; Stritih and Novak, 1996; Neeper, 2000; Onishi et al., 2001; Nikolić et al., 2003; Heim and Clarke, 2004), Energain is not suitable for use in Temixco during May because its melting temperature is not 1.0°C to 3.0°C above the respective comfort temperature. Then, in order to investigate the thermal performance and the optimal melting temperature of this PCM, they were considered the following variations on thickness and melting temperature of the PCM: thickness variations from 5 mm to 50 mm (in multiples of 5 mm); and variations of 1.0°C on melting temperature from $T_c - 10$°C to $T_c + 10$°C for each city. The variations in the melting temperature were conducted by a shift of the effective specific heat function shown in Figure 6.1.

To evaluate the thermal performance of the PCM-wall the following parameters were chosen: the heating and cooling loads (HL and CL, respectively) for the AC condition and the heat and cold discomfort degree hours (DDH_{hot} and DDH_{cold}, respectively) for the nAC

condition. They were calculated per day according to the following equations (Barrios et al., 2012),

$$CL = \int \mu_i \left[T_{is} - T_c\right] dt, \qquad T_{is} > T_c, \tag{6.1}$$

$$HL = -\int \mu_i \left[T_{is} - T_c\right] dt, \qquad T_{is} < T_c, \tag{6.2}$$

$$DDH_{hot} = \int \left[T_i - (T_c + \Delta T_c)\right] dt, \qquad T_i > T_c + \Delta T_c, \tag{6.3}$$

$$DDH_{cold} = -\int \left[T_i - (T_c - \Delta T_c)\right] dt, \qquad T_i < T_c - \Delta T_c, \tag{6.4}$$

The parameters DDH_{hot} and DDH_{cold} are null when the indoor temperature is inside the thermal comfort zone. The set of evaluation parameters (HL, CL, DDH_{hot}, and DDH_{cold}) will be referred as Thermal Performance Evaluation Parameters (hereafter TPEPs).

The study cases analyzed in this work were: 1) Temixco for the typical day of May under AC condition, 2) Temixco for the typical day of May under nAC condition, 3) Toluca for the typical day of January under AC condition, 4) Toluca for the typical day of January under nAC condition.

6.4 Results and discussion

This section shows the results of the analysis of the thermal performance of the PCM-wall subject to variations in its thickness, e, and melting temperature, T_m, along with an analysis of the PCM-wall thickness selection. The analysis was carried out under AC and nAC conditions in two different climates, and the differences between these cases were investigated.

6.4.1 Thickness and melting temperature analysis

Figure 6.3 shows the percentage variation of each TPEP for each study case, considering different values of thickness, e, and melting temperature, T_m, of the PCM. The percentage variation of a TPEP (shown in gray scale) was calculated with respect to the minimum value of the corresponding TPEP for a single thickness and for each value of T_m. The white color corresponds to the minimum variation and the black color corresponds to the maximum variation. This allows to quantify the magnitude of the thermal performance variations when varying T_m for a given e, as well as to identify the value of T_m that minimizes the TPEP for each e. It can be observed that higher variations occur in Temixco, particularly for the nAC condition, with thermal performance variations of up to 43% in the AC condition; whereas in Toluca the variations are small, with thermal performance variations of up to 6% in the nAC condition. It can be concluded that in Temixco the selection of T_m has a great impact on the PCM thermal performance, whereas in Toluca the the selection of T_m has a small

impact on the PCM thermal performance. In Temixco, for both use conditions, the T_m that minimizes the TPEP increases as the PCM-wall thickness increases, reaching a limit value of 29.1°C for the AC condition and 31.1°C for the nAC condition. In Toluca, up to a thickness of 30 mm, there is a unique T_m (21.6°C) that minimizes the TPEP for both conditions; for greater thicknesses the the magnitude of the thermal performance variations is reduced significantly. In Temixco the T_m that minimizes the TPEP for each thickness is higher than the comfort temperature, 1.0°C and 3.0°C for the AC and nAC condition, respectively. In Toluca, for both use conditions, the T_m that minimizes the TPEP for each thickness is 4.0°C higher than the comfort temperature.

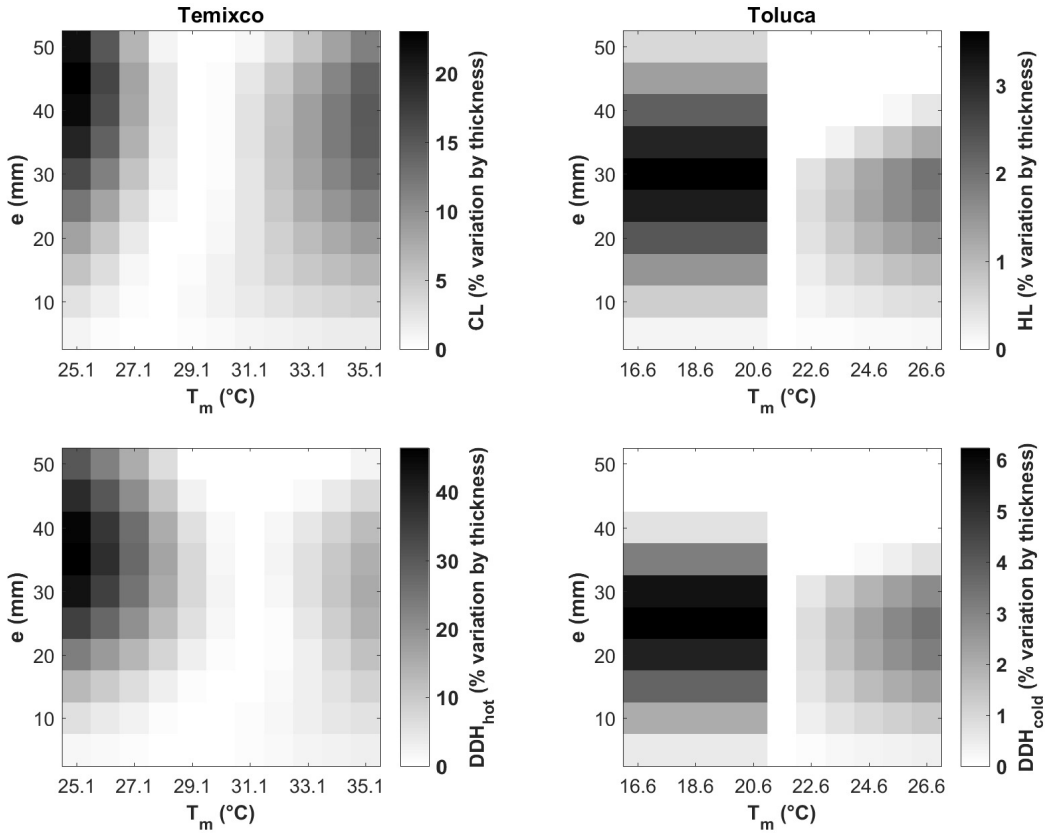

Figure 6.3: Percentage variation of the corresponding TPEP relative the minimum value of each thickness as function of the melting temperature and thickness, for the four study cases.

Also, it is interesting to show the magnitude of the thermal performance variations when the variations in thickness and melting temperature are conjointly considered. Figure 6.4 shows the percentage variation of each TPEP for each study case. The percentage variation of a TPEP (shown in gray scale) was calculated with respect to the minimum value of the corresponding TPEP for all of the combinations of e and T_m. The white color corresponds to the minimum variation and the black color corresponds to the maximum variation. Hereinafter the minimum value of percentage variation will be referred to as the global minimum.

From Figure 6.4 it can be observed that for all of the cases, except for the nAC condition in Toluca, variations in melting temperature and thickness of the PCM-wall impact strongly on the PCM thermal performance. Temixco exhibits the highest thermal performance variations for both operation conditions, with variations of up to 200% for the AC condition; whereas the thermal performance variations in Toluca for the nAC condition are small (barely 15%). This means that the PCM thermal performance in Toluca for the nAC condition is hardly affected by the entire range of variations in e and T_m considered, which suggests that the use of a PCM-wall with a thickness greater than 5 mm in Toluca for the nAC condition would not be profitable.

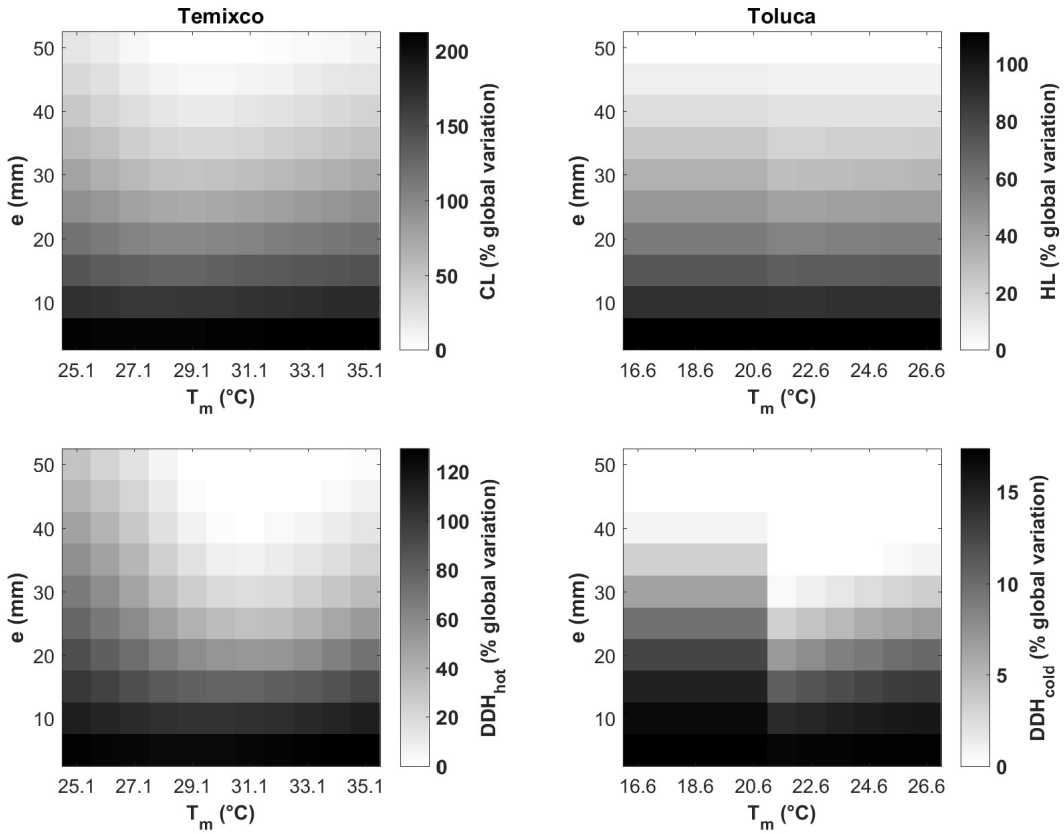

Figure 6.4: Percentage of relative variation of the corresponding TPEP from the global minimum, as function of the melting temperature and thickness, for the four study cases.

In order to find an explanation of the differences of the PCM thermal performance variations between the two climates, the effects of the symmetry of the effective specific heat function were investigated. Numerical simulations were carried out considering different configurations of the effective specific heat function (Figure 6.5), which are a combination of the original effective specific heat function (Figure 6.1), plus a smoothed symmetric function (Figure 6.5d).

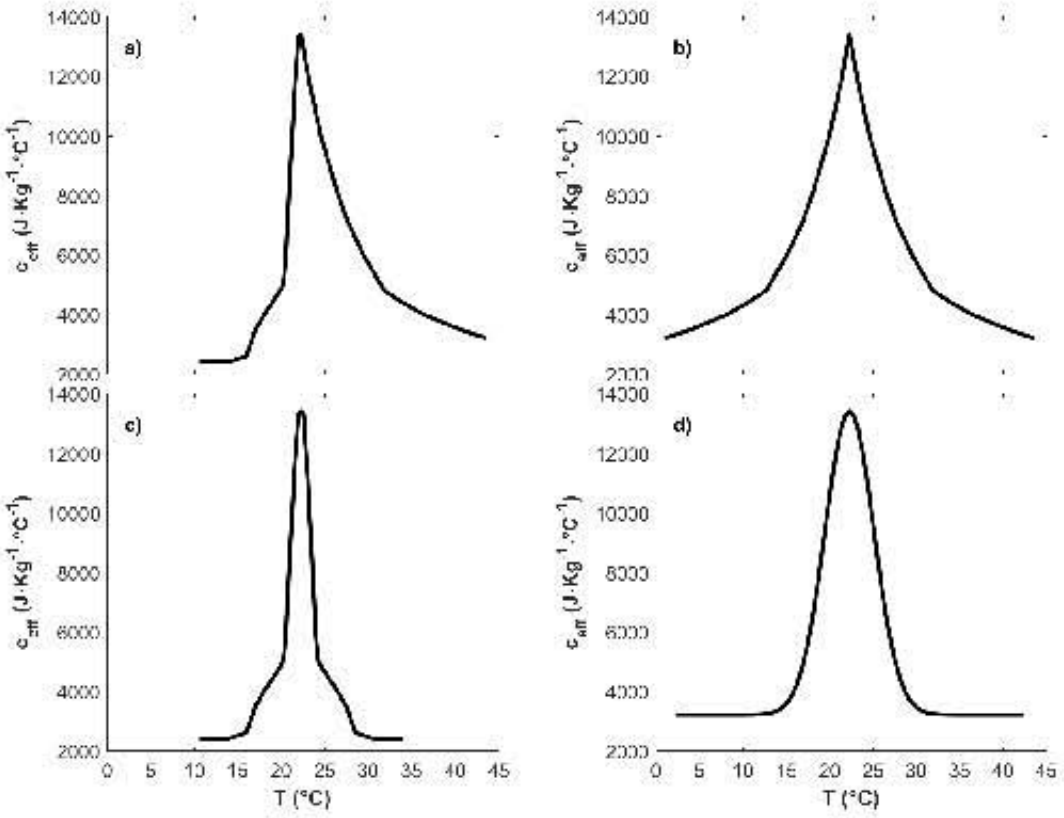

Figure 6.5: Different effective specific heat curves c_{eff} tested.

The same analysis of the PCM thermal performance variations shown in Figures 6.3 and 6.4 was carried out for the four effective specific heat functions presented in Figure 6.5. It was found that the PCM thermal performance variations are similar to the ones obtained with the original effective specific heat function. This result suggests that the thermal performance of the PCM depends slightly on the symmetry of the effective specific heat function, but it strongly depends on the environmental forcing, the sol-air temperature. Then, there is no a general rule that allows to select a melting temperature that minimizes the TPEP in AC and nAC conditions. So as to find the optimum thermophysical properties of a PCM in every application, a numerical simulation that includes all the factors that impact its thermal performance, principally the environmental forcing, had better be performed.

6.4.2 PCM-wall thickness selection

In this subsection the thermal performance of the PCM-wall varying its thickness was analyzed. For this analysis the optimum value of the melting temperature for each thickness obtained from Figure 6.3 was considered. Then, the corresponding TPEP values were plotted with the aim of finding a limit value of thickness, i.e., a thickness in which there is no a

significant improvement in the PCM thermal performance if the thickness is increased.

Figure 6.6 shows the reductions in the TPEPs for each thickness increment of 5 mm (ΔTPEP), along with the reductions with respect to the PCM-wall 5 mm-thick, for the four study cases. For the AC condition, in Temixco and Toluca, ΔTPEP decreases as thickness increases, with the maximum reduction obtained with the PCM-wall 10 mm-thick. For the nAC condition, in Temixco and Toluca, ΔTPEP first increases as thickness increases, and then ΔTPEP decreases as thickness increases, with the maximum reduction obtained with the PCM-wall 20 mm-thick. This suggests that the thermal performance of the PCM-wall under nAC is more complex than in the AC condition.

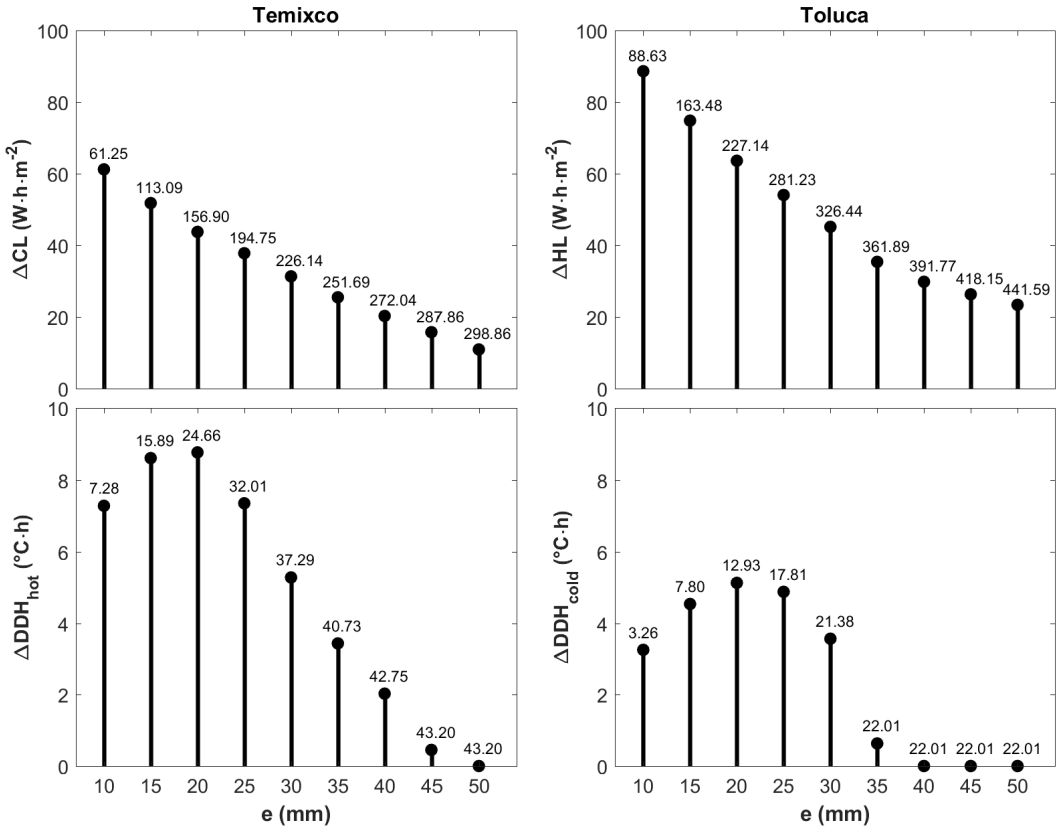

Figure 6.6: Reductions in the TPEPs (ΔTPEP) for each thickness increment of 5 mm in the PCM-wall, with respect to that of the previous thickness. The numbers above the dots represent the reductions in the TPEP respect to the PCM-wall 5 mm-thick.

On the other hand, concerning the TPEP reduction with respect to the PCM-wall 5 mm-thick, it is observed for the nAC condition that it decreases until reaching a limit value, indicating that there is a limit in the enhancement of the thermal performance of the PCM-wall by increasing its thickness (that limit is achieved with a thickness of 45 mm for Temixco and 35 mm for Toluca). For the AC condition there is no such limit. For this condition, the reductions in Toluca are higher than in Temixco, indicating that the PCM-wall performs

better thermally in Toluca for the AC condition. The maximum reduction in Toluca is 1.5 times the maximum reduction in Temixco. In contrast, for the nAC condition, the reductions in Temixco are higher than in Toluca, with a maximum reduction in Temixco of 2 times the maximum reduction in Toluca. The maximum reductions with respect to the PCM-wall 5 mm-thick are shown in Table 6.2.

Table 6.2: Maximum reductions in the TPEPs with respect to the PCM-wall 5 mm-thick.

Operation condition	City	Thickness (mm)	TPEP maximum reduction
AC	Temixco	50	$298.9\,\mathrm{W\cdot h\cdot m^{-2}}$ (67.4%)
	Toluca	50	$441.6\,\mathrm{W\cdot h\cdot m^{-2}}$ (52.5%)
nAC	Temixco	45	$43.2°\mathrm{C\cdot h}$ (55.2%)
	Toluca	35	$22.0°\mathrm{C\cdot h}$ (14.3%)

From Table 6.2 it can be observed that the TPEP maximum reductions are quite significant for all cases (higher than 50%), except in Toluca for the nAC condition. Then it can be confirmed that the use of the PCM-wall is not profitable in that case.

6.5 Comparison of the PCM-wall with a cement board wall

To contrast the thermal performance of the PCM-wall (with the effective specific heat function of Figure 6.1) versus one of the most commonly used lightweight walls worldwide (the cement board wall described in Section 6.3), the thermal performance of the cement board wall was studied. For the comparison it was considered the optimum value of melting temperature of the PCM-wall for each thickness as obtained from Figure 6.3.

Figure 6.7 shows the TPEPs for the PCM-wall and the cement board wall. From Figure 6.7 it can be seen that for all thicknesses considered the thermal performance of the PCM-wall is always better than that of the cement board wall. With respect to the cement board wall, the PCM-wall has greater benefits in Temixco than in Toluca for both operation conditions. Also, Figure 6.8 shows the absolute value of the percentage relative variation of the corresponding TPEP for the PCM-wall with respect to the cement board wall: differences ranging from 1% to 52% were obtained. From Figure 6.8 it is possible to identify the thickness that gives the maximum benefit of the PCM-wall. For the AC condition the maximum benefit is achieved with the maximum thickness considered, 50 mm; but in the nAC condition it is achieved in an intermediate thickness, 40 mm for Temixco and 30 mm for Toluca. Table 6.3 summarizes the maximum TPEP reduction (in physical units and in absolute values of the percentage relative variation) obtained with the PCM-wall with respect to the cement board wall.

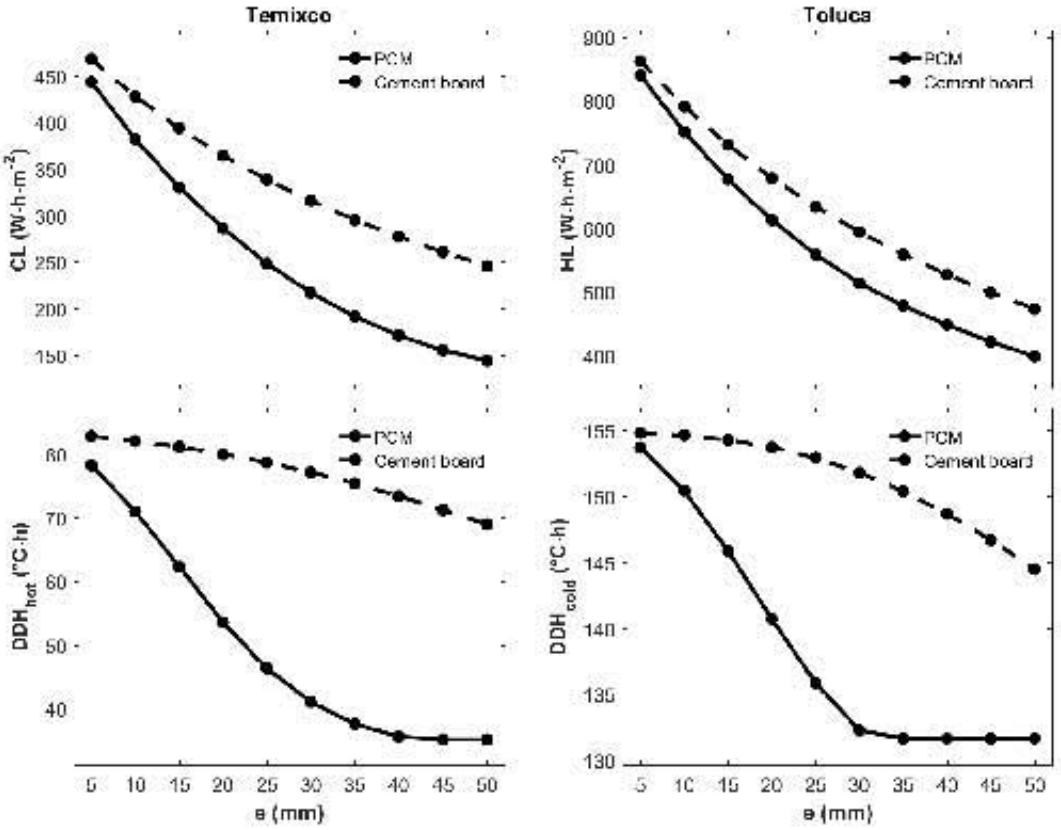

Figure 6.7: Comparison of the PCM-wall thermal performance versus the cement board wall.

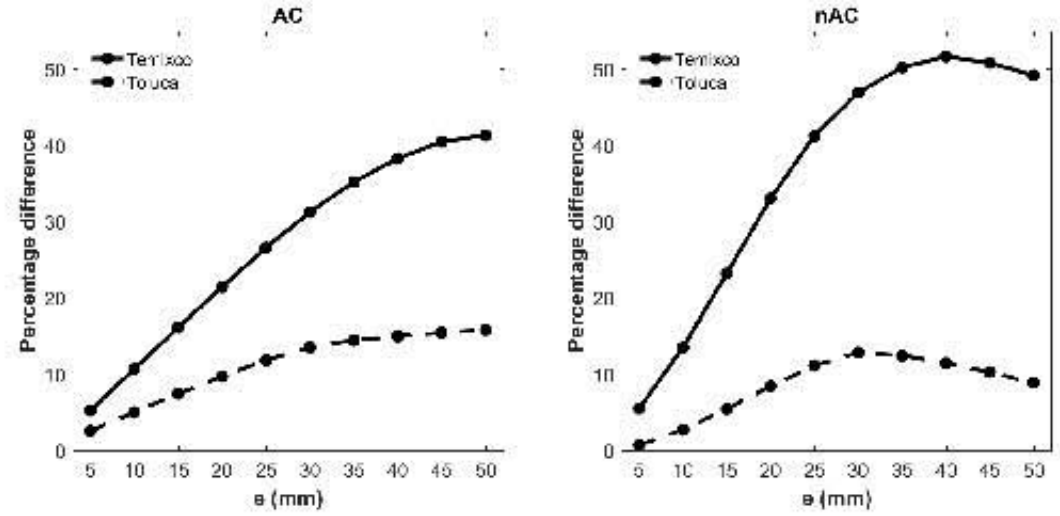

Figure 6.8: Absolute value of the percentage relative variation of the corresponding TPEP for the PCM-wall with respect to the cement board wall.

Table 6.3: Maximum TPEP reduction obtained with the PCM-wall with respect to the cement board wall for the proposed study cases. The reductions are presented in physical units and in absolute values of the percentage relative variation.

Operation condition	City	Thickness (mm)	TPEP reduction
AC	Temixco	50	$CL = 101.7\,\mathrm{W{\cdot}h{\cdot}m^{-2}}$ (41.3%)
	Toluca	50	$HL = 74.9\,\mathrm{W{\cdot}h{\cdot}m^{-2}}$ (15.8%)
nAC	Temixco	40	$DDH_{hot} = 37.9°\mathrm{C{\cdot}h}$ (51.6%)
	Toluca	30	$DDH_{cold} = 19.5°\mathrm{C{\cdot}h}$ (12.8%)

6.6 Conclusions

In this work, numerical simulations of the thermal performance of a PCM lightweight wall for two different climates in Mexico (a hot and a cold), under AC and nAC conditions; along with a comparison between the PCM-wall and a common lightweight wall with no phase change, were carried out.

It was found that there are significant differences in the thermal performance between the two climates and between the two operation conditions. For the hot climate the variations in the PCM melting temperature, given a thickness, have a huge effect on the thermal performance of the PCM-wall; whereas for the cold climate the variations in the PCM melting temperature do not significantly impact the thermal performance of the PCM-wall.

It was shown that the thermal performance of the PCM-wall strongly depends on the environmental forcing (the sol-air temperature) and on the operation condition (AC or nAC), and that the symmetry of the effective specific heat function has a small effect on its thermal performance. Moreover, for the study cases considered in this work, there is a limit in the thermal performance of the PCM-wall for the nAC condition (evaluated using the cooling and heating loads) in both climates, but a limit does not exist for the AC condition (evaluated using the hot and cold discomfort degree hours) (see Table 6.2).

The best thermal performance of the PCM-wall in the hot climate is obtained with a melting temperature 1.0°C higher than the comfort temperature for the AC condition, and 3.0°C higher than the comfort temperature for the nAC condition. In the cold climate the best thermal performance is obtained with a melting temperature 4.0°C higher than the comfort temperature for both conditions. Compared with the optimum melting temperatures reported in the literature, from 1.0°C to 3.0°C above the comfort temperature (Peippo et al., 1991; Stritih and Novak, 1996; Neeper, 2000; Onishi et al., 2001; Nikolić et al., 2003; Heim and Clarke, 2004), the results obtained in this work are similar to those. In the case of a mixed use of both operations conditions in the hot climate, a melting temperature of 2.0°C above the comfort temperature is suggested, as the variations in the thermal performance of the PCM-wall, from the thermal performance considering the optimum melting temperatures for both conditions, are small.

Compared with the cement board wall, the thermal performance of the PCM-wall is better in the hot climate than in the cold climate for both operation conditions. For the hot climate the energy reduction is up to 41% for the AC condition with a thickness of 50 mm and the discomfort reduction is up to 52% for nAC condition with a thickness of 40 mm; whereas for the cold climate the reductions are up to 16% and 13% for AC and nAC condition, with thicknesses of 50 mm and 30 mm, respectively. From the numerical results, the PCM-wall is recommended for use in the hot climate for both conditions due to reductions in the TPEPs are significant. However, its use in the cold climate for both conditions may not be profitable as the cement board wall has a similar thermal performance to the PCM-wall.

According to the results of this study, there is no a general rule that allows to select an optimum PCM. Besides technical issues, selecting a PCM may also involve economic issues and last but not least environmental criteria in order to satisfy sustainability standards in buildings. A cost-benefit analysis and annual simulations of the thermal performance of the PCM-wall are proposed as future research.

Chapter 7

Hysteresis effects on the thermal performance of building envelope PCM-walls

Manuscript submitted
E. Moreles, G. Huelsz and G. Barrios. Hysteresis effects on the thermal performance of building envelope PCM-walls. Submitted to *Building Simulation* on June 2, 2017. Under review.

Abstract

This work presents a numerical study of the combined effects of the hysteresis temperature difference, peak melting temperature, and thickness of a building envelope PCM-wall on its thermal performance in air-conditioning and non-air-conditioning conditions. The study was carried out considering complete melting-freezing daily cycles of the PCM in a climate exhibiting both hot and cold thermal discomfort. A time-dependent one-dimensional heat conduction code, which uses the effective specific heat method to simulate the heat transfer through the PCM was developed. Insights into the effects of the hysteresis phenomenon were obtained, it was found that hysteresis improves the thermal performance of PCM-walls. The higher the hysteresis temperature difference the better the thermal performance, but there is a limit in the improvement of the thermal performance, which is achieved when the entire phase change process take place at temperatures outside of the thermal comfort zone. Maximum improvements from 4% to 29% for air-conditioning and from 4% to 30% for non-air-conditioning, for a BioPCM wall with thicknesses from 6 mm to 18 mm, were found. Suggested criteria to achieve the maximum possible thermal performance of PCM-walls given a thickness and use condition were obtained. This work proposes the basis of a methodology to optimize simultaneously any pair of variables of a PCM-wall for different use conditions (AC, nAC, or a combined use of AC and nAC).

Keywords: thermal performance; time-dependent; PCM-wall; hysteresis; optimization

List of symbols

AC	air-conditioning
c	specific heat ($\mathrm{J{\cdot}kg^{-1}{\cdot}{^\circ}C^{-1}}$)
c_{eff}	effective specific heat ($\mathrm{J{\cdot}kg^{-1}{\cdot}{^\circ}C^{-1}}$)
CL	cooling load ($\mathrm{W{\cdot}h{\cdot}m^{-2}}$)
d	the distance from the indoor surface where the heat transfer is supposed to be zero (m)
DDH_{hot}	hot discomfort degree hours (°C·h)
DDH_{cold}	cold discomfort degree hours (°C·h)
e	thickness (mm)
h	specific enthalpy ($\mathrm{J{\cdot}kg^{-1}}$)
HL	heating load ($\mathrm{W{\cdot}h{\cdot}m^{-2}}$)
k	thermal conductivity ($\mathrm{W{\cdot}m^{-1}{\cdot}K^{-1}}$)
L	phase change enthalpy per volume ($\mathrm{J{\cdot}kg^{-1}}$)
LTPZ	limit thermal performance zone
MAPE	mean absolute percentage error (%)
MPE	absolute percentage error (%)
nAC	non-air-conditioning
q_{is}	heat flux across the indoor surface ($\mathrm{W{\cdot}m^{-2}}$)
q_{os}	heat flux across the outdoor surface ($\mathrm{W{\cdot}m^{-2}}$)
PCM	phase change material
t	time (s)
T	temperature (°C)
T_a	outdoor air temperature (°C)
T_c	comfort temperature (°C)
T_f	peak freezing temperature (°C)
T_{fe}	freezing ending temperature (°C)
T_{fo}	freezing onset temperature (°C)
T_i	indoor air temperature (°C)
T_{is}	temperature at the indoor surface (°C)
T_m	peak melting temperature (°C)
T_{me}	melting ending temperature (°C)
T_{mo}	melting onset temperature (°C)
T_{os}	temperature at the outdoor surface (°C)
T_{sa}	sol-air temperature (°C)
TCZ	thermal comfort zone
TPEP	thermal performance evaluation parameter
x	space (m)

α	the difference between T_{mo} and T_f (°C)
β	the difference between T_f and T_{fo} (°C)
Γ	the limit for which the entire melting process takes place above the corresponding thermal comfort limit (°C)
ΔH	hysteresis temperature difference (°C)
ΔT_c	half of the amplitude of TCZ (°C)
μ_i	indoor film coefficient ($W \cdot m^{-2} \cdot K^{-1}$)
μ_o	outdoor film coefficient ($W \cdot m^{-2} \cdot K^{-1}$)
ρ	density ($kg \cdot m^{-3}$)
Ψ	fraction of the liquid phase
Ω	the limit for which the entire freezing process takes place below the corresponding thermal comfort limit (°C)
Subscripts	
a	air
Superscripts	
new	current time step
old	previous time step

7.1 Introduction

Worldwide the use of energy in buildings (residential, commercial, and public) represents the largest energy-consuming sector in the economy (with 35% of the final consumption). The use of fossil fuels as the main source of energy production has led a progressive increase in the levels of atmospheric CO_2, being the buildings responsible for approximately one-third of these emissions (IEA, 2013). It is therefore necessary to develop and implement building technologies to reduce both energy consumption and CO_2 emissions.

A key component in buildings to reduce their energy consumption and improve their thermal performance is the envelope (IEA, 2013; Kośny, 2015; Akeiber et al., 2016). Recently, the latent heat energy storage through the use of phase change materials (PCMs) placed in the building envelope has become an interesting alternative to achieve these goals (Kośny, 2015; Lee et al., 2015; Akeiber et al., 2016; Lei et al., 2016; Ramakrishnan et al., 2017; Soares et al., 2017).

A successful implementation of PCMs requires that their melting temperature, thickness, and location within the constructive system are selected according to the climate and use condition (air-conditioning or non-air-conditioning). Several works have studied the thermal performance of specific PCM-constructive-systems and have found optimal values of melting temperature (Neeper, 2000; Heim and Clarke, 2004; Zhou et al., 2007; Jiang et al., 2011; Moreles and Huelsz, 2015b), thickness (Chen et al., 2008), location (Halford and Boehm, 2007; Jin et al., 2013) and melting temperature and thickness (Peippo et al., 1991; Stritih

and Novak, 1996; Soares et al., 2014; Ascione et al., 2014). However, an important feature of PCMs, the thermal hysteresis phenomenon, has hardly been studied and included in building thermal simulations.

Kuznik and Virgone (2009), Gowreesunker et al. (2012), and Gowreesunker and Tassou (2013) showed the importance of considering hysteresis in the numerical simulations to describe accurately the temperature evolution of PCMs. Moreles and Huelsz (2015a) studied the heat conduction through a PCM-wall subjected to variations in the hysteresis temperature difference (the difference between the peak melting and freezing temperatures) of 10.0°C and found differences of up to 12°C in short periods and 4°C for longer periods in the indoor surface temperature. Nonetheless, there are no research concerning the effects of the hysteresis temperature difference on the thermal performance of PCM-walls, nor how it modifies the selection of optimal thermophysical properties for different use conditions.

Therefore, the main aim of this paper is to numerically study the combined effects of the hysteresis temperature difference, peak melting temperature, and thickness of a building envelope PCM-wall on its thermal performance. The second aim of this paper is to propose the basis of a methodology to select optimal values of hysteresis temperature difference, peak melting temperature, and thickness for the air-conditioning and non-air-conditioning use conditions. The analysis was carried out using a time-dependent model, considering complete melting-freezing daily cycles of the PCM in a climate exhibiting both hot and cold thermal discomfort. Also, in order to develop a numerical code that can be integrated into other building energy simulation programs (EnergyPlus or Ener-Habitat), the analysis was carried out in a one-dimensional approach.

From this work a comprehensive analysis of the thermal performance of PCM-walls was carried out and an optimization procedure was developed. Also, criteria to achieve the maximum possible thermal performance of PCM-walls and some topics for future work were suggested.

7.2 Methodology

This section describes the model developed to simulate the heat transfer through PCMs, the characteristics of the simulated PCM constructive system, and the proposed methodology to study its thermal performance.

This work focuses on studying the hysteresis phenomenon and its effects on the thermal performance of PCM-walls. Other phenomena related to the study of PCM-walls and that can affect their behavior, e.g., convection and sub-cooling, were not addressed. The objective is to separate the hysteresis effects from the effects of other phenomena and provide results only related to the hysteresis phenomenon.

7.2.1 Mathematical model

A scheme of the one-dimensional heat transfer through a PCM-wall is shown in Figure 7.1. T_{sa} is the sol-air temperature (ASHRAE, 2005), which represents the outdoor conditions, T_i is the indoor air temperature, T_{os} is the temperature at the outdoor surface of the PCM-wall, T_{is} is the temperature at the indoor surface of the PCM-wall, and d is a distance measured from the indoor surface to the indoor space at which the heat transfer is supposed to be zero. When evaluating a wall, d is the distance at which an adiabatic or a symmetry condition is assumed, the center of the room (Barrios et al., 2016).

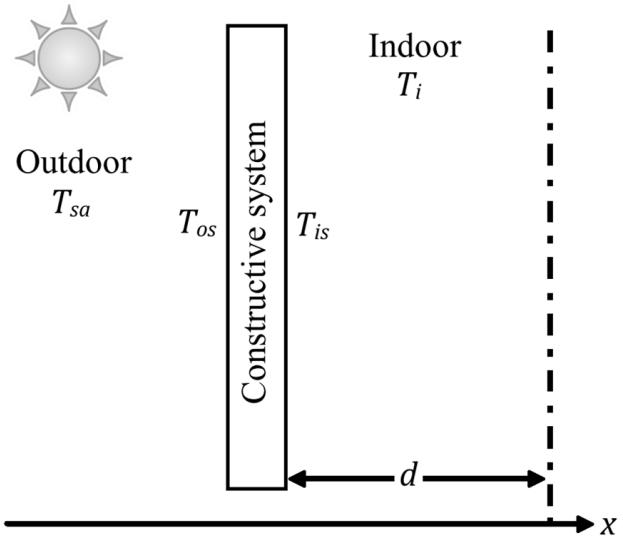

Figure 7.1: Scheme of heat transfer through the building envelope. T_{sa} is the sol-air temperature, T_i is the indoor air temperature, T_{os} is the temperature at the outdoor surface, T_{is} is the temperature at the indoor surface, x is the spatial coordinate, and d is a distance measured from the indoor surface to the indoor space at which the heat transfer is supposed to be zero.

In order to address the problem described above, the time-dependent one-dimensional heat equation for the PCM-wall was considered using the effective specific heat method. This method addresses the solidification/melting of multicomponent systems which solidify in a temperature interval leading to a spatial mushy region between solid and liquid phases. This method expresses the heat transfer only as a function of the PCM temperature grouping the non-linear latent and specific heat effects in a single term, the effective specific heat, c_{eff}. Its formulation is (Samarskii and Vabishchevich, 1995)

$$\rho\, c_{eff} \frac{\partial T}{\partial t} = \operatorname{div}\left(k \operatorname{grad} T\right), \tag{7.1}$$

where T is the temperature as function of time, t, and space, x, ρ is the density, and k is the thermal conductivity. The key in this method lies in the expression of the c_{eff} function,

which is usually obtained from testing data with calorimetric methods or using analytical or numerical approximations (AL-Saadi and Zhai, 2013).

In this work the boundary conditions were specified via the heat flux across the outdoor surface, q_{os}, and the heat flux across the indoor surface, q_{is}. At the outdoor surface, os, and at the indoor surface, is, these conditions are:

$$q_{os} = -k\frac{\partial T}{\partial x}\bigg|_{os} = \mu_o \left(T_{sa} - T_{os}\right), \tag{7.2}$$

$$q_{is} = -k\frac{\partial T}{\partial x}\bigg|_{is} = \mu_i \left(T_{is} - T_i\right), \tag{7.3}$$

where $\mu_o = 13.0\,\mathrm{W{\cdot}m^{-2}{\cdot}K^{-1}}$ and $\mu_i = 8.1\,\mathrm{W{\cdot}m^{-2}{\cdot}K^{-1}}$ are the outdoor and indoor film coefficients, respectively, which were taken from the Mexican official standard NOM-ENER-020-2011 (SENER, 2011).

The specification of T_{sa} and T_i in Equations (7.2) and (7.3) was made according to the following procedure. T_{sa} was specified using mean climate variables as described in Section 7.2.4, whereas T_i was calculated according to two use conditions: the non-air-conditioning (nAC) condition and the air-conditioning (AC) condition.

For the nAC condition it was considered that the rate of change of the energy of the indoor air is equal to the heat flux across the indoor surface. Using Equation (7.3) this is expressed as

$$d\rho_a c_a \frac{dT_i}{dt} = \mu_i \left(T_{is} - T_i\right), \tag{7.4}$$

where ρ_a is the density of the air and c_a is the specific heat of the air.

For the AC condition an air-conditioning system of the energy saving type was chosen. If T_i is within the thermal comfort zone (TCZ) the air-conditioning is turned off and T_i is calculated according to Equation (7.4). If T_i is greater than the upper limit of the TCZ the air-conditioning cools the space with the upper limit of the TCZ as the setpoint. If T_i is below the lower limit of the TCZ then the air-conditioning heats the space with the lower limit of the TCZ as the setpoint.

The following assumptions were taken into account in the model formulation: *i*) the solid and liquid phases of the PCM are homogeneous and isotropic with constant thermophysical properties, *ii*) indoor air perfectly mixed, so T_i is homogeneous, *iii*) the heat transfer between the surrounding media and the PCM-wall is instantaneous *iv*) there are no internal heat gains or infiltration, and *v*) the air-conditioning system can supply any amount of cooling or heating load. Finally, according to Barrios et al. (2016) a value of 2.5 m for the distance d was considered.

7.2.2 Numerical model

The model discretization was made using a control-volume formulation. In this formulation the domain is discretized using several grid points, with nonoverlapping control volumes surrounding the grid points, and with the temperature specified at each grid point. Alike the space discretization, the temperature is calculated in discrete time intervals. Then, Equation (7.1) is integrated over each control volume and the discretization equations are obtained. The most attractive attribute of this formulation is that the energy conservation principle holds for every control volume and for any number of grid points (Patankar, 1980).

The grid considered for the PCM-wall is shown in Figure 7.2. The PCM-wall was discretized in $Nx - 1$ complete control volumes and two half control volumes adjacent to the boundaries, which are denoted by the points 0 and Nx. Each complete control volume i has a length $(\delta x_l)_i + (\delta x_r)_i$ and the interfaces between the control volumes are specified by s_i.

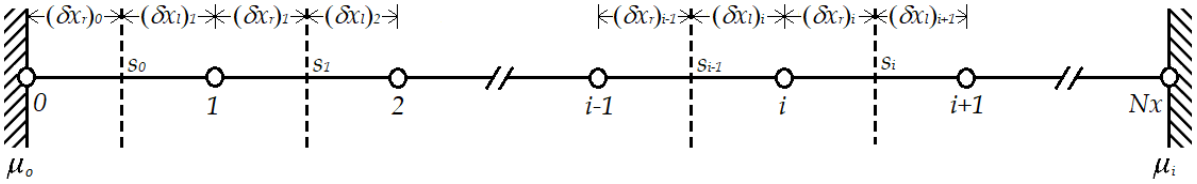

Figure 7.2: Grid considered for the PCM-wall. Each control volume i has a length $(\delta x_l)_i + (\delta x_r)_i$ and the interfaces between the control volumes are specified by s_i. The outdoor and indoor surface nodes are denoted by 0 and Nx, respectively. The outdoor and indoor film coefficients are μ_o and μ_i, respectively.

The discretization equations were obtained considering a fully implicit scheme and were solved using an iterative scheme with a particular form of the Gaussian-elimination method (the TriDiagonal-Matrix Algorithm) as explained by Patankar (1980). Detailed calculation of these procedures can be found in Section 3.3.

In this work the c_{eff} function was calculated using a numerical approximation. From a provided specific enthalpy curve, $h\,(T)$, c_{eff} was calculated using a temporal averaging proposed by Morgan et al. (1978),

$$c_{eff} = \frac{h\,(T^{new}) - h\left(T^{old}\right)}{T^{new} - T^{old}}, \tag{7.5}$$

where *new* represents the current time step and *old* represents the previous time step in iterative schemes.

Moreover, a T_{sa} function with daily periodicity was used. Then simulations were carried out for a day and the numerical code was iterated until obtaining periodic solutions of T and T_i, i.e., until the difference in the temperature values of each node of the PCM-wall for $t = 0$ h and $t = 24$ h was less than a tolerance value, ζ[1]. The periodicity of the solutions

[1]In this work a tolerance value $\zeta = 0.0001$°C was considered.

implies that the energy absorbed by the indoor air is equal to the energy released by it for the 24 hours period.

According to the above description, for this model the input data for the properties of PCMs are the enthalpy curves, density, specific heat in solid and liquid phases, thermal conductivity, and thickness. The validation of the numerical code is shown in Appendix 7.5.

7.2.3 Selected PCM and constructive system

The use of PCMs into building envelopes as a component in constructive systems (not PCMs incorporated into the construction materials by direct incorporation, immersion, or microencapsulation), e.g., using sheets of macro-encapsulated PCM pouches or PCM panels, represents a promising use of the phase change technology as the PCMs are low cost and easy to install, specially for retrofitting purposes (Sage-Lauck and Sailor, 2014). A PCM of this kind that exhibits hysteresis is BioPCM, which was considered in this work.

There are very limited data concerning the hysteresis of commercial PCMs and consequently of their melting and freezing enthalpy curves. Energain is one of the few PCMs whose melting and freezing enthalpy curves have been reported (Kuznik and Virgone, 2009). However, its phase change interval is wide (of about 20°C) and it may not complete melting-freezing cycles by increasing the hysteresis temperature difference at a certain level (see Subsection 7.2.6), which is an aim of this paper. In contrast, BioPCM has a less wide phase change interval and it is useful for the analysis proposed in this paper (see Subsections 7.2.5 and 7.2.6).

BioPCM is an organic based PCM in the form of a gel contained within a multitude of pouches (40 mm × 45 mm base and 20 mm-thick) in a flexible roll of plastic film (BioPCM). Because BioPCM is not packaged as a continuous layer, the manufacturer (BioPCM) proposed an effective thickness $e = 6$ mm in order to consider it as a continuous layer and be able to simulate it using a one-dimensional approach. Hereinafter the effective thickness will be referred to as thickness. Table 7.1 shows the thermophysical properties of BioPCM. The curves of h and c_{eff} (calculated as dh/dT) of BioPCM for the melting process are shown in Figure 7.3. The peak melting temperature is $T_m = 28.2$°C, the phase change onset temperature is 26.0°C, and the phase change ending temperature is 31.0°C.

Numerical studies of the thermal performance of BioPCM, without considering internal convection in the liquid phase or sub-cooling, and the corresponding experimental validation have been carried out by Sage-Lauck and Sailor (2014) and Muruganantham (2010). Due to the fact that there is no clear information concerning the freezing curve of BioPCM, certain assumptions had to be done to construct it and be able to study the hysteresis phenomenon (Subsection 7.2.5).

In this work it was considered the PMC as the only component of the wall. Strictly, BioPCM cannot be used directly as the only component of the constructive system due to its lack of rigidity, however it can be placed between two thin metal plates to obtain a rigid constructive system. Such a constructive system has practically the same thermal performance as that of the BioPCM due to the low thermal mass and thermal resistance of

the thin metal plates.

Table 7.1: Thermophysical properties of BioPCM. k is the thermal conductivity, ρ is the density, c is the specific heat, L is the phase change enthalpy per volume, and e is the thickness.

k	ρ	c frozen	c melted	L	e
$[\mathrm{W{\cdot}m^{-1}{\cdot}K^{-1}}]$	$[\mathrm{kg{\cdot}m^{-3}}]$	$[\mathrm{J{\cdot}kg^{-1}{\cdot}{^\circ}C^{-1}}]$	$[\mathrm{J{\cdot}kg^{-1}{\cdot}{^\circ}C^{-1}}]$	$[\mathrm{J{\cdot}kg^{-1}}]$	[mm]
0.2	860.0	1620.0	1620.0	205127.0	6

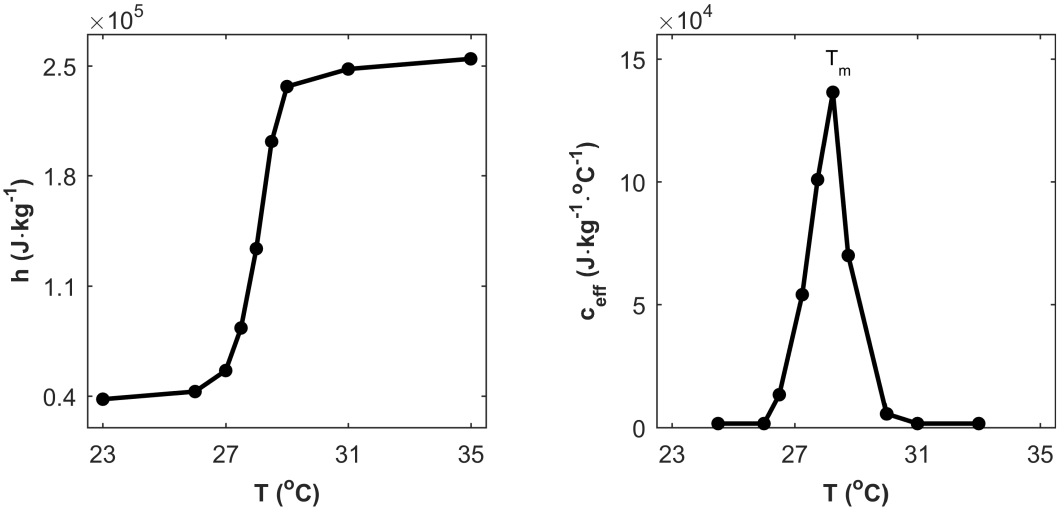

Figure 7.3: Specific enthalpy, h, and effective specific heat, c_{eff}, curves of BioPCM for the melting process as functions of temperature, T. T_m is the peak melting temperature

.

7.2.4 Simulated climate

A climate exhibiting hot and cold thermal discomfort during the day was considered, Nogales, Sonora, Mexico (31°19′N, 110°56′W, 1199 m altitude) in April. The climate conditions for this month were represented by T_{sa} for the typical day of April. A periodic function of the outdoor air temperature, T_a, was constructed using the methodology proposed by Chow and Levermore (2007). Then, using the maximum and minimum values of T_a, the time when they occur, and the daily average of the incident solar radiation over the surface, T_{sa} was calculated. These values were obtained from a typical year using Meteonorm.

A west facing wall was selected because this one exhibits the highest and lowest values of T_{sa} respect to those of north, south, and east orientations. A wall with a solar absorptivity of 0.4 (light color) was considered. T_{sa}, T_a, the comfort temperature, T_c, the upper limit

of the TCZ, $T_c + \Delta T_c$, and the lower limit of the TCZ, $T_c - \Delta T_c$, for this wall and climate are shown in Figure 7.4. T_c (= 23.1°C) was calculated as proposed by Humphreys and Nicol (2000) and ΔT_c (= 2.2°C) was calculated as proposed by Morillón-Gálvez et al. (2004).

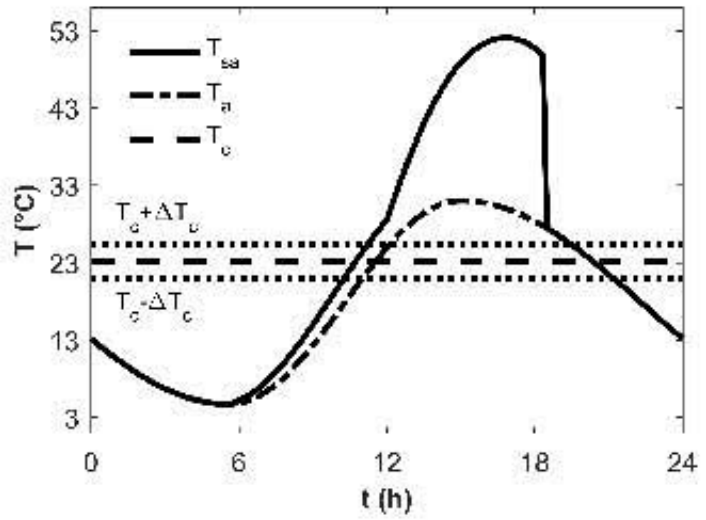

Figure 7.4: Temperature variables (the sol-air temperature, T_{sa}, the outdoor air temperature, T_a, the comfort temperature, T_c, the upper limit of the thermal comfort zone, $T_c + \Delta T_c$, and the lower limit of the thermal comfort zone, $T_c - \Delta T_c$) as functions of time, t, in Nogales, Sonora in April for a west facing wall with a solar absorptivity of 0.4.

7.2.5 Hysteresis simulation

To simulate hysteresis both melting and freezing enthalpy curves have to be considered. Experiments carried out by J. Belaunzarán Zamudio (2015), Delcroix et al. (2015a) and Delcroix et al. (2015b) shown that BioPCM exhibits hysteresis, however there is no clear information concerning its freezing curve. Therefore, in order to study the effects of the hysteresis temperature difference, the freezing curve had to be constructed hypothetically. According to Bony and Citherlet (2007), the freezing curve was constructed by means of a shifting the melting curve to a lower temperature according to a hysteresis temperature difference value, ΔH,

$$\Delta H = T_m - T_f, \tag{7.6}$$

where T_f is the peak freezing temperature. Figure 7.5 shows an example of a freezing curve constructed with the aforementioned methodology. In this figure T_{mo} is the melting onset temperature, T_{me} is the melting ending temperature, T_{fo} is the freezing onset temperature, and T_{fe} is the freezing ending temperature. Two important parameters are the difference

between the onset of melting and the peak melting temperature, α, and the difference between the peak freezing temperature and the onset of freezing, β,

$$\alpha = T_m - T_{mo}, \tag{7.7}$$

$$\beta = T_{fo} - T_f. \tag{7.8}$$

The parameters α and β are intrinsic properties of a particular PCM. According to the proposed methodology to construct freezing curves, for BioPCM $\alpha = 2.2$°C and $\beta = 2.8$°C.

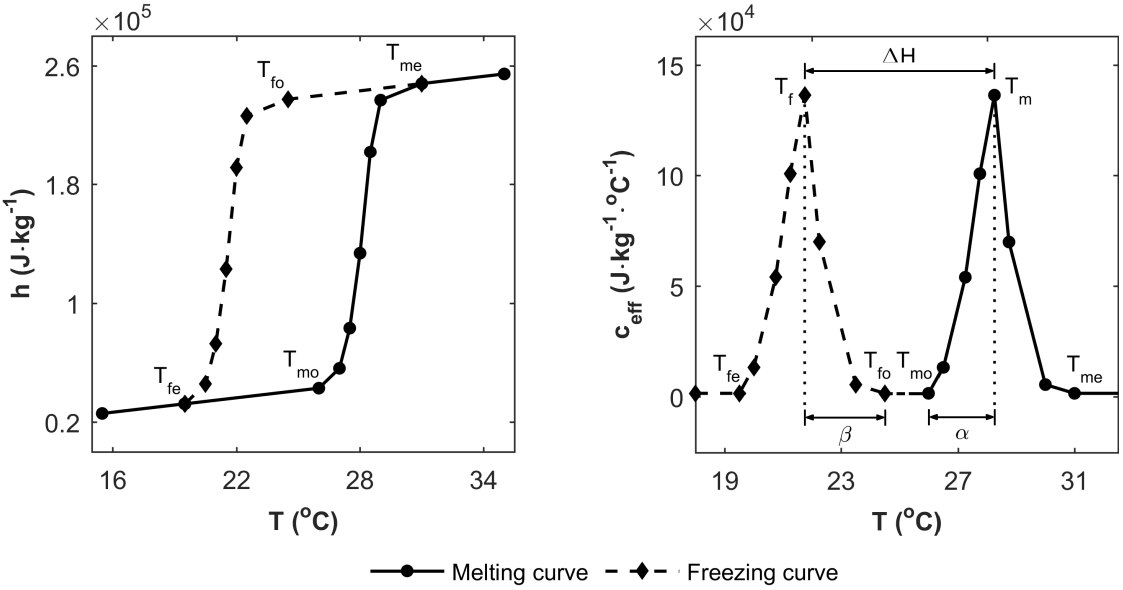

Figure 7.5: Specific enthalpy, h, and effective specific heat, c_{eff}, curves of BioPCM for the melting and freezing processes as functions of temperature, T. ΔH is the hysteresis temperature difference, T_{mo} is the melting onset temperature, T_{me} is the melting ending temperature, T_{fo} is the freezing onset temperature, T_{fe} is the freezing ending temperature, T_m is the peak melting temperature, T_f is the peak freezing temperature, $\alpha = T_m - T_{mo}$, and $\beta = T_{fo} - T_f$.

7.2.6 Study cases

In order to analyze the effects of the hysteresis phenomenon, a wide range of values of ΔH, from 0.0°C (no hysteresis) to 30.0°C, was considered. The study cases analyzed in this work were a west facing wall in Nogales, Sonora for the typical day of April under AC and nAC condition, considering six thicknesses ($e =$ 6 mm, 9 mm, 12 mm, 15 mm, 18 mm, and 21 mm), and ΔH from 0.0°C to 30.0°C. The space of simulated temperatures is shown in Figure 7.6. The ΔH values, with increments of 0.8°C, are represented in gray scale (in color scale online), the vertical axis represents T_m, and the horizontal axis represents T_f. From the

line representing the cases with no hysteresis ($\Delta H = 0.0$°C), ΔH increases as T_f decreases and T_m increases.

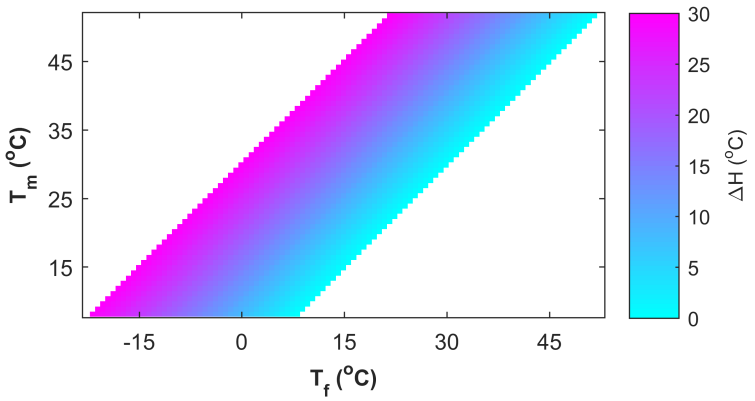

Figure 7.6: Space of simulated temperatures, where the hysteresis temperature difference, ΔH, is represented in gray scale (in color scale online). T_m is the peak melting temperature and T_f is the peak freezing temperature. From the line $\Delta H = 0.0$°C, ΔH increases as T_f decreases and T_m increases.

As reported by Sage-Lauck and Sailor (2014), Lee et al. (2015) and Lei et al. (2016), to fully utilize the latent heat storage of a PCM, it has to complete melting-freezing daily cycles. Therefore, in this work to evaluate the thermal performance of the PCM-wall only the cases that fulfill the criterion of complete melting-freezing daily cycles were considered. A necessary but not sufficient condition for the PCM to complete daily melting-freezing cycles, is that $T_{sa_{max}} > T_{me}$ and $T_{sa_{min}} < T_{fe}$, where $T_{sa_{max}}$ and $T_{sa_{min}}$ are the maximum and minimum values of T_{sa}, respectively. The duration of periods when T_{sa} is close to its maximum value and its minimum value and the PCM thickness also play a role on this.

The process followed for the construction of the freezing enthalpy curve by means of a shifting of the melting enthalpy curve, in combination with the conditions of periodic solutions of T and T_i and complete melting-freezing daily cycles, implies that the energy absorbed by each of the control volumes of the PCM-wall (see Figure 7.2) is equal to the energy released by them for the 24 hours period, thus, the daily energy flux at each of the interfaces of the control volumes and at the outdoor and indoor surfaces is equal to zero.

7.2.7 Thermal performance evaluation parameters

A common thermal performance parameter for the AC condition is the energy per unit area consumed in a day to maintain T_i within the TCZ (the cooling load, CL, when $T_i > T_c + \Delta T_c$ and the heating load, HL, when $T_i < T_c - \Delta T_c$). For the nAC condition a useful parameter is the duration and intensity of T_i when it is outside the TCZ during a day (the hot discomfort degree hours, DDH_{hot}, when $T_i > T_c + \Delta T_c$ and the cold discomfort degree hours, DDH_{cold}, when $T_i < T_c - \Delta T_c$) (Barrios et al., 2012).

The parameters for hot thermal discomfort are CL and DDH_{hot}, where the relevant thermal comfort limit is the upper limit of the TCZ, $T_c + \Delta T_c$; whereas the parameters for cold thermal discomfort are HL and DDH_{cold}, where the relevant thermal comfort limit is the lower limit of the TCZ, $T_c - \Delta T_c$. Each of these parameters will be referred to as a Thermal Performance Evaluation Parameter (hereinafter TPEP). The smaller the TPEP values the better the thermal performance.

7.3 Results and discussion

This section shows the results of the thermal performance evaluation of the PCM-wall for each of the study cases.

The TPEP values for each of the study cases in the space of simulated temperatures are shown in Figure 7.7. The TPEP values are represented in gray scale (in color scale online), the vertical axis represents T_m, the horizontal axis represents T_f, and the dotted lines indicate the corresponding thermal comfort limit for each TPEP ($T_c + \Delta T_c$ for CL and DDH_{hot} and $T_c - \Delta T_c$ for HL and DDH_{cold}). Figure 7.7 shows the generated spaces of temperatures for the cases that fulfill the criterion of complete melting-freezing cycles, which are isosceles right triangles with the corresponding 45° slope line passing through the origin of the coordinate system $T_f - T_m$ as the hypotenuse. Due to the calculation of T_i in the AC condition, the space of temperatures that meet the condition of complete melting-freezing cycles in the AC condition is smaller than in the nAC condition. In order to obtain the TPEP values in the rest of space of simulated temperatures (Figure 7.6) it is necessary to assume a hysteresis model for the incomplete melting-freezing cycles, which is matter of future research; that is the reason why the TPEP values in this zone are not shown.

From Figure 7.7 it can be seen that the selection of T_m and T_f has a great effect on the thermal performance. Significant variations of the maximum value of the TPEP with respect to the corresponding minimum value were found: for the AC condition variations of $113\,\mathrm{W{\cdot}h{\cdot}m^{-2}}$ (25%) for $e_1 = 6$ mm and variations of $112\,\mathrm{W{\cdot}h{\cdot}m^{-2}}$ (242%) for $e_6 = 21$ mm in HL were found; whereas for the nAC condition variations of 26°C·h (25%) for $e_1 = 6$ mm and variations of 35°C·h (577%) for $e_6 = 21$ mm in DDH_{cold} were found. The dimensional difference was calculated as the difference between the maximum value of the TPEP and the corresponding minimum value; whereas the percentage difference was calculated as the dimensional difference divided by the minimum TPEP value and expressed in percentage form.

Also, Figure 7.7 shows that hysteresis improves the thermal performance of the PCM-wall: the minimum value of the TPEP for each ΔH decreases as ΔH increases. However, there is a limit on the thermal performance achievable by the PCM-wall, when conjointly $T_m \geq \Gamma$ and $T_f \leq \Omega$ the TPEP values will no longer change and will have the same value, defined as its limit minimum value. Γ indicates the limit for which the entire melting process takes place above the corresponding thermal comfort limit, i.e., when

$$T_{mo} \geq \begin{cases} T_c + \Delta T_c & \text{for } CL \text{ and } DDH_{hot}, \\ T_c - \Delta T_c & \text{for } HL \text{ and } DDH_{cold}. \end{cases} \tag{7.9}$$

Ω indicates the limit for which the entire freezing process takes place below the corresponding thermal comfort limit, i.e., when

$$T_{fo} \leq \begin{cases} T_c + \Delta T_c & \text{for } CL \text{ and } DDH_{hot}, \\ T_c - \Delta T_c & \text{for } HL \text{ and } DDH_{cold}. \end{cases} \tag{7.10}$$

From Equations (7.7), (7.8), (7.9), and (7.10), Γ and Ω are specified by the following relationships, in which the values of Γ and Ω for the analyzed situation are also indicated,

$$\Gamma = \begin{cases} (T_c + \Delta T_c) + \alpha = 27.6°\text{C} & \text{for } CL \text{ and } DDH_{hot} \\ (T_c - \Delta T_c) + \alpha = 23.1°\text{C} & \text{for } HL \text{ and } DDH_{cold} \end{cases} \tag{7.11}$$

$$\Omega = \begin{cases} (T_c + \Delta T_c) - \beta = 22.6°\text{C} & \text{for } CL \text{ and } DDH_{hot} \\ (T_c - \Delta T_c) - \beta = 18.1°\text{C} & \text{for } HL \text{ and } DDH_{cold} \end{cases} \tag{7.12}$$

The zone that defines the region where the limit minimum value in the thermal performance is located will be referred hereinafter as the limit thermal performance zone, LTPZ, which satisfies

$$T_m \geq \Gamma \text{ and } T_f \leq \Omega. \tag{7.13}$$

Equation defining the LTPZ (Equation (7.13)) is valid only if the condition of daily complete melting-freezing cycles is fulfilled. Figure 7.7 shows that as the thickness increases the number of cases that fulfill the criterion of complete melting-freezing cycles is reduced, and then for the larger thicknesses ($e \geq 21$ mm for CL, $e \geq 15$ mm for HL, $e \geq 21$ mm for DDH_{hot}, and $e \geq 18$ mm for DDH_{cold}) the limit minimum value in the thermal performance cannot be calculated and consequently the LTPZ cannot be defined.

In order to quantify the improvement of the thermal performance by hysteresis for a given thickness, Table 7.2 shows the dimensional and percentage differences of the minimum value of the TPEP for $\Delta H = 0.0°$C with respect to its corresponding limit minimum value, which is reached at $\Delta H = 5.0°$C for all the cases. The dimensional difference was calculated as the difference between the minimum value of the TPEP for $\Delta H = 0.0°$C and the limit minimum value; whereas the percentage difference was calculated as the dimensional difference divided by the limit minimum value and expressed in percentage form. It is observed that hysteresis improves the thermal performance of the PCM-wall from 4% for $e = 6$ mm to 29% for $e = 18$ mm in CL for the AC condition; whereas in the nAC condition the improvement is from 4% for $e = 6$ mm to 30% for $e = 18$ mm in DDH_{hot}.

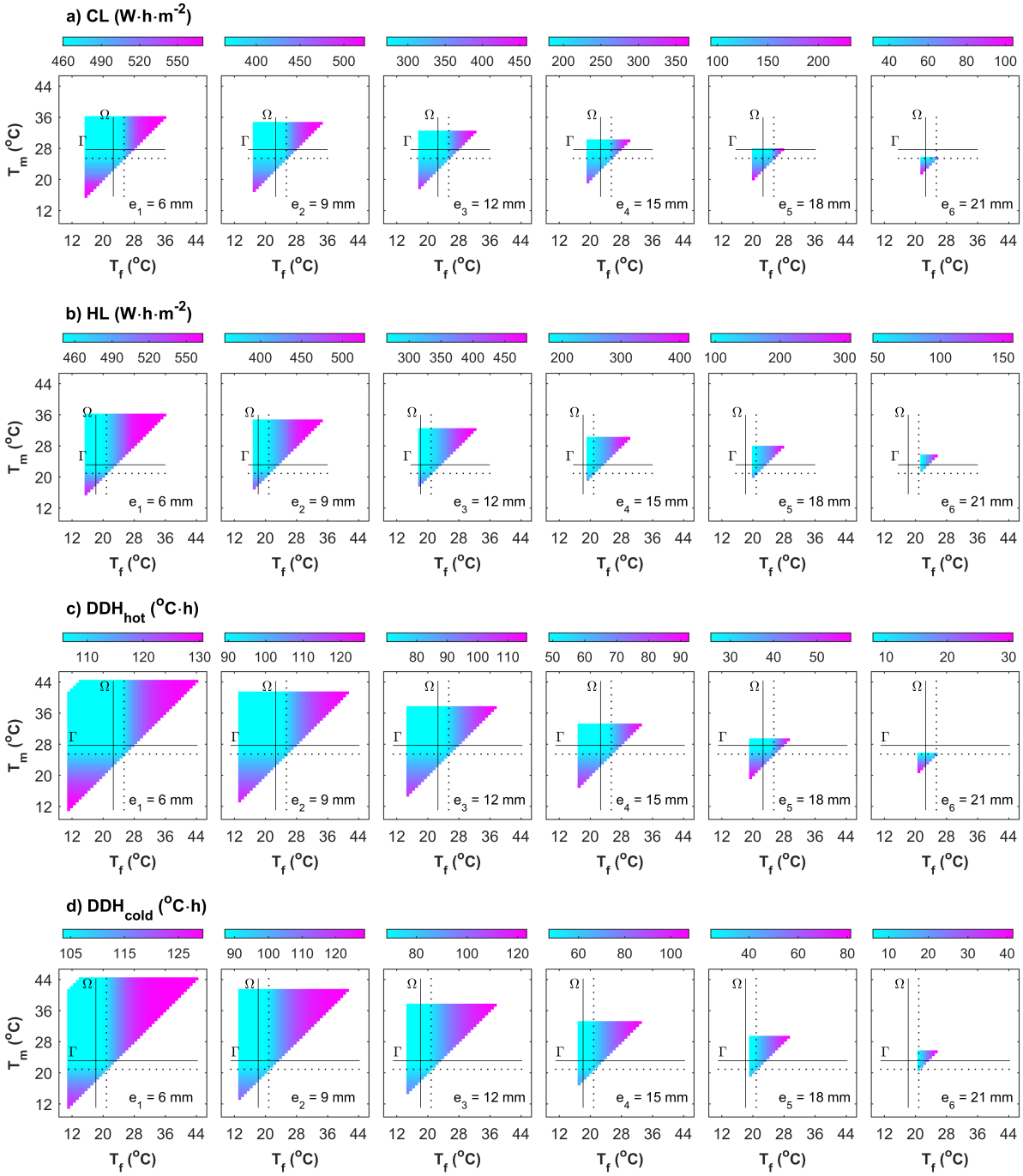

Figure 7.7: Thermal performance of the PCM-wall. The TPEP values (a) for CL, b) for HL, c) for DDH_{hot}, and d) for DDH_{cold}) are represented in gray scale (in color scale online), T_m is the peak melting temperature, T_f is the peak freezing temperature, e is the thickness, the dotted lines indicate the corresponding thermal comfort limit for each TPEP, the horizontal black solid lines indicate the limit for which the entire melting process takes place above the corresponding thermal comfort limit, Γ, and the vertical black solid lines indicate the limit for which the entire freezing process takes place below the corresponding thermal comfort limit, Ω.

Table 7.2: Dimensional and percentage differences of the minimum value of the TPEPs for a null hysteresis temperature difference, $\Delta H = 0.0$°C, with respect to its corresponding limit minimum value for a given thickness. For all the cases the limit minimum value is reached at $\Delta H = 5.0$°C. e is the thickness, CL is the cooling load, HL is the heating load, DDH_{hot} are the hot discomfort degree hours, and DDH_{cold} are the cold discomfort degree hours.

e [mm]	CL [W·h·m^{-2}]	HL [W·h·m^{-2}]	DDH_{hot} [°C·h]	DDH_{cold} [°C·h]
6	19.1 (4%)	25.8 (5%)	4.5 (4%)	4.6 (4%)
9	28.3 (7%)	36.3 (9%)	6.4 (7%)	6.6 (7%)
12	31.6 (10%)	43.4 (14%)	7.9 (10%)	8.5 (11%)
15	34.7 (16%)		9.4 (16%)	10.1 (18%)
18	38.6 (29%)		10.9 (30%)	

The thermal performance patterns of the PCM-wall exhibited in Figure 7.7 are described below. To complement the description of these patterns, Figure 7.8 shows T_{is} as function of t for $e_1 = 6$ mm and different values of T_m and T_f and how they modify the values of CL and HL. The curves in this figure are arranged in increasing order of thermal performance.

1. For a specific T_f and $T_m \geq \Gamma$ (the entire melting process takes place above the corresponding thermal comfort limit), the corresponding TPEP has the same value.

   For example, Figure 7.8a shows that CL has the same value for a specific T_f and $T_m \geq 27.6$°C (dark-gray and dashed curves). The curves of these cases below $T_c + \Delta T_c$ are the same, and thus the energy exiting through the indoor surface is the same. Then, by energy conservation (the daily energy flux must be zero) the energy entering through the indoor surface must be the same, and thus the energy to be removed from the indoor air to set $T_i = T_c + \Delta T_c$, i.e., CL, must be the same.

   In addition, Figure 7.8a shows that HL has the same value for a specific T_f and $T_m \geq 23.1$°C (black, dark-gray, and dashed curves). The curves of these cases below $T_c - \Delta T_c$ are the same, and thus the energy transferred from the indoor air to the indoor surface is the same. Then, the energy to be added to the indoor air to set $T_i = T_c - \Delta T_c$, i.e., HL, is the same.

2. For a specific T_f and $T_m < \Gamma$ (the entire melting process does not take place above the corresponding thermal comfort limit), the corresponding TPEP increases as T_m decreases.

   For example, Figure 7.8a shows that for a specific T_f and $T_m < 27.6$°C, CL increases as T_m decreases (black, light-gray, and dotted curves); whereas that for a specific T_f and $T_m < 23.1$°C, HL increases as T_m decreases (light-gray and dotted curves).

3. For a specific T_m and $T_f \leq \Omega$ (the entire freezing process takes place below the corresponding thermal comfort limit), the corresponding TPEP has the same value.

For example, Figure 7.8b shows that CL has the same value for a specific T_m and $T_f \leq 22.6°C$ (black, dark-gray, and dashed curves). The curves of these cases above $T_c + \Delta T_c$ are the same, and thus the energy transferred from the indoor surface to the indoor air is the same. Then, the energy to be removed from the indoor air to set $T_i = T_c + \Delta T_c$, i.e., CL, is the same.

In addition, Figure 7.8b shows that HL has the same value for a specific T_m and $T_f \leq 18.1°C$ (dark-gray and dashed curves). The curves of these cases above $T_c - \Delta T_c$ are the same, and thus the energy entering through the indoor surface is the same. Then, by energy conservation (the daily energy flux must be zero) the energy exiting through the indoor surface must be the same, and thus the energy to be added to the indoor air to set $T_i = T_c - \Delta T_c$, i.e., HL, must be the same.

4. For a specific T_m and $T_f > \Omega$ (the entire freezing process does not take place below the corresponding thermal comfort limit), the corresponding TPEP increases as T_f increases.

   For example, Figure 7.8b shows that for a specific T_m and $T_f > 22.6°C$, CL increases as T_f increases (light-gray and dotted curves); whereas that for a specific T_m and $T_f > 18.1°C$, HL increases as T_f increases (black, light-gray, and dotted curves).

From the previous analysis, criteria to select an optimal PCM-wall, i.e., criteria to obtain the maximum possible thermal performance, can be derived. If the PCM does not exhibit hysteresis ($T_m = T_f$), the optimal T_m is close to the corresponding thermal comfort limit (Figure 7.7), which agrees with the results of previous research (Heim and Clarke, 2004; Neeper, 2000; Zhou et al., 2007; Jiang et al., 2011; Moreles and Huelsz, 2015b; Peippo et al., 1991; Stritih and Novak, 1996; Soares et al., 2014; Ascione et al., 2014), which optimized T_m without considering hysteresis. On the other hand, if the PCM exhibits hysteresis, the optimal values of T_m and T_f are within the LTPZ (Equation (7.13)).

Despite the TPEP values within the LTPZ are the same (Figure 7.7), Figure 7.8 shows that the highest value of T_m and the lowest value of T_f (dashed curves) are preferred because they prevent abrupt increases in T_{is} and reduce the duration of their higher values when it is above the TCZ, also they prevent abrupt decreases in T_{is} and reduce the duration of their lower values when it is below the TCZ. This observation similarly applies for T_i in the nAC condition.

Figure 7.9 shows the minimum value of the corresponding TPEP for the AC and nAC condition and each thickness considered. As it is expected, the thermal performance is improved by increasing the thickness. The rate of decrease of the TPEP values for all of them has small variations in the range of thicknesses studied. Technically, there is no a clear recommendation for the optimal thickness. Also, there is no a direct correlation between the behavior of the rate of decrease of the TPEP values and the fact that the limit minimum value in the thermal performance is reached.

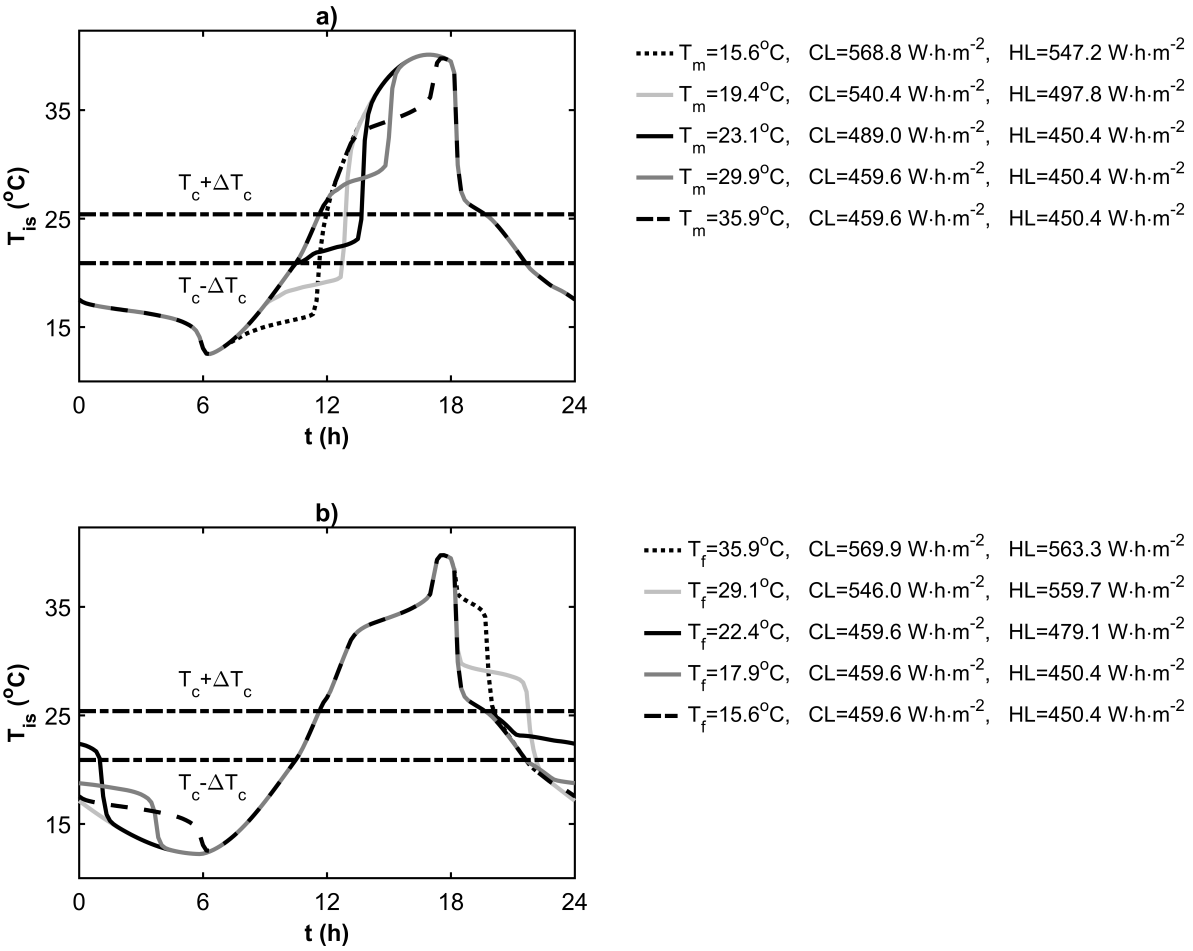

Figure 7.8: Indoor surface temperature, T_{is}, as function of time, t, for the thickness $e_1 = 6$ mm. a) corresponds to a fixed peak freezing temperature $T_f = 15.6$°C and different values of T_m, whereas b) corresponds to a fixed peak melting temperature $T_m = 35.9$°C and different values of T_f. CL is the cooling load, HL is the heating load, T_c is the comfort temperature, and the upper and lower limits of the thermal comfort zone are indicated by dashed-dotted lines.

Based on the results, the following criteria are suggested when selecting a peak melting temperature, a peak freezing temperature, and a hysteresis temperature difference of PCM-walls in order to maximize their thermal performance. These criteria were derived for a given PCM thickness and considering that the PCM completes melting-freezing daily cycles.

- For applications in hot conditions (sol-air temperature predominantly above the thermal comfort zone), select a PCM such that the entire melting process takes place above the upper thermal comfort limit and the entire freezing process takes place below the upper thermal comfort limit, i.e.,

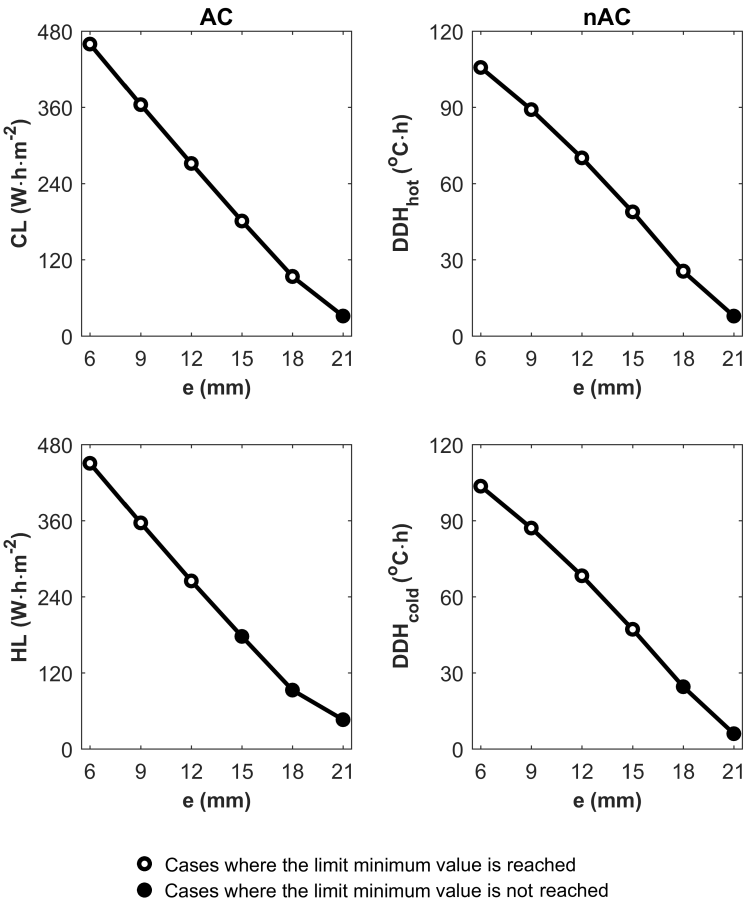

Figure 7.9: Minimum values of the TPEPs for the AC and nAC condition and each thickness, e, considered. CL is the cooling load, HL is the heating load, DDH_{hot} are the hot discomfort degree hours, and DDH_{cold} are the cold discomfort degree hours.

$$T_m \geq (T_c + \Delta T_c) + \alpha, \tag{7.14}$$
$$T_f \leq (T_c + \Delta T_c) - \beta, \tag{7.15}$$

which implies

$$\Delta H = T_m - T_f \geq \alpha + \beta. \tag{7.16}$$

- For applications in cold conditions (sol-air temperature predominantly below the thermal comfort zone), select a PCM such that the entire freezing process takes place below the lower thermal comfort limit and the entire melting process takes place above the lower thermal comfort limit, i.e.,

$$T_m \geq (T_c - \Delta T_c) + \alpha, \tag{7.17}$$
$$T_f \leq (T_c - \Delta T_c) - \beta, \tag{7.18}$$

which implies

$$\Delta H = T_m - T_f \geq \alpha + \beta. \tag{7.19}$$

- For applications in hot and cold conditions (sol-air temperature crossing the thermal comfort zone), select a PCM such that the entire melting process takes place above the upper thermal comfort limit and the entire freezing process takes place below the lower thermal comfort limit. The separation between the melting and freezing processes (the separation between the melting onset temperature and the freezing onset temperature) has to be at least the width of the thermal comfort zone, i.e.,

$$T_m \geq (T_c + \Delta T_c) + \alpha, \tag{7.20}$$
$$T_f \leq (T_c - \Delta T_c) - \beta, \tag{7.21}$$

which implies

$$\Delta H = T_m - T_f \geq \alpha + 2\Delta T_c + \beta. \tag{7.22}$$

- Despite the maximum thermal performance of PCM-walls is achieved with the equality condition in Equations (7.16), (7.19), and (7.22), select a PCM with the highest possible ΔH because it will improve the behavior of T_{is} or T_i for the AC or nAC condition, respectively.

In this work only complete melting-freezing cycles were considered. For future research, to study the behavior of PCMs in partial melting-freezing cycles and its effects on the thermal performance, it is necessary to consider a model to simulate them. There are three models to simulate partial melting-freezing cycles: Chandrasekharan et al. (2013) considered that the PCM follows a specific enthalpy curve (melting or freezing curve) until it melts or freezes completely, then the PCM follows the corresponding enthalpy curve; Bony and Citherlet (2007) proposed a model that considers transitions between the enthalpy curves in partial melting-freezing cycles; whereas Delcroix et al. (2015a) through experimental and numerical studies found that in partial melting-freezing cycles transitions occur and the PCM follows enthalpy curves located between the original ones until the end of phase change. Nevertheless, no conclusive studies have yet been made about an appropriate model to simulate partial melting-freezing cycles in PCMs.

7.4 Conclusions

Hysteresis is an important phenomenon that should be included in simulations to have an accurate description of the thermal performance of building envelopes incorporating phase change materials (PCMs). In this work a numerical code that simulates hysteresis was develop and a comprehensive analysis of the thermal performance of a PCM-wall exposed to outdoor conditions in a climate exhibiting hot and cold climate discomfort was carried out, considering variations in hysteresis temperature difference, ΔH, peak melting temperature, T_m, and thickness, e, for different use conditions (air-conditioning, AC, and non-air-conditioning, nAC). This work only considers the cases that fulfill the criterion of complete melting-freezing daily cycles of the PCM.

From this work insights into the effects of the hysteresis phenomenon were obtained and suggested criteria to maximize the thermal performance of PCM-walls were derived . It was found that hysteresis improves the thermal performance of PCM-walls, the higher the hysteresis temperature difference the better the thermal performance. Additionally, mathematical expressions to select optimal values of the peak melting temperature and the peak freezing temperature were obtained (Equations (7.14)-(7.22)). It was found that there is a limit in the improvement of the thermal performance achievable by a PCM-wall, which is achieved when the entire processes of melting and freezing take place at temperatures outside of the thermal comfort zone (equality condition in Equations (7.16), (7.19), and (7.22)). Increments of the hysteresis temperature difference beyond such condition will not produce a better thermal performance, however, higher values of ΔH prevent abrupt increases or decreases in the indoor surface temperature or in the indoor temperature and reduce the duration of their higher or lower values for the AC or nAC condition, respectively. For the case analyzed in this work (a BioPCM wall) there were found the following improvements in the thermal performance of the PCM-wall by hysteresis: improvements from 4% for $e = 6$ mm to 29% for $e = 18$ mm in the cooling load for the AC condition and improvements from 4% for $e = 6$ mm to 30% for $e = 18$ mm in the hot discomfort degree hours for the nAC condition.

In this work a simultaneous optimization of the peak melting temperature and the peak freezing temperature of a PCM-wall was conducted with the aid of a graphic tool (Figure 7.7). This graphic tool can be used to optimize any pair of variables of a PCM-wall for different use conditions (AC, nAC, or a combined use of AC and nAC). The PCM-wall thermal performance optimization analysis carried out in this work can be enhanced by incorporating the location of the PCM in a multilayered constructive system as a new variable to be optimized and simulations for the whole year (or simulations for the hot or cold season). Thus, the technical aspects of the thermal performance of PCM-walls can be subsequently optimized.

As subject matters of future research it is proposed: *i*) to carry out experiments to determine the hysteresis curves of PCMs and the model that better describes their behavior in partial melting-freezing cycles; *ii*) to perform a similar study to the present, but including partial melting-freezing cycles of PCMs; and *iii*) to perform a holistic optimization analysis for the PCM implementation on building envelopes, i.e., an analysis considering technical,

economic, and environmental aspects.

7.5 Appendix: Validation of the numerical code

The validation of the numerical code was made using a one-dimensional numerical benchmark (Johannes et al., 2011) proposed by the International Energy Agency. In this benchmark the one-dimensional thermal behavior of a building wall containing PCM in time-dependent conditions was simulated by different working groups (groups of France, Norway, and China). Each working group developed a numerical code to this end: the group of France developed a code under TRNSYS software using the effective specific heat method, the group of Norway did not provide details concerning the model they used, whereas the group of China developed a code using the enthalpy method written in FORTRAN.

Nine cases (Table 7.3) were analyzed by all the working groups. The thermal properties of the materials which undergo no phase change are presented in Table 7.4. For the PCM, $\rho = 1100.0\,\mathrm{kg\cdot m^{-3}}$, whereas its values of c_{eff} and k are functions of T (Figure 7.10). In this benchmark the radiative heat transfer was not considered, the indoor and outdoor convection heat transfer coefficients were equal to $2.5\,\mathrm{W\cdot m^{-2}\cdot K^{-1}}$ and $8.0\,\mathrm{W\cdot m^{-2}\cdot K^{-1}}$, respectively, and the indoor air temperature was supposed constant and equal to 20.0°C. The outdoor air temperature varied according to $12.0^\circ\mathrm{C} + 20.0^\circ\mathrm{C/h} \times t$ for $t \leq 1\,\mathrm{h}$ and 32°C for $t > 1\,\mathrm{h}$.

Table 7.3: Cases analyzed in the benchmark carried out by Johannes et al. (2011).

Case	Outdoor layer	Indoor layer
1	5 mm PCM	
2	10 mm PCM	
3	50 mm PCM	
4	30 mm concrete	10 mm PCM
5	10 mm PCM	30 mm concrete
6	200 mm concrete	10 mm PCM
7	10 mm PCM	200 mm concrete
8	100 mm insulation	10 mm PCM
9	10 mm PCM	100 mm insulation

All the cases analyzed in the benchmark were simulated using the numerical code developed in this work[2] and the results were compared with those obtained by the different working groups. Figure 7.11 shows the indoor surface temperature T_{is} as function of time t of the wall for each case obtained with the numerical code developed in this work, by the group of France, and by the group of Norway (the comparison with the group of China was not possible because the temperature values at the indoor surface for different times were

[2] A time-step of 1 min and a grid-size of 0.5 mm were used.

not reported in Johannes et al. (2011)). Figure 7.11 shows that the results of the numerical code developed in this work are in good agreement with those of the benchmark.

Table 7.4: Thermal properties of the materials with no no phase change used in the benchmark carried out by Johannes et al. (2011). k is the thermal conductivity, ρ is the density, and c is the specific heat.

Material	k [W·m^{-1}·K^{-1}]	ρ [kg·m^{-3}]	c [J·kg^{-1}·°C^{-1}]
Concrete	1.2	2000.0	1000.0
Insulation	0.04	50.0	1000.0

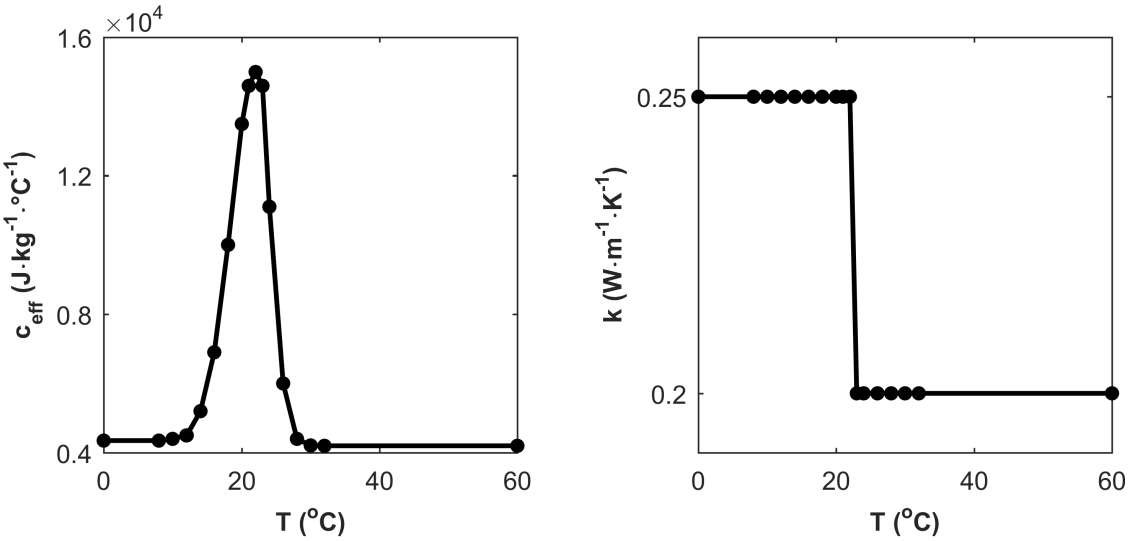

Figure 7.10: Effective specific heat, c_{eff}, and thermal conductivity, k, of the PCM used in the benchmark carried out by Johannes et al. (2011), as functions of temperature, T.

In addition to the qualitative comparison, a quantitative comparison was made in terms of the absolute value of the maximum percentage error, MPE, and the mean absolute percentage error, MAPE. Table 7.5 shows that the maximum differences with the group of France are 10% in the MPE for case 2 and 2% in the MAPE for cases 2 and 3; whereas with the group of Norway the maximum differences are 4% in the MPE for case 4 and 2% in the MAPE for cases 3, 4, 6, and 7.

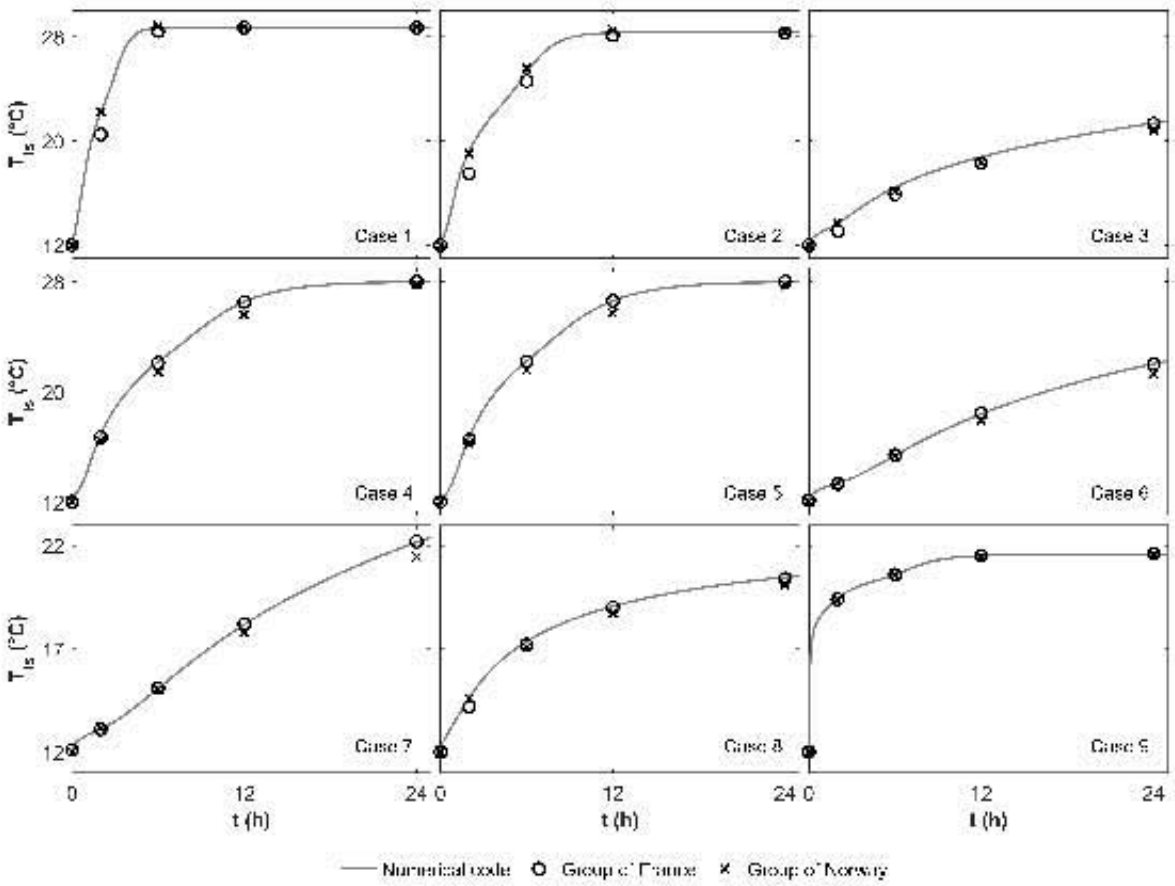

Figure 7.11: Graphical comparison of the results of the numerical code developed in this work with those of the benchmark carried out by Johannes et al. (2011). It is shown the indoor surface temperature, T_{is}, as function of time, t, of the wall for each case obtained with the numerical code developed in this work, by the group of France, and by the group of Norway.

Table 7.5: Quantitative comparison of the results of the numerical code developed in this work with those of the benchmark carried out by Johannes et al. (2011). MPE is the absolute value of the maximum percentage error and MAPE is the mean absolute percentage error.

	France		**Norway**	
Case	**MPE (%)**	**MAPE (%)**	**MPE (%)**	**MAPE (%)**
1	8	1	1	1
2	10	2	1	1
3	4	2	3	2
4	1	1	4	2
5	1	1	3	1
6	1	1	3	2
7	1	1	3	2
8	3	1	2	1
9	1	1	1	1

Chapter 8

Hysteresis models for PCMs

A successful calculation of the thermal performance of a PCM requires accurate values of the stored/released energy by the PCM, which are obtained via the temperature-enthalpy curve. An enthalpy curve can contain a curve for the melting process and other curve for the freezing process (phenomenon known as hysteresis), particularly for organic PCMs (Kośny, 2015). Kuznik and Virgone (2009), Gowreesunker et al. (2012), and Gowreesunker and Tassou (2013) performed numerical simulations of PCMs that exhibit hysteresis and found that the PCM temperature evolution is accurately described by incorporating this phenomenon into the numerical simulations. These studies considered complete melting-freezing cycles, in which the PCM melts following the melting enthalpy curve and freezes following the freezing enthalpy curve.

Nevertheless, little research concerning the PCM behavior in partial melting-freezing cycles has been done and there is no conclusive research of a physical model of the hysteresis phenomenon in PCMs. There are three different models to simulate hysteresis in PCMs: two of them are proposed models to simulate PCMs in general, whereas the third one is derived from experimental and numerical studies for a particular PCM (BioPCM). In order to advance in the study of the hysteresis phenomenon, the objective of this chapter is to contrast the thermal behavior of a PCM-wall in partial melting-freezing cycles considering the three hysteresis models. To do this a numerical analysis was carried out.

8.1 Hysteresis models

In recent years two models to simulate the PCM behavior in partial melting-freezing cycles, considering the hysteresis phenomenon, were proposed. The first one considers that the process returns following the current enthalpy curve until it reaches the solid or liquid phase (Chandrasekharan et al., 2013), in this work this hysteresis model will be referred to as the NT model; whereas the second one considers that the process undergoes transitions between the melting and freezing curves through a straight line with a slope equal to the minimum specific heat in the solid or liquid phases (Bony and Citherlet, 2007; Jaworski et al., 2014),

in this work this hysteresis model will be referred to as the WT model. Figure 8.1 illustrates these models as trajectories in the phase space[1].

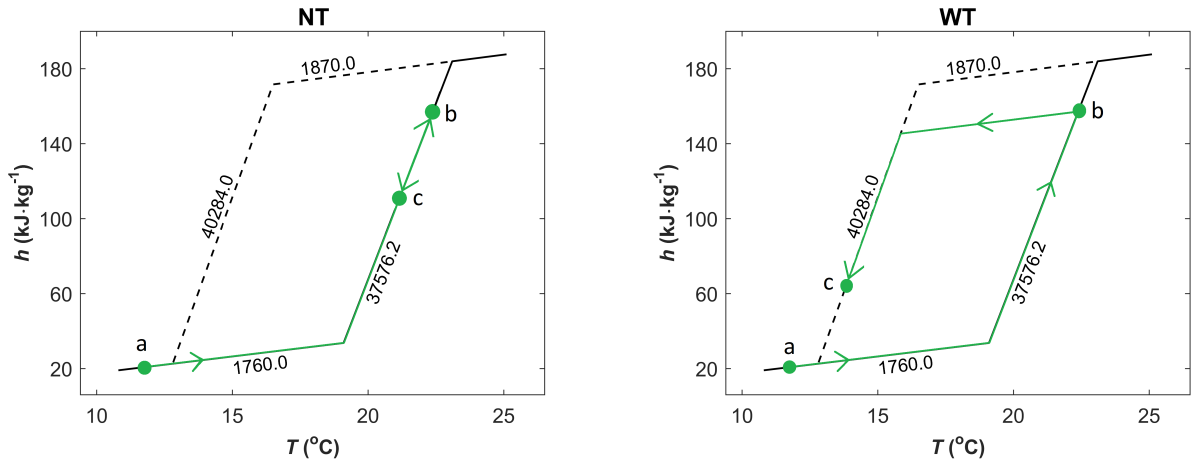

Figure 8.1: Schemes for the NT and WT models to simulate incomplete melting-freezing cycles of PCMs. h is the specific enthalpy, T is the temperature, the numbers represent the slope of each segment of the enthalpy curve, i.e., the specific heat value, and the letters indicate an example of a possible trajectory in the phase space.

To test the two hysteresis models described above, Delcroix et al. (2015a) studied experimentally and numerically the thermal behavior of a PCM-equipped-wall (a wall consisting of a double layer of plastic film with BioPCM pouches placed between two plywood panels) subject to incomplete melting-freezing cycles and found another type of transitions. The transitions were through a straight line of constant specific heat close to the solid and liquid values, then the PCM evolved following an enthalpy curve located between the heating and cooling curves until the end of the phase change. They found that the intermediate enthalpy curves are different in the interrupted heating and cooling processes. In this work this hysteresis model will be referred to as the WIT model. Figure 8.2 illustrates the WIT model as trajectories in the phase for the cases of interrupted heating and interrupted cooling. In this work the transitions were taken using straight line with a slope equal to the minimum specific heat in the solid or liquid phases.

[1]The term phase space refers to the thermodynamic phase space that is parametrized by the macroscopic states of a system, in this case by the temperature and specific enthalpy.

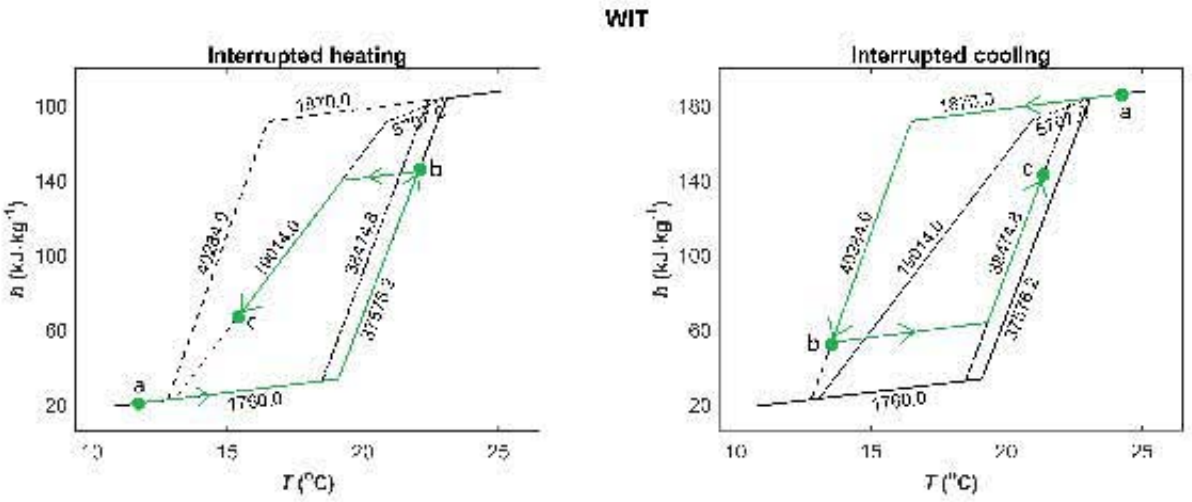

Figure 8.2: Scheme for the WIT model to simulate incomplete melting-freezing cycles of PCMs for the cases of interrupted heating and interrupted cooling. h is the specific enthalpy, T is the temperature, the numbers represent the slope of each segment of the enthalpy curve, i.e., the specific heat value, and the letters indicate an example of a possible trajectory in the phase space.

8.2 Constructive system, evaluation parameters and study cases

A constructive system consisting of a wall made only of BioPCM was considered. Despite the behavior of BioPCM is described by the WIT model, for research purposes and to take into account the objective of this chapter, it was considered that the PCM can also behave as described by the other two hysteresis models.

The numerical code described in Chapter 5 was used to simulate the heat transfer through a PCM-wall. In order to simulate BioPCM as a continuous layer in a one-dimensional approach, Delcroix et al. (2015a) proposed an effective thickness $e = 8.5$ mm, hereinafter it will be referred to as thickness, a thermal conductivity $k = 0.042\ \mathrm{W \cdot m^{-1} \cdot K^{-1}}$, and a density $\rho = 223.0\ \mathrm{kg \cdot m^{-3}}$.

An east facing wall with a solar absorptivity of 0.4 (light color) for the typical day of March in Nogales, Sonora, Mexico (31°19′N, 110°56′W, 1199 m altitude) was considered. The climate conditions for this month and wall were represented by a periodic function of T_{sa}. This climate was chosen such that when the thickness of the PCM increases, T_{is} only takes values within the mushy zone and the differences between the three hysteresis models can be distinguished. T_{sa}, T_a, T_c, the upper limit of the TCZ, $T_c + \Delta T_c$, and the lower limit of the TCZ, $T_c - \Delta T_c$, for this wall and climate are shown in Figure 8.3. T_c (= 21.2°C) was calculated as proposed by Humphreys and Nicol (2000) and ΔT_c (= 2.2°C) was calculated as proposed by Morillón-Gálvez et al. (2004).

The parameters used to evaluate the thermal performance of the PCM-wall are the same as those described in Subsection 7.2.7.

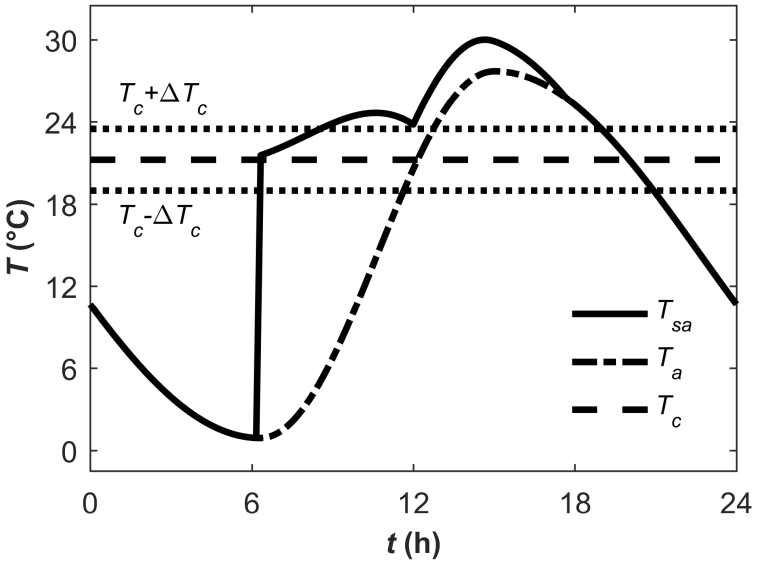

Figure 8.3: Temperature variables (the sol-air temperature, T_{sa}, the outdoor air temperature, T_a, the comfort temperature, T_c, the upper limit of the thermal comfort zone, $T_c + \Delta T_c$, and the lower limit of the thermal comfort zone, $T_c - \Delta T_c$) as functions of time, t, in Nogales, Sonora in March for an east facing wall with a solar absorptivity of 0.4.

The study cases analyzed in this work were an east facing wall in Nogales, Sonora for the typical day of March under AC and nAC condition, considering three thicknesses ($e =$ 8.5 mm, 25.5 mm, and 42.5 mm) and the three hysteresis models described above.

8.3 Results and discussion

The analysis of the differences in the PCM behavior between the three hysteresis models was performed qualitatively and quantitatively. The qualitative analysis was performed using Figures 8.4, 8.5, 8.6, 8.7, 8.8, and 8.9. These figures present the values of temperature, T, effective specific heat (hereinafter it will be referred to as specific heat and denoted by c), and specific enthalpy, h, for the outdoor surface node, os, and the indoor surface node, is, of the PCM-wall (see Figure 3.2), considering the three hysteresis models. The temperature and specific heat are plotted as functions of time, whereas the specific enthalpy is plotted in the phase space. In the graphs of temperature vs time the gray dotted lines represent the TCZ. In the graphs of specific enthalpy the specific enthalpy curves considered in the WIT model were included as a visual aid (they were plotted using gray lines).

For all of the study cases there are no differences in the PCM behavior between the three hysteresis models for the outdoor surface node (first six figures in Figures 8.4, 8.5, 8.6, 8.7, 8.8, and 8.9). For the three hysteresis models this node take the same values of T, c, and h taken during the day. This node always complete melting-freezing cycles, which can be observed by noting that the specific enthalpy values taken by this node completely run the

loop of the external curves of melting and freezing.

For the indoor surface node there are differences in the PCM behavior between the three hysteresis models (last six figures in Figures 8.4, 8.5, 8.6, 8.7, 8.8, and 8.9). Due to the boundary condition in the AC condition, the amplitude of T_{is} is higher in the nAC condition than in the AC condition. For the cases with $e =$ 8.5 mm the differences in T_{is} between the hysteresis models are negligible. However, as the thickness of the PCM increases, T_{is} and h_i take values within the mushy zone and the differences between the hysteresis models can be distinguished.

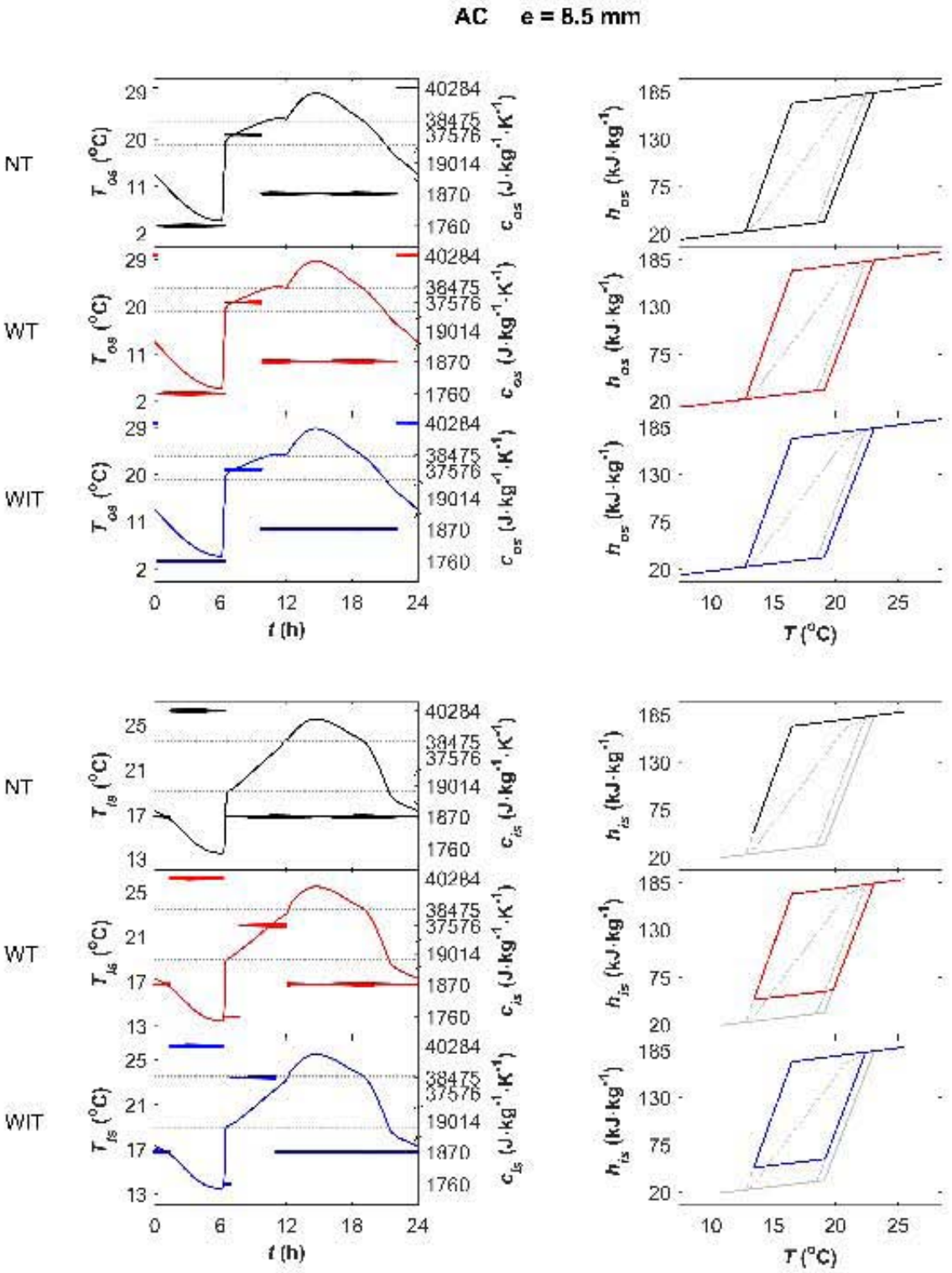

Figure 8.4: Values of temperature, T, and specific heat, c, as functions of time, t, along with the values of the specific enthalpy, h, in the phase space for the indoor, is, and outdoor, os, surfaces. Results for the AC condition with a PCM-thickness of 8.5 mm considering three different hysteresis models: NT, WT, and WIT.

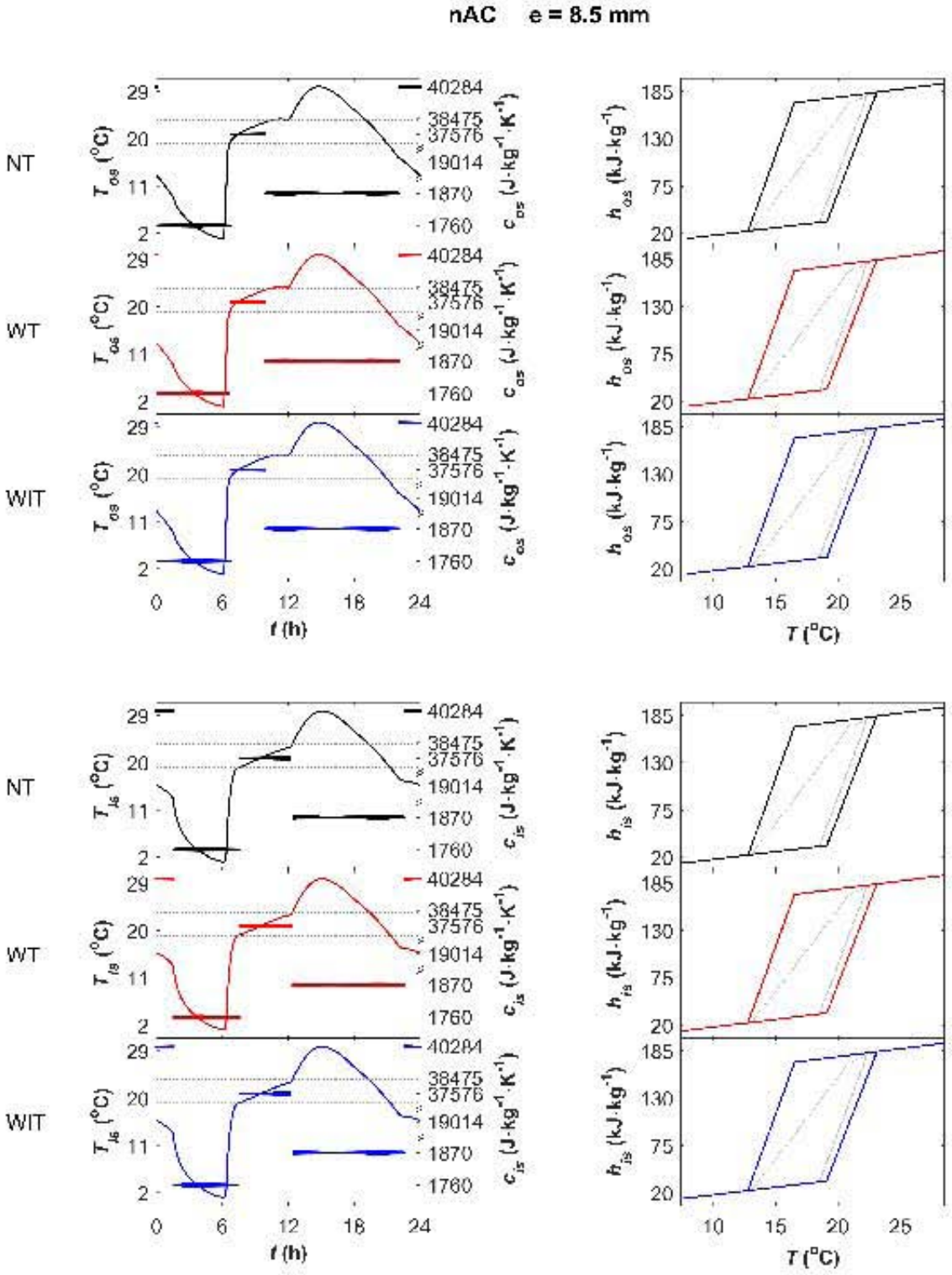

Figure 8.5: Values of temperature, T, and specific heat, c, as functions of time, t, along with the values of the specific enthalpy, h, in the phase space for the indoor, is, and outdoor, os, surfaces. Results for the nAC condition with a PCM-thickness of 8.5 mm considering three different hysteresis models: NT, WT, and WIT.

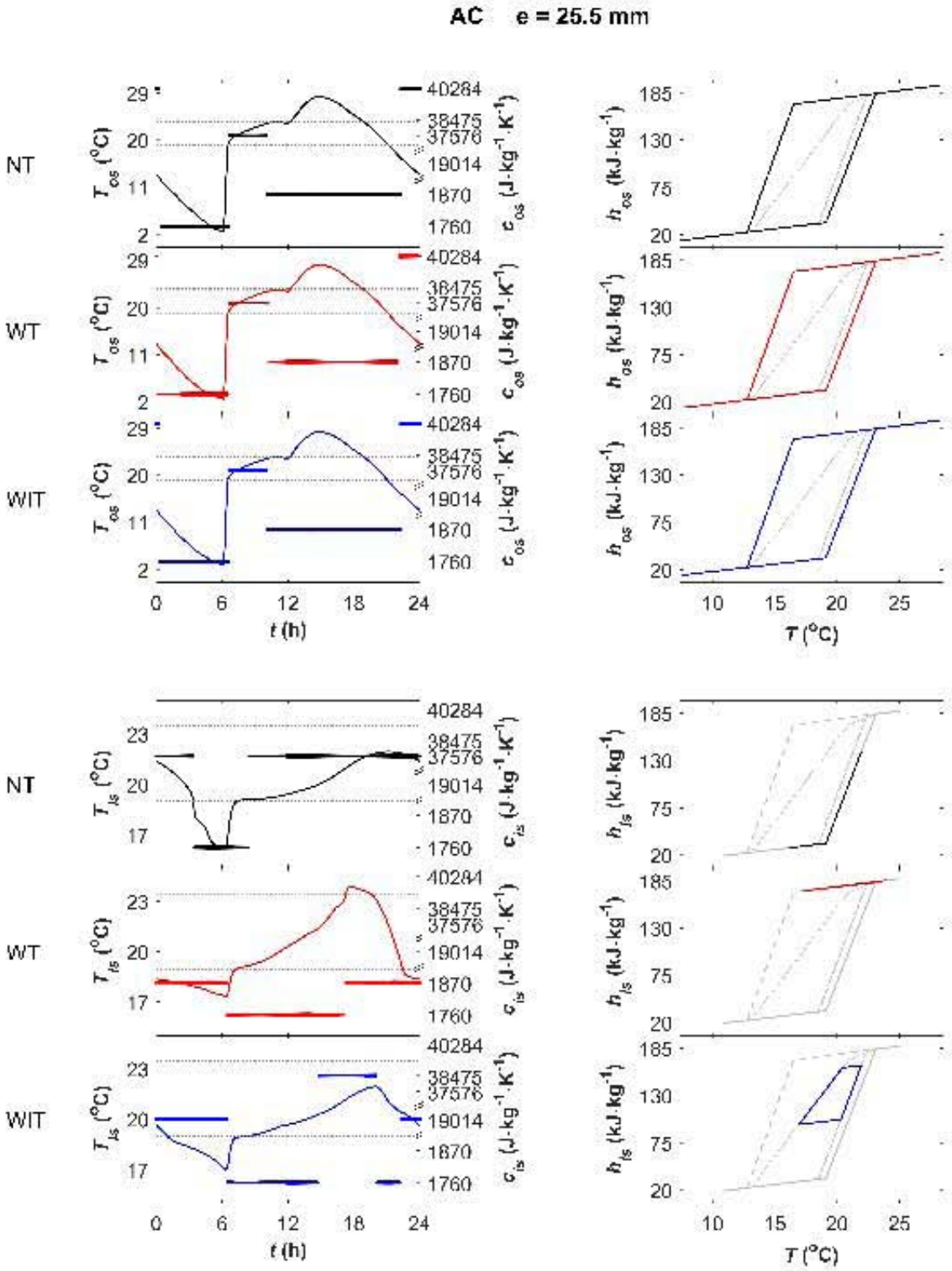

Figure 8.6: Values of temperature, T, and specific heat, c, as functions of time, t, along with the values of the specific enthalpy, h, in the phase space for the indoor, is, and outdoor, os, surfaces. Results for the AC condition with a PCM-thickness of 25.5 mm considering three different hysteresis models: NT, WT, and WIT.

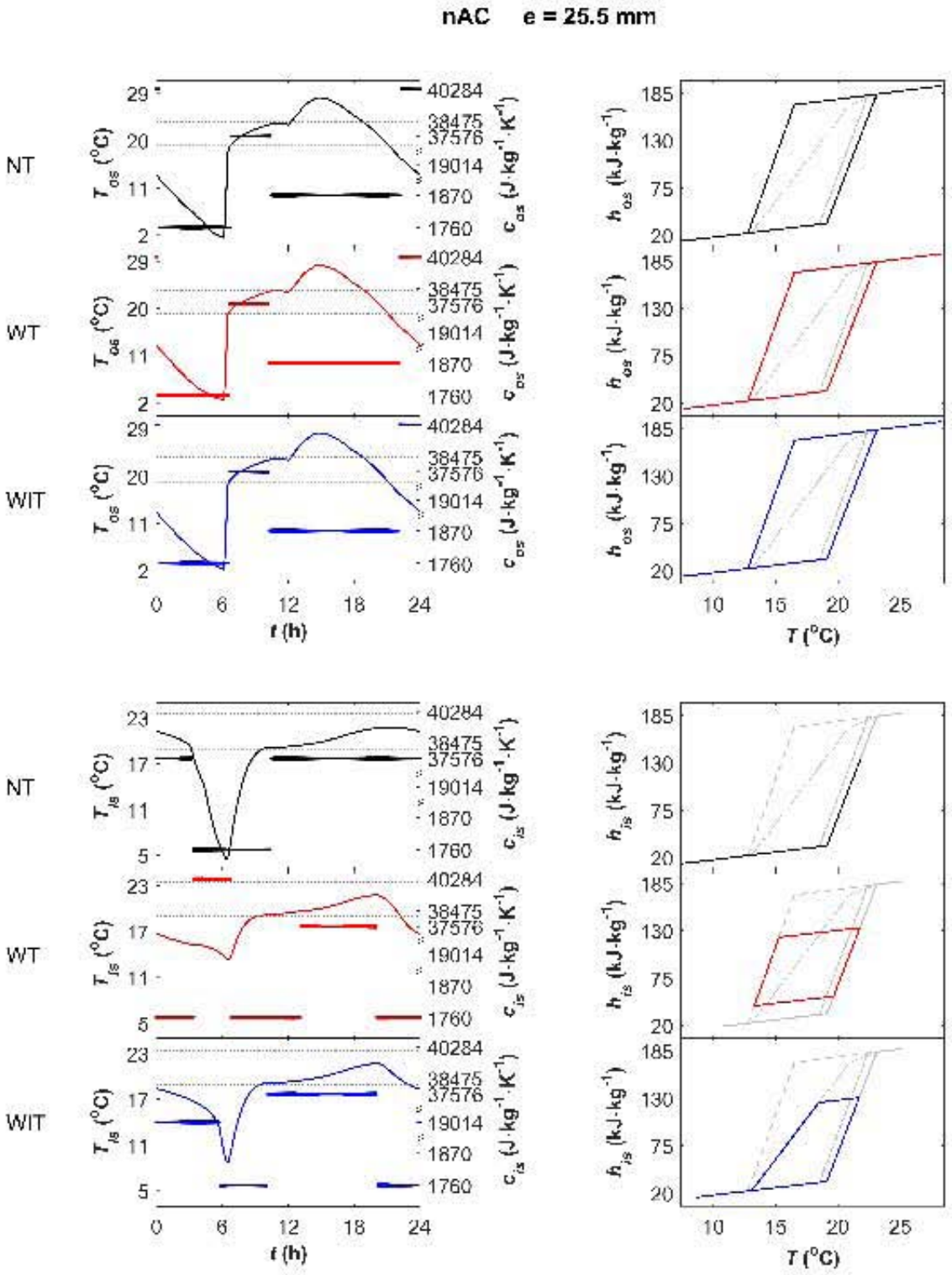

Figure 8.7: Values of temperature, T, and specific heat, c, as functions of time, t, along with the values of the specific enthalpy, h, in the phase space for the indoor, is, and outdoor, os, surfaces. Results for the nAC condition with a PCM-thickness of 25.5 mm considering three different hysteresis models: NT, WT, and WIT.

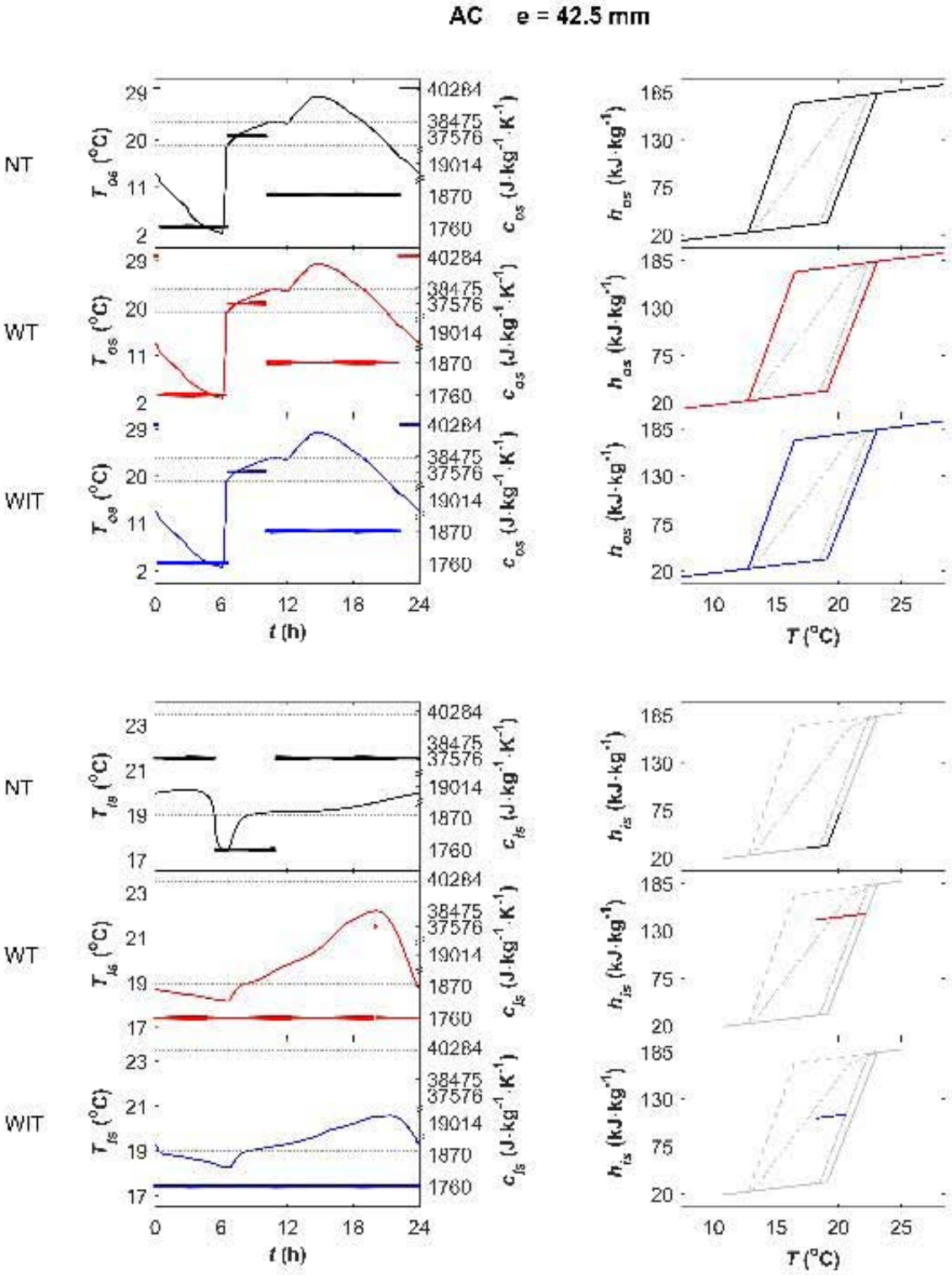

Figure 8.8: Values of temperature, T, and specific heat, c, as functions of time, t, along with the values of the specific enthalpy, h, in the phase space for the indoor, is, and outdoor, os, surfaces. Results for the AC condition with a PCM-thickness of 42.5 mm considering three different hysteresis models: NT, WT, and WIT.

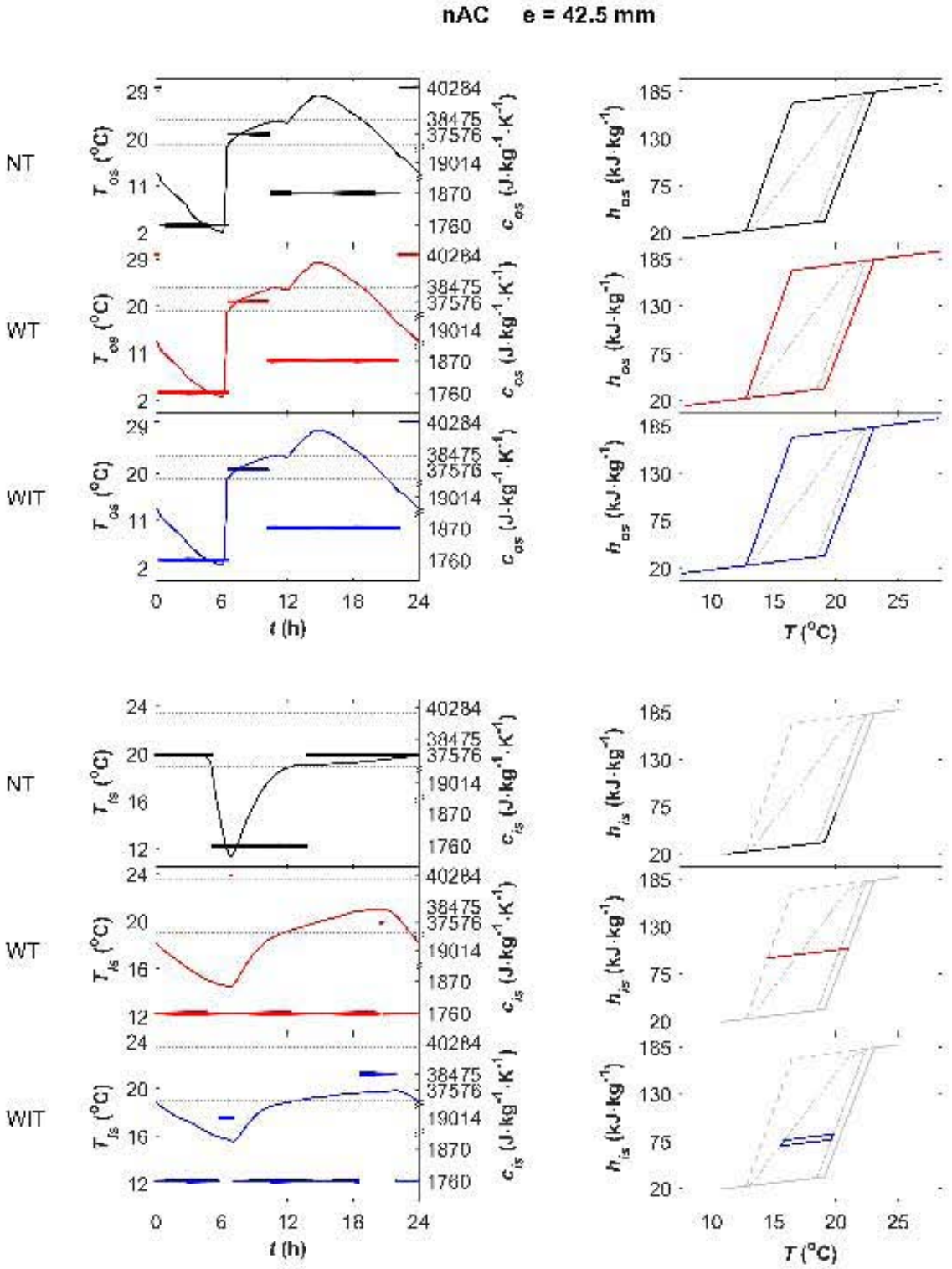

Figure 8.9: Values of temperature, T, and specific heat, c, as functions of time, t, along with the values of the specific enthalpy, h, in the phase space for the indoor, is, and outdoor, os, surfaces. Results for the nAC condition with a PCM-thickness of 42.5 mm considering three different hysteresis models: NT, WT, and WIT.

In order to quantify the differences between the thermal performance of the PCM-wall considering the three hysteresis models, Figure 8.10 shows the amplitude of T_{is} (defined as T_{is}^{A}) and the corresponding TPEP values for all of the study cases. Also, the percentage difference in the values of the TPEPs and T_{is}^{A} between the three hysteresis models is displayed. The percentage difference was calculated with respect to the maximum value of each case.

For the thicknesses of $e =$ 25.5 mm and $e =$ 42.5 mm the situation is mainly of cold thermal discomfort. As it is expected, the values of T_{is}^{A} and the TPEPs decrease as e increases. However, there is no a direct correlation between the TPEP values and the T_{is}^{A} values, because the TPEP values are determined by the behavior of T_{is} outside the TCZ. The differences in T_{is} and thermal performance for all of the study cases is presented below.

- For the cases with $e =$ 8.5 mm the differences in T_{is} and thermal performance between the hysteresis models are negligible.

- For the case with $e =$ 25.5 mm in AC condition it was found that the smallest value of T_{is}^{A} was obtained with the WIT model (5.0°C) and the largest value of T_{is}^{A} was obtained with the WT model (6.5°C), with a percentage difference of 24.2%. Regarding the thermal performance, the best thermal performance was obtained with the WIT model ($HL = 52.7\,\mathrm{W{\cdot}h{\cdot}m^{-2}}$) and the worst thermal performance was obtained with the WT model ($HL = 75.7\,\mathrm{W{\cdot}h{\cdot}m^{-2}}$), with a percentage difference of 30.4%.

- For the case with $e =$ 25.5 mm in nAC condition it was found that the smallest value of T_{is}^{A} was obtained with the WT model (8.4°C) and the largest value of T_{is}^{A} was obtained with the NT model (17.2°C), with a percentage difference of 51.4%. Regarding the thermal performance, the best thermal performance was obtained with the WIT model ($DDH_{cold} = 30.1\,\mathrm{°C{\cdot}h}$) and the worst thermal performance was obtained with the NT model ($DDH_{cold} = 41.3\,\mathrm{°C{\cdot}h}$), with a percentage difference of 27.1%.

- For the case with $e =$ 42.5 mm in AC condition it was found that the smallest value of T_{is}^{A} was obtained with the WIT model (2.3°C) and the largest value of T_{is}^{A} was obtained with the WT model (4.0°C), with a percentage difference of 42.4%. Regarding the thermal performance, the best thermal performance was obtained with the NT model ($HL = 24.6\,\mathrm{W{\cdot}h{\cdot}m^{-2}}$) and the worst thermal performance was obtained with the WT model ($HL = 38.9\,\mathrm{W{\cdot}h{\cdot}m^{-2}}$), with a percentage difference of 36.8%.

- For the case with $e =$ 42.5 mm in nAC condition it was found that the smallest value of T_{is}^{A} was obtained with the WIT model (4.3°C) and the largest value of T_{is}^{A} was obtained with the NT model (8.6°C), with a percentage difference of 50.3%. Regarding the thermal performance, the best thermal performance was obtained with the WIT model ($DDH_{cold} = 20.7\,\mathrm{°C{\cdot}h}$) and the worst thermal performance was obtained with the NT model ($DDH_{cold} = 29.5\,\mathrm{°C{\cdot}h}$), with a percentage difference of 29.8%.

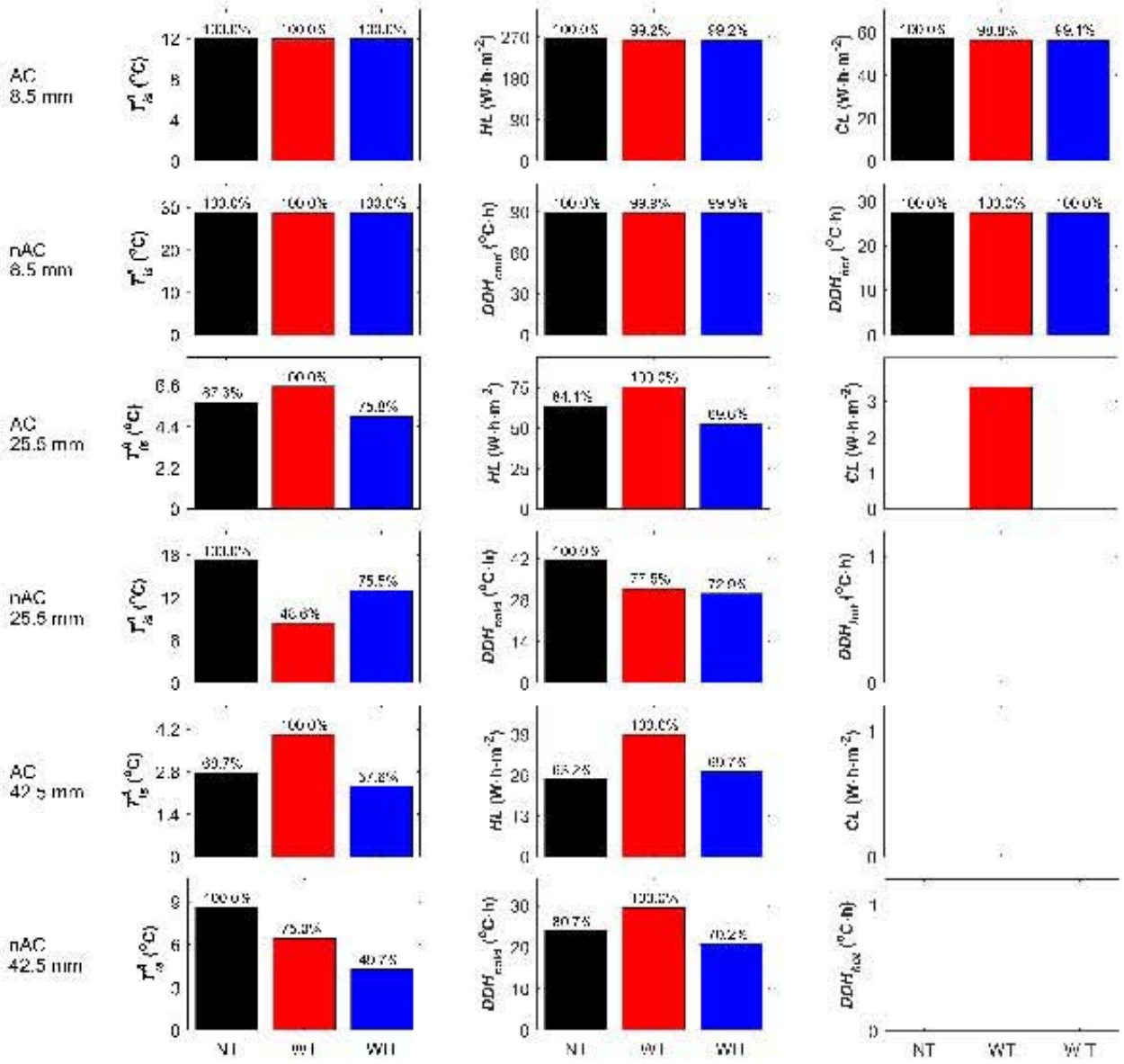

Figure 8.10: Thermal performance of the PCM-wall for all of the study cases considering three hysteresis models: NT, WT, and WIT. T_{is}^{A} is the amplitude of the indoor surface temperature, HL is the heating load, and DDH_{cold} are the cold discomfort degree hours. The percentage differences in the values of HL, DDH_{cold}, and T_{is}^{A} between the three hysteresis models are also displayed.

It is observed that not always the same hysteresis model produces the smallest values of T_{is}^A and the TPEPs, but for many of the analyzed cases with the WIT model the smallest values are obtained. It is expected that the thermal performance of the PCM-wall depends on the energy stored by it during the day. Large values of energy stored correspond to a high thermal inertia, which produce small T_{is}^A values and consequently small TPEPs values; whereas small values of energy stored correspond to a low thermal inertia, which produce large T_{is}^A values and consequently large TPEPs values. The following two hypotheses are proposed in order to explain the differences between the thermal performance of the PCM-wall considering the three hysteresis models:

- An inverse relationship exists between T_{is}^A and the energy stored by the PCM-wall for the 24-hours period, e_{PCM}.

- An inverse relationship exists between the TPEPs (CL, HL, DDH_{cold}, and DDH_{hot}) values and the energy stored by the PCM-wall for the 24-hours period, e_{PCM}.

Figure 8.11 shows scatter plots of T_{is}^A, HL, CL, DDH_{cold} and DDH_{hot} with the energy stored by the PCM-wall for the 24-hours period, ${e_{PCM}}^2$, for all of the study cases. According to these hypotheses it is expected a negative slope in the scatter plots, however this is not observed, except in the scatter plot of HL for $e =$ 42.5 mm in the AC condition.

Since the previous hypothesis could not be verified, it is suggested to consider specific relationships of the specific heat with T_{is}^A. It is expected that the T_{is} amplitude, T_{is}^A, depends on the values of the specific heat taken by the PCM-wall during the day. Large values of specific heat correspond to a high thermal inertia, which produce small T_{is}^A values; whereas small values of specific heat correspond to a low thermal inertia, which produce large T_{is}^A values. Six hypotheses are suggested:

1. An inverse relationship exists between T_{is}^A and the mean value of the specific heat for the 24-hours period, $\bar{c}$. $\bar{c}$ is calculated using all the grid nodes of the PCM-wall.

2. An inverse relationship exists between T_{is}^A and the mean value of the specific heat for the 2-hours period when the PCM-wall achieves the higher temperature values, $c_{T_{max}}$. $c_{T_{max}}$ is calculated using all the grid nodes of the PCM-wall.

3. An inverse relationship exists between T_{is}^A and the mean value of the specific heat for the 2-hours period when the PCM-wall achieves the lower temperature values, $c_{T_{min}}$. $c_{T_{min}}$ is calculated using all the grid nodes of the PCM-wall.

4. An inverse relationship exists between T_{is}^A and the duration of the three higher values of the specific heat for the 24-hours period. The calculation considers all the grid nodes of the PCM-wall.

[2]The energy stored by the PCM-wall, e_{PCM}, was calculated by the positive integral of the energy flux through it, $EF_{PCM} = \mu_o (T_{sa} - T_{os}) - \mu_i (T_{is} - T_i)$, i.e., $e_{PCM} = \int EF_{PCM} dt$ when $E_{PCM} > 0$.

5. An inverse relationship exists between T_{is}^{A} and the duration of the three higher values of the specific heat for the 2-hours period when the PCM-wall achieves the higher temperature values. The calculation considers all the grid nodes of the PCM-wall.

6. An inverse relationship exists between T_{is}^{A} and the duration of the three higher values of the specific heat for the 2-hours period when the PCM-wall achieves the lower temperature values. The calculation considers all the grid nodes of the PCM-wall.

In order to verify the hypotheses 1, 2, and 3, Figure 8.12 shows scatter plots of T_{is}^{A} with $\bar{c}$, $c_{T_{max}}$, and $c_{T_{min}}$ for all of the study cases. According to the hypotheses 1, 2, and 3, it is expected a negative slope in the scatter plots, however the results exhibited in Figure 8.12 can not verify these hypotheses, except in the scatter plot of $c_{T_{min}}$ for $e =$ 25.5 mm in the nAC condition.

To verify the hypothesis 4, Figure 8.13 shows scatter plots of T_{is}^{A} with the duration of the three higher values of the specific heat for the 24-hours period for all of the study cases. According to the hypothesis 4 it is expected a negative slope in the scatter plots, however this is not observed, so this hypothesis can not be verified. In addition to the scatter plots, the duration of each value of the specific heat for the time period considered is also shown in Figure 8.13.

To verify the hypothesis 5, Figure 8.14 shows scatter plots of T_{is}^{A} with the duration of the three higher values of the specific heat for the 2-hours period when the PCM-wall achieves the higher temperature values for all of the study cases. According to the hypothesis 5 it is expected a negative slope in the scatter plots, however this is not observed, so this hypothesis can not be verified. In addition to the scatter plots, the duration of each value of the specific heat for the time period considered is also shown in Figure 8.14.

To verify the hypothesis 6, Figure 8.15 shows scatter plots of T_{is}^{A} with the duration of the three higher values of the specific heat for the 2-hours period when the PCM-wall achieves the lower temperature values for all of the study cases. According to the hypothesis 6 it is expected a negative slope in the scatter plots, however this is not observed, so this hypothesis can not be verified. In addition to the scatter plots, the duration of each value of the specific heat for the time period considered is also shown in Figure 8.15.

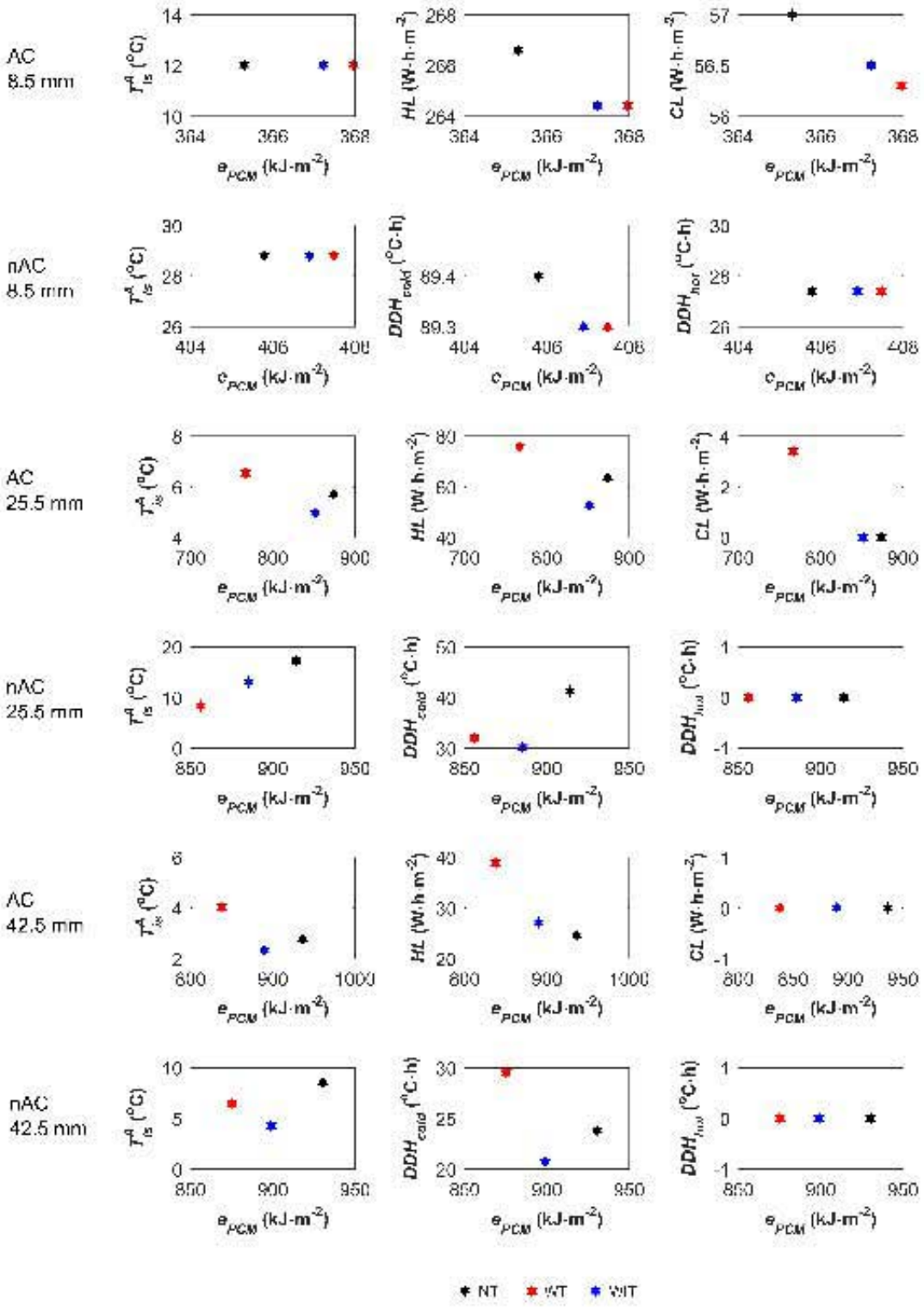

Figure 8.11: Scatter plots of the amplitude of the indoor surface temperature, T_{is}^A and the TPEPs, HL, CL, DDH_{cold}, and DDH_{hot}, as functions of the energy stored by the PCM-wall for the 24-hours period, e_{PCM}. NT, WT, and WIT represents the three different hysteresis models.

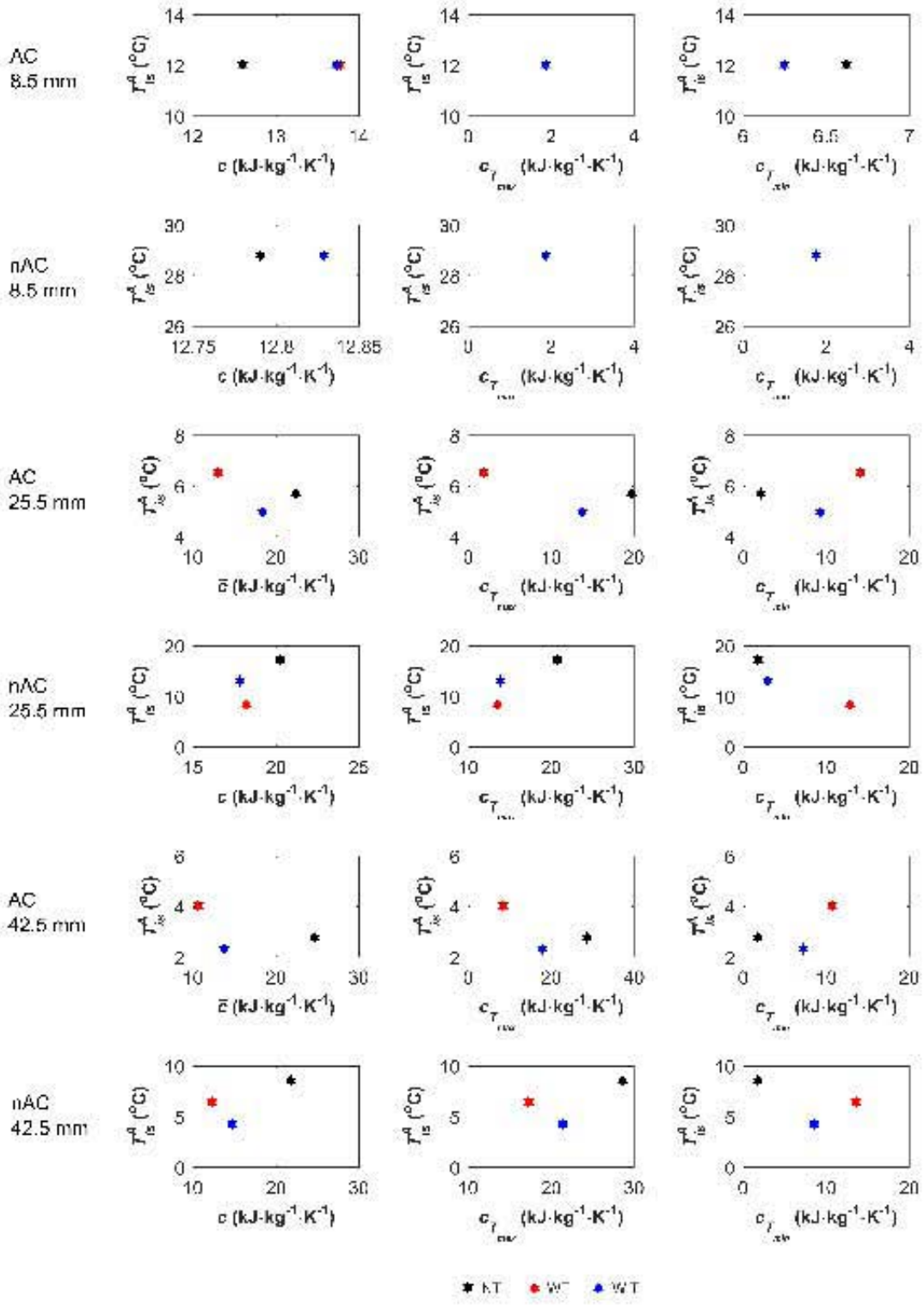

Figure 8.12: Scatter plots of the amplitude of the indoor surface temperature, T_{is}^{A}, as function of the mean value of the specific heat for the 24-hours period, $\bar{c}$, the mean value of the specific heat for the 2-hours period when the PCM-wall achieves the maximum temperature values, $c_{T_{max}}$, and the mean value of the specific heat for the 2-hours period when the PCM-wall achieves the minimum temperature values, $c_{T_{min}}$. NT, WT, and WIT represents the three different hysteresis models.

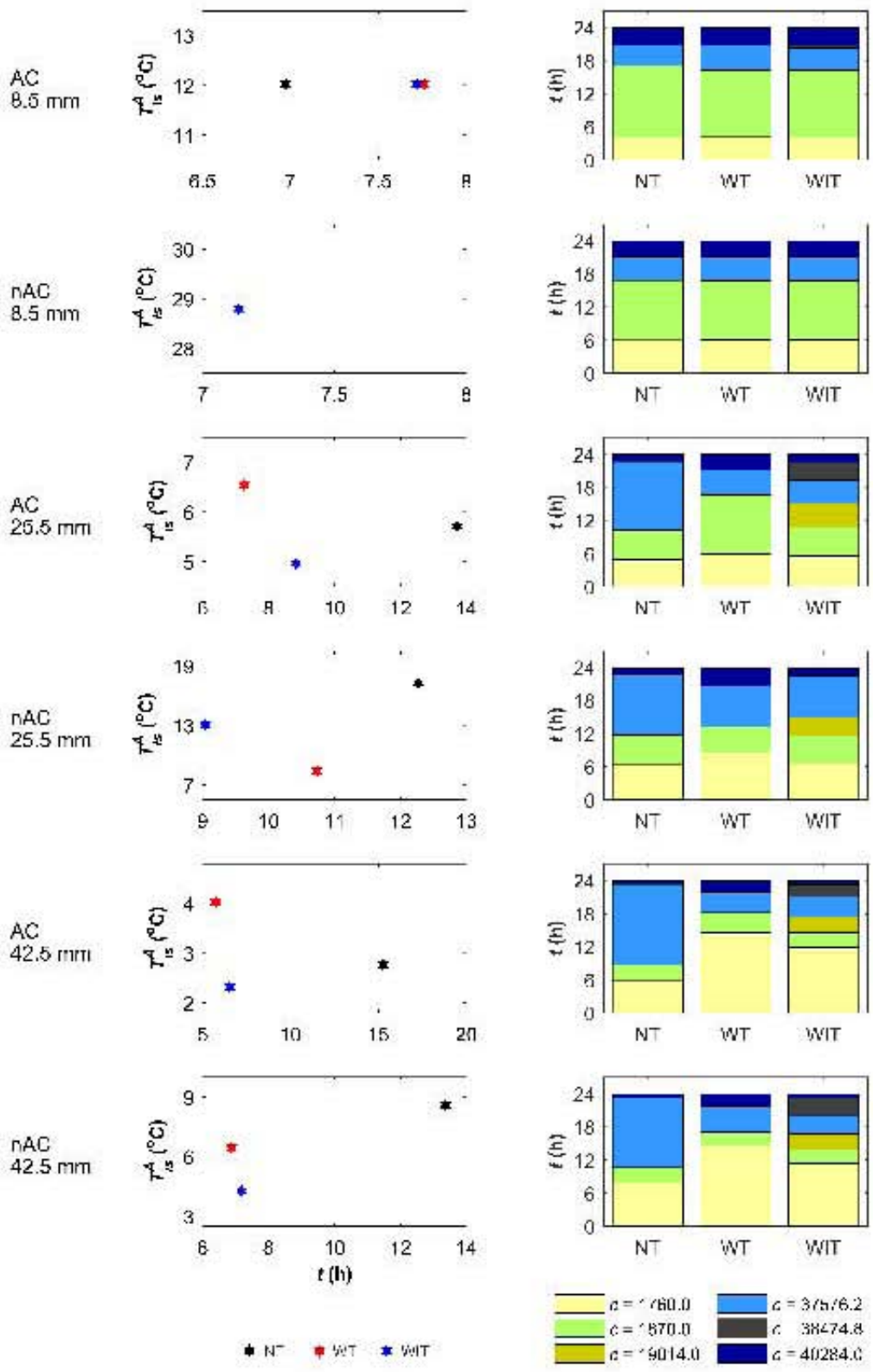

Figure 8.13: Scatter plots of the amplitude of the indoor surface temperature, T_{is}^A, with the duration of the three higher values of the specific heat for the 24-hours period for all of the study cases. NT, WT, and WIT represents the three different hysteresis models. The duration of each value of the specific heat for the 24-hours period is also shown.

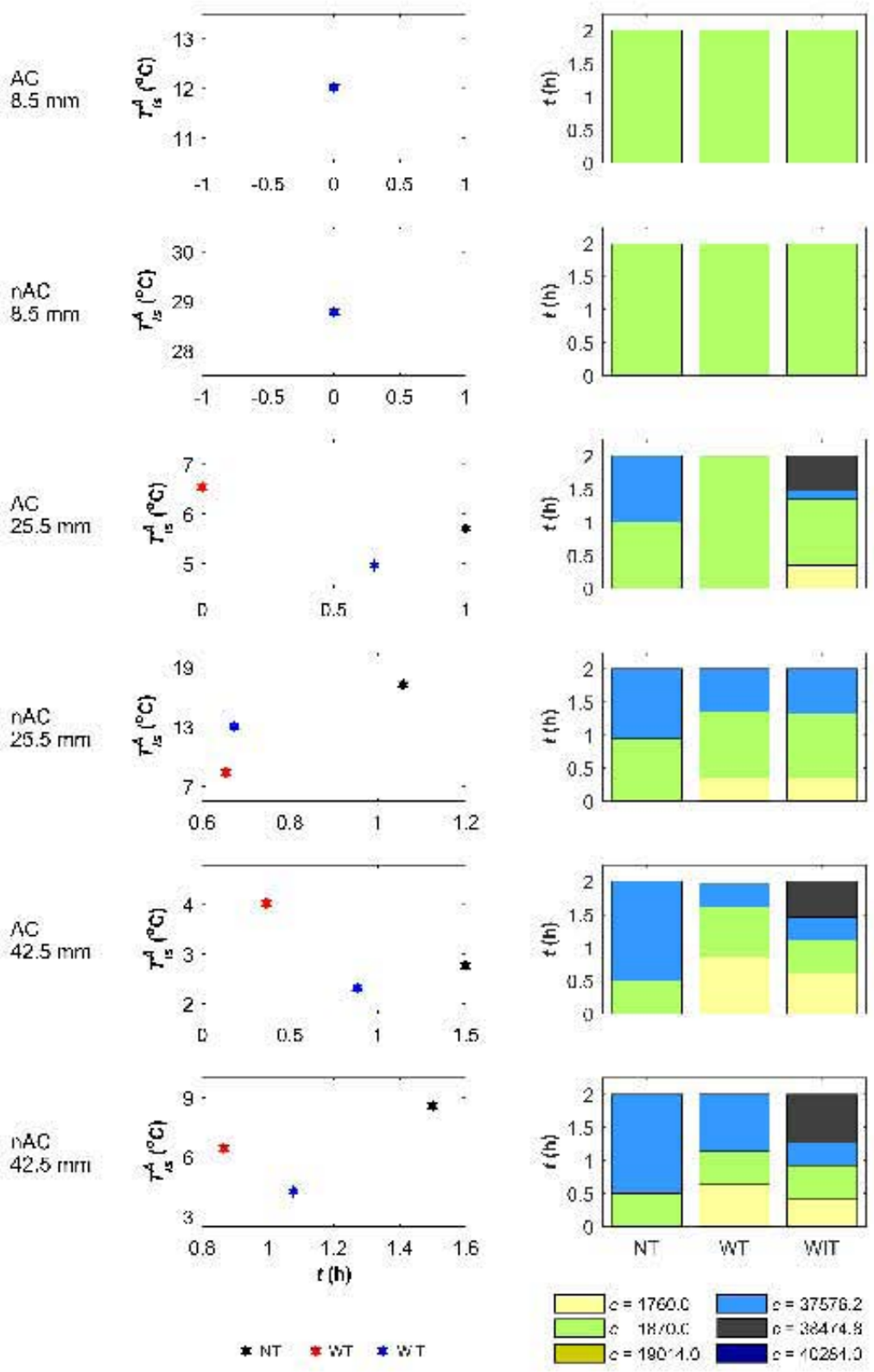

Figure 8.14: Scatter plots of the amplitude of the indoor surface temperature, T_{is}^A, with the duration of the three higher values of the specific heat for the the 2-hours period when the PCM-wall achieves the higher temperature values for all of the study cases. NT, WT, and WIT represents the three different hysteresis models. The duration of each value of the specific heat for the time period considered is also shown.

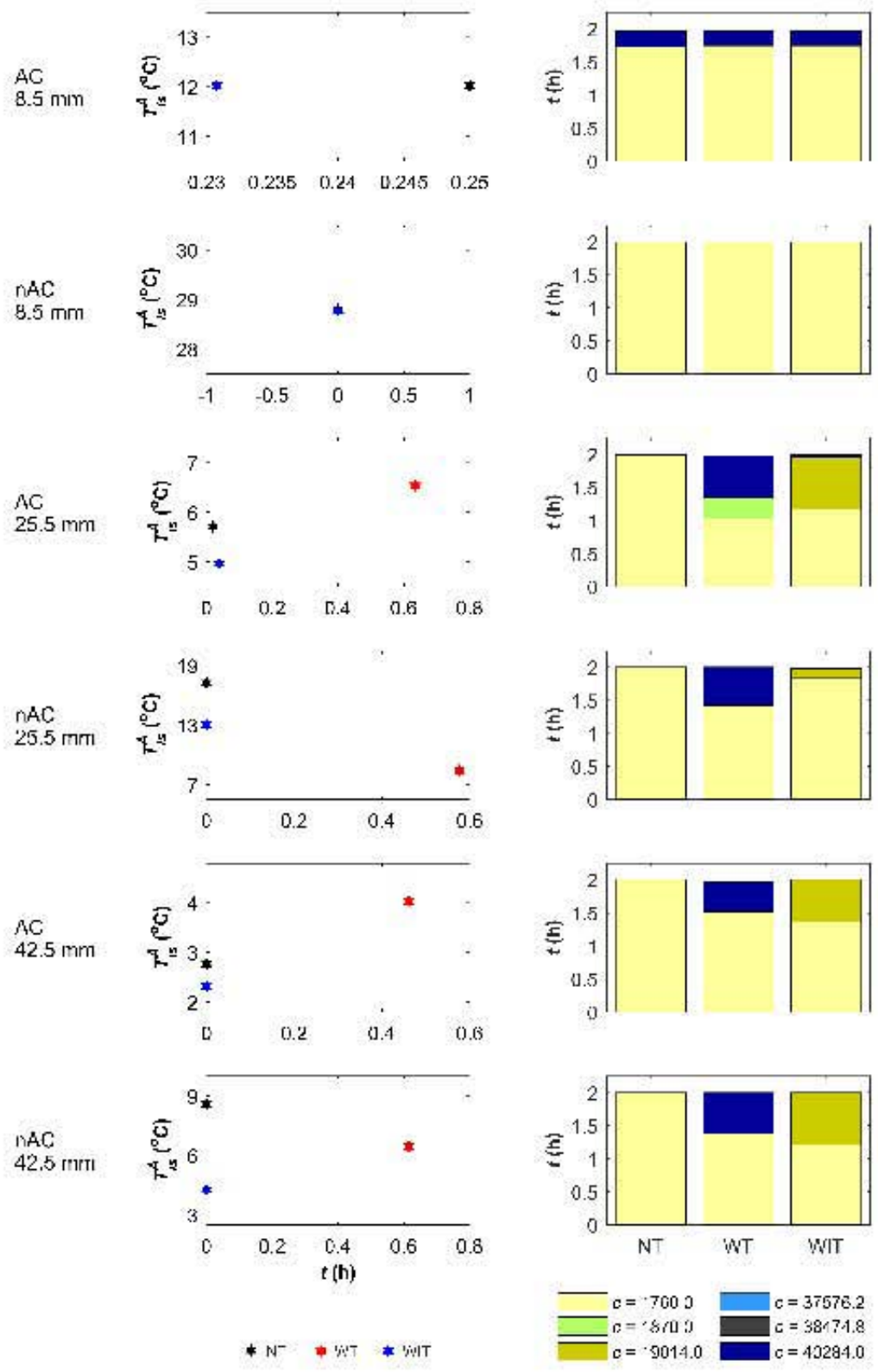

Figure 8.15: Scatter plots of the amplitude of the indoor surface temperature, T_{is}^A, with the duration of the three higher values of the specific heat for the the 2-hours period when the PCM-wall achieves the lower temperature values for all of the study cases. NT, WT, and WIT represents the three different hysteresis models. The duration of each value of the specific heat for the time period considered is also shown.

8.4 Conclusions

It was found that there are important differences in the thermal behavior of the PCM-wall for the different hysteresis models considered. Differences in T_{is}^{A} of up to 8.9°C (51.4% with respect to the maximum value) for the case with $e =$ 25.5 mm in nAC condition, differences in HL of up to 23.0 $\mathrm{W{\cdot}h{\cdot}m^{-2}}$ (30.4% with respect to the maximum value) for the case with $e =$ 25.5 mm in AC condition, and differences in DDH_{cold} of up to 11.2°C·h (27.1% with respect to the maximum value) for the case with $e =$ 25.5 mm in nAC condition. The largest differences were obtained with the intermediate thickness.

No relationships between the PCM-wall thermal performance with specific evaluations of the specific heat (the mean value of the specific heat for the 24-hours period, the mean value of the specific heat for the 2-hours period when the PCM-wall achieves the higher temperature values, the mean value of the specific heat for the 2-hours period when the PCM-wall achieves the lower temperature values, the duration of the three higher values of the specific heat for the 24-hours period, the duration of the three higher values of the specific heat for the 2-hours period when the PCM-wall achieves the higher temperature values, and the duration of the three higher values of the specific heat for the 2-hours period when the PCM-wall achieves the lower temperature values) and stored energy could be found. The presented results show the complex behavior of PCMs. A deep understanding of the hysteresis phenomenon, along with extensive numerical and experimental studies concerning PCMs varying their thermal properties in different use conditions are needed in order to fully understand their behavior.

Chapter 9

Conclusions

The utilization of PCMs in the building envelope is an attractive option to increase the thermal mass of the envelope without a significant increase in the thickness, thus contributing to improve the thermal comfort and reduce the use of air-conditioning. A successful application of PCMs in the building envelope requires that their thermophysical properties are selected according to the climate and use condition (AC or nAC). Is is known that the thermal performance of constructive systems depends on the use condition (Barrios et al., 2011). So, it is needed to compare the thermal performance of PCMs in AC and nAC conditions in different climates, and to find optimal values of key thermophysical properties for each case and use condition.

Another important aspect for a proper implementation of PCMs is to perform an adequate simulation of the hysteresis phenomenon. However it is just being studied and there is no a definitive theory of this phenomenon. There are three models for the hysteresis phenomenon (Chandrasekharan et al., 2013; Bony and Citherlet, 2007; Jaworski et al., 2014; Delcroix et al., 2015a), yet there are no studies concerning the effects of the hysteresis phenomenon on the thermal performance of PCMs nor how it modifies the selection of optimal thermophysical properties for different use conditions.

In this work a numerical a numerical study was carried out to address these aspects. The contributions made are described below.

It was developed a numerical code that solves the one-dimensional heat transfer through PCM-constructive-systems in the building envelope, considering the three different hysteresis models (Chapter 5). The numerical code was validated using a one-dimensional numerical benchmark (Johannes et al., 2011) proposed by the International Energy Agency (IEA). Also, a sensitivity analysis on the grid size and time step was performed with good results on convergence and grid size independence.

It was studied the thermal performance of a PCM-wall in AC and nAC conditions in a hot and a cold climate in Mexico, considering variations in the peak melting temperature and thickness of the PCM-wall (Chapter 6). It was supposed that the PCM-wall does not exhibit hysteresis. It was found that there are significant differences in the thermal performance between the two climates and between the two operation conditions. For the hot climate

the variations in the peak melting temperature, given a thickness, have a huge effect on the thermal performance of the PCM-wall; whereas for the cold climate the variations in the peak melting temperature do not significantly impact the thermal performance of the PCM-wall. In the case of a mixed use of AC and nAC conditions, a peak melting temperature of 2.0°C above the comfort temperature is suggested. This result is in agreement with previous findings on the literature.

The comparison of a PCM-wall with one of the most commonly used lightweight walls worldwide (the Durock panel, a cement board wall) was performed (Chapter 6). It was found that the thermal performance of the PCM-wall is better that that of the cement board wall, considering the same thickness for both of them. An adequate selection of the peak melting temperature of the PCM-wall 50 mm-thick produced a daily saving of $102\,\mathrm{W{\cdot}h{\cdot}m^{-2}}$ (41%) in the cooling load for the AC condition; similarly, the PCM-wall 40 mm-thick produced a daily reduction of 38°C·h (52%) in the hot discomfort degree hours for the nAC condition.

A study of the combined effect of the hysteresis temperature difference, peak melting temperature and thickness of a PCM-wall on its thermal performance was carried out (Chapter 7). The study was made considering complete melting-freezing cycles of the PCM-wall in a location exhibiting both hot and cold thermal discomfort. It was found that hysteresis improves the thermal performance and suggested recommendations for selecting a peak melting temperature, a peak freezing temperature, and a hysteresis temperature difference to maximize the thermal performance of PCM-walls were obtained. Also, the basis of a methodology to optimize simultaneously any pair of variables of a PCM-wall for different use conditions (AC, nAC, or a combined use of AC and nAC) were proposed.

Finally, the thermal performance of a PCM-wall considering three different hysteresis models, considering AC and nAC use conditions for different values of thicknesses was studied (Chapter 8). It was found that there are important differences in the thermal behavior of the PCM-wall for the different hysteresis models, with the largest differences for an intermediate thickness. The complex behavior of PCMs was evidenced and no relationships between the PCM-wall thermal performance and specific evaluations of the specific heat (the mean value of the specific heat for the 24-hours period, the mean value of the specific heat for the 2-hours period when the PCM-wall achieves the higher temperature values, the mean value of the specific heat for the 2-hours period when the PCM-wall achieves the lower temperature values, the duration of the three higher values of the specific heat for the 24-hours period, the duration of the three higher values of the specific heat for the 2-hours period when the PCM-wall achieves the higher temperature values, and the duration of the three higher values of the specific heat for the 2-hours period when the PCM-wall achieves the lower temperature values) and stored energy could be found.

The study cases shown in this thesis demonstrated the advantages of PCMs in the building envelope to improve the thermal performance of buildings, compared to traditional constructive systems (with no phase change). The rich behavior of the PCM-constructive-systems and the complexity to study the heat transfer through them, makes not possible to derive a general rule that allows selecting optimal thermophysical properties of them. A case-by-case analysis considering technical, economic, and environmental issues should be done before

opting for PCMs as a part of the building envelope constructive systems.

Finally, from this work the following is suggested for future research:

- Consider other phenomena related to the study of PCM-constructive-systems (e.g., convection and sub-cooling) in more complex geometries.
- Perform full-scale experiments with different PCM-constructive-systems to investigate the hysteresis exhibited by them, and thus gain a better understanding of this phenomenon.
- Integrate the hysteresis phenomenon in whole building energy simulation programs (e.g., EnergyPlus).
- Carry out annual simulations of the thermal performance of different PCM-constructive-systems to find the optimal configuration considering a technical, economic, and environmental analysis.

Bibliography

A. Abhat. Low temperature latent heat thermal energy storage: Heat storage materials. *Solar Energy*, 30(4):313 – 332, 1983. doi: 10.1016/0038-092X(83)90186-X.

M. Ahmad, A. Bontemps, H. Sallée, and D. Quenard. Experimental investigation and computer simulation of thermal behaviour of wallboards containing a phase change material. *Energy and Buildings*, 38(4):357 – 366, 2006. doi: 10.1016/j.enbuild.2005.07.008.

H. Akeiber, P. Nejat, M. Z. A. Majid, M. A. Wahid, F. Jomehzadeh, I. Z. Famileh, J. K. Calautit, B. R. Hughes, and S. A. Zaki. A review on phase change material (PCM) for sustainable passive cooling in building envelopes . *Renewable and Sustainable Energy Reviews*, 60:1470 – 1497, 2016. doi: 10.1016/j.rser.2016.03.036.

S. N. AL-Saadi and Z. J. Zhai. Modeling phase change materials embedded in building enclosure: A review. *Renewable and Sustainable Energy Reviews*, 21:659 – 673, 2013. doi: 10.1016/j.rser.2013.01.024.

M. Alam, H. Jamil, J. Sanjayan, and J. Wilson. Energy saving potential of phase change materials in major australian cities. *Energy and Buildings*, 78:192 – 201, 2014. doi: 10.1016/j.enbuild.2014.04.027.

Amy Saunders and Emma Davidson. Global Cement Magazine: Cement boards, January 2014. URL `http://www.globalcement.com/images/stories/documents/articles/eGC-Jan14-32web.pdf`. .

K. Anderson. *Design Energy Simulation for Architects: Guide to 3D Graphics*. Routledge, New York, 1 edition, 2014. ISBN 978-0415840668.

F. Ascione, N. Bianco, R. F. D. Masi, F. de' Rossi, and G. P. Vanoli. Energy refurbishment of existing buildings through the use of phase change materials: Energy savings and indoor comfort in the cooling season. *Applied Energy*, 113:990 – 1007, 2014. doi: 10.1016/j.apenergy.2013.08.045.

ASHRAE. *ASHRAE Handbook - Fundamentals*. American Society of Heating, Refrigerating and Air-Conditioning Engineers, United States, 2005. ISBN 9781931862714.

A. Athienitis, C. Liu, D. Hawes, D. Banu, and D. Feldman. Investigation of the thermal performance of a passive solar test-room with wall latent heat storage. *Building and Environment*, 32(5):405 – 410, 1997. doi: 10.1016/S0360-1323(97)00009-7.

R. Baetens, B. P. Jelle, and A. Gustavsen. Phase change materials for building applications: A state-of-the-art review. *Energy and Buildings*, 42(9):1361 – 1368, 2010. doi: 10.1016/j.enbuild.2010.03.026.

G. Barrios, G. Huelsz, R. Rechtman, and J. Rojas. Wall/roof thermal performance differences between air-conditioned and non air-conditioned rooms. *Energy and Buildings*, 43(1):219 – 223, 2011. doi: 10.1016/j.enbuild.2010.09.015.

G. Barrios, G. Huelsz, J. Rojas, J. M. Ochoa, and I. Marincic. Envelope wall/roof thermal performance parameters for non air-conditioned buildings. *Energy and Buildings*, 50:120–127, 2012. doi: 10.1016/j.enbuild.2012.03.030.

G. Barrios, G. Huelsz, and J. Rojas. Ener-Habitat: A Cloud Computing Numerical Tool to Evaluate the Thermal Performance of Walls/Roofs. *Energy Procedia*, 57:2042 – 2051, 2014. doi: 10.1016/j.egypro.2014.10.169. 2013 ISES Solar World Congress.

G. Barrios, J. Casas, G. Huelsz, and J. Rojas. Ener-Habitat: An online numerical tool to evaluate the thermal performance of homogeneous and non-homogeneous envelope walls/roofs. *Solar Energy*, 131(Supplement C):296 – 304, 2016. doi: 10.1016/j.solener.2015.12.017.

BioPCM. Phase Change Energy Solutions. www.phasechange.com and by personal communication.

J. Bony and S. Citherlet. Numerical model and experimental validation of heat storage with phase change materials. *Energy and Buildings*, 39(10):1065 – 1072, 2007. doi: 10.1016/j.enbuild.2006.10.017.

A. Chan. Energy and environmental performance of building facades integrated with phase change material in subtropical hong kong. *Energy and Buildings*, 43(10):2947 – 2955, 2011. doi: 10.1016/j.enbuild.2011.07.021.

R. Chandrasekharan, S. L. Edwin, D. E. Fisher, and P. S. Deokar. An enhanced simulation model for building envelopes with phase change materials. *ASHRAE Transactions*, 119(2): 1 – 10, 2013.

C. Chen, H. Guo, Y. Liu, H. Yue, and C. Wang. A new kind of phase change material (PCM) for energy-storing wallboard. *Energy and Buildings*, 40(5):882 – 890, 2008. doi: 10.1016/j.enbuild.2007.07.002.

D. Chow and G. J. Levermore. New algorithm for generating hourly temperature values using daily maximum, minimum and average values from climate models. *Building Services Engineering Research and Technology*, 28(3):237–248, 2007. doi: 10.1177/0143624407078642.

K. Darkwa and J. S. Kim. Heat transfer in neuron composite laminated phase-change drywall. *Proceedings of the Institution of Mechanical Engineers, Part A: Journal of Power and Energy*, 218(2):83–87, 2004. doi: 10.1243/095765004773644085.

K. Darkwa and J. S. Kim. Thermal Analysis of Composite Phase Change Drywall Systems. *Journal of Solar Energy Engineering*, 127(3):352–356, 2005. doi: 10.1115/1.1877492.

L. W. Davis and P. J. Gertler. Contribution of air conditioning adoption to future energy use under global warming. *Proceedings of the National Academy of Sciences*, 112(19):5962 – 5967, 2015. doi: 10.1073/pnas.1423558112.

B. Delcroix, M. Kummert, and A. Daoud. Thermal behavior mapping of a phase change material between the heating and cooling enthalpy-temperature curves. *Energy Procedia*, 78:225 – 230, 2015a. doi: 10.1016/j.egypro.2015.11.612. 6th International Building Physics Conference, IBPC 2015.

B. Delcroix, M. Kummert, A. Daoud, and J. Bouchard. Influence of experimental conditions on measured thermal properties used to model phase change materials. *Building Simulation*, 8(6):637 – 650, 2015b. doi: 10.1007/s12273-015-0241-8.

B. M. Diaconu and M. Cruceru. Novel concept of composite phase change material wall system for year-round thermal energy savings. *Energy and Buildings*, 42(10):1759 – 1772, 2010. doi: 10.1016/j.enbuild.2010.05.012.

Ener-Habitat. Ener-Habitat Evaluación térmica de la envolvente arquitectónica. URL `http://www.enerhabitat.unam.mx/Cie2/`. .

EnergyPlus. U.S. Department of Energy, Energy Efficiency & Renewable Energy. EnergyPlus Energy Simulation Software. U.S. Department of Energy, Energy Efficiency & Renewable Energy. URL `https://energyplus.net/`. .

S. J. Farlow. *Partial Differential Equations for Scientists and Engineers*. Dover Publications, Inc., United States of America, 1 edition, 1993. ISBN 0-486-67620-X.

N. Gershenfeld. *The Nature of Mathematical Modeling*. Cambridge University Press, Cambridge, United Kingdom, 1999. ISBN 0521570956.

J. C. Glenn, E. Florescu, and The-Millennium-Project-Team. *2015-16 State of the Future*. The Millennium Project, Washington, D.C., U.S.A., 1 edition, 2015. ISBN 978-0-9882639-2-5.

B. Gowreesunker and S. Tassou. Effectiveness of CFD simulation for the performance prediction of phase change building boards in the thermal environment control of indoor spaces. *Building and Environment*, 59:612 – 625, 2013. doi: 10.1016/j.buildenv.2012.10.004.

B. Gowreesunker, S. Tassou, and M. Kolokotroni. Improved simulation of phase change processes in applications where conduction is the dominant heat transfer mode. *Energy and Buildings*, 47:353 – 359, 2012. doi: 10.1016/j.enbuild.2011.12.008.

C. Halford and R. Boehm. Modeling of phase change material peak load shifting. *Energy and Buildings*, 39(3):298 – 305, 2007. doi: 10.1016/j.enbuild.2006.07.005.

D. Heim and J. A. Clarke. Numerical modelling and thermal simulation of PCMâĂŞgypsum composites with ESP-r. *Energy and Buildings*, 36(8):795 – 805, 2004. doi: 10.1016/j.enbuild.2004.01.004.

M. A. Humphreys and F. J. Nicol. Outdoor temperature and indoor thermal comfort-raising the precision of the relationship for the 1998 ASHRAE database files studies. *ASHRAE Trans.*, 106(2):485–492, 2000.

S. R. Idelsohn, M. A. Storti, and L. A. Crivelli. Numerical methods in phase-change problems. *Archives of Computational Methods in Engineering*, 1(1):49 – 74, 1994. doi: 10.1007/BF02736180.

IEA. *Transition to Sustainable Buildings: Strategies and Opportunities to 2050*. IEA, Paris, France, 2013. ISBN 9789264202955. doi: 10.1787/9789264202955-en.

IEA. *World Energy Balances 2016*. OECD Publishing, Paris, France, 2016a. ISBN 9789264263116. doi: 10.1787/9789264263116-en.

IEA. *World Energy Outlook 2016*. IEA, Paris, France, 2016b. ISBN 9789264264953. doi: 10.1787/weo-2016-en.

IPCC. Climate Change. The physical Scientific Basis. Working Group I. Technical report, Intergovernmental Panel on Climate Change, 2013.

J. Belaunzarán Zamudio. Estudios de un sistema constructivo con cambio de fase, 2015. Tesis de maestría, Universidad Nacional Autónoma de México, Instituto de Energías Renovables.

M. Jaworski, P. apka, and P. Furmański. Numerical modelling and experimental studies of thermal behaviour of building integrated thermal energy storage unit in a form of a ceiling panel. *Applied Energy*, 113:548 – 557, 2014. doi: 10.1016/j.apenergy.2013.07.068.

F. Jiang, X. Wang, and Y. Zhang. A new method to estimate optimal phase change material characteristics in a passive solar room. *Energy Conversion and Management*, 52(6):2437 – 2441, 2011. doi: 10.1016/j.enconman.2010.12.051. 9th International Conference on Sustainable Energy Technologies (SET 2010).

X. Jin, M. A. Medina, and X. Zhang. On the importance of the location of PCMs in building walls for enhanced thermal performance. *Applied Energy*, 106:72 – 78, 2013. doi: 10.1016/j.apenergy.2012.12.079.

K. Johannes, J. Virgone, F. Kuznik, X. Wang, T. Haavi, and G. Fraisse. Applying energy storage in buildings of the future. Technical report, IEA - TASK C/Annex 23: Development of Sustainable Energy Storage Designs for a variety of Ultra-low energy building thermal, phase change materials and electrical storage options, February 2011.

X. Kong, S. Lu, Y. Li, J. Huang, and S. Liu. Numerical study on the thermal performance of building wall and roof incorporating phase change material panel for passive cooling application. *Energy and Buildings*, 81:404 – 415, 2014. doi: 10.1016/j.enbuild.2014.06.044.

J. Kośny. *PCM-Enhanced Building Components - An Application of Phase Change Materials in Building Envelopes and Internal Structures*. Engineering Materials and Processes. Springer International Publishing, Cham, Switzerland, 1 edition, 2015. ISBN 978-3-319-14285-2. doi: 10.1007/978-3-319-14286-9.

F. Kuznik and J. Virgone. Experimental investigation of wallboard containing phase change material: Data for validation of numerical modeling. *Energy and Buildings*, 41(5):561 – 570, 2009. doi: 10.1016/j.enbuild.2008.11.022.

F. Kuznik, D. David, K. Johannes, and J.-J. Roux. A review on phase change materials integrated in building walls. *Renewable and Sustainable Energy Reviews*, 15(1):379 – 391, 2011. doi: 10.1016/j.rser.2010.08.019.

F. Kuznik, K. Johannes, and D. David. Integrating phase change materials (PCMs) in thermal energy storage systems for buildings. In L. F. Cabeza, editor, *Advances in Thermal Energy Storage Systems: Methods and Applications*, Woodhead Publishing Series in Energy (Book 66), chapter 13, page 336. Elsevier Science, Cambridge, UK, 1 edition, 10 2014.

K. O. Lee, M. A. Medina, E. Raith, and X. Sun. Assessing the integration of a thin phase change material (PCM) layer in a residential building wall for heat transfer reduction and management. *Applied Energy*, 137:699 – 706, 2015. doi: 10.1016/j.apenergy.2014.09.003.

J. Lei, J. Yang, and E.-H. Yang. Energy performance of building envelopes integrated with phase change materials for cooling load reduction in tropical singapore. *Applied Energy*, 162:207 – 217, 2016. doi: 10.1016/j.apenergy.2015.10.031.

E. C. Lemmon. Phase-change techniques for finite element conduction codes. In R. W. Lewis and K. Morgan, editors, *Numerical Methods in Thermal Problems*, pages 149–158, 1979.

L. Long and H. Ye. The roles of thermal insulation and heat storage in the energy performance of the wall materials: a simulation study. *Scientific Reports*, 6(24181):1 – 9, 2016. doi: 10.1038/srep24181.

H. Mehling and L. F. Cabeza. *Heat and cold storage with PCM. An up to date introduction into basics and applications*. Heat and Mass Transfer. Springer-Verlag Berlin Heidelberg, Berlin, 1 edition, 2008. ISBN 978-3-540-68557-9. doi: 10.1007/978-3-540-68557-9.

Meteonorm. Meteonorm. Irradiation data for every place on Earth. URL `http://meteonorm.com`. .

E. Moreles and G. Huelsz. Hysteresis effect on the thermal performance of lightweight walls of the building envelope with phase change materials. In *Poster session at Third International Symposium on Renewable Energy and Sustainability (ISRES)*, Morelos, Mexico, Sep. 9-11 2015a.

E. Moreles and G. Huelsz. Thermal performance of lightweight walls with phase change materials. In *Proceedings of the 10th Conference on Advanced Building Skins*, pages 47 – 56, Bern, Switzerland, Nov. 3-4 2015b. Economic Forum.

K. Morgan, R. W. Lewis, and O. C. Zienkiewicz. An improved algrorithm for heat conduction problems with phase change. *International Journal for Numerical Methods in Engineering*, 12(7):1191 – 1195, 1978. doi: 10.1002/nme.1620120710.

D. Morillón-Gálvez, R. Saldaña-Flores, and A. Tejeda-Martínez. Human bioclimatic atlas for Mexico. *Solar Energy*, 76(6):781 – 792, 2004. doi: 10.1016/j.solener.2003.11.008.

K. Muruganantham. Application of phase change material in buildings: Field data vs. energyplus simulation. Master's thesis, Arizona State University, 12 2010.

D. Neeper. Thermal dynamics of wallboard with latent heat storage. *Solar Energy*, 68(5): 393 – 403, 2000. doi: 10.1016/S0038-092X(00)00012-8.

R. Nikolić, M. Marinović-Cincović, S. Gadzurić, and I. Zsigrai. New materials for solar thermal storageâĂŤsolid/liquid transitions in fatty acid esters. *Solar Energy Materials and Solar Cells*, 79(3):285 – 292, 2003. doi: 10.1016/S0927-0248(02)00412-9.

J. Onishi, H. Soeda, and M. Mizuno. Numerical study on a low energy architecture based upon distributed heat storage system. *Renewable Energy*, 22(1):61 – 66, 2001. doi: 10.1016/S0960-1481(00)00049-5.

S. V. Patankar. *Numerical Heat Transfer and Fluid Flow*. Taylor and Francis, Washington, United States, 1980. ISBN 9780891165224.

K. Peippo, P. Kauranen, and P. Lund. A multicomponent PCM wall optimized for passive solar heating. *Energy and Buildings*, 17(4):259 – 270, 1991. doi: 10.1016/0378-7788(91)90009-R.

S. Ramakrishnan, X. Wang, J. Sanjayan, and J. Wilson. Thermal performance of buildings integrated with phase change materials to reduce heat stress risks during extreme heatwave events. *Applied Energy*, 194:410 – 421, 2017. doi: 10.1016/j.apenergy.2016.04.084.

S. B. Sadineni, S. Madala, and R. F. Boehm. Passive building energy savings: A review of building envelope components. *Renewable and Sustainable Energy Reviews*, 15(8):3617 – 3631, 2011. doi: 10.1016/j.rser.2011.07.014.

J. Sage-Lauck and D. Sailor. Evaluation of phase change materials for improving thermal comfort in a super-insulated residential building. *Energy and Buildings*, 79:32 – 40, 2014. doi: 10.1016/j.enbuild.2014.04.028.

A. A. Samarskii and P. N. Vabishchevich. *Computational Heat Transfer - Mathematical Modelling*, volume 1. John Wiley and Sons Ltd, Chichester, United Kingdom, 1995. ISBN 978-0-471-95659-4.

SENER. SENER Norma oficial Mexicana NOM-020-ENER-2011 para eficiencia energética en edificaciones - Envolvente de edificios para uso habitacional, 9 de agosto 2011. Diario Oficial de la Federación, 44-89.

SENER. *Balance Nacional de Energía 2013*. Secretaría de Energía, México, 1 edition, 2014.

SENER. *Balance Nacional de Energía 2015*. Secretaría de Energía, México, 1 edition, 2016.

A. Sharma, V. Tyagi, C. Chen, and D. Buddhi. Review on thermal energy storage with phase change materials and applications. *Renewable and Sustainable Energy Reviews*, 13(2):318 – 345, 2009. doi: 10.1016/j.rser.2007.10.005.

S. D. Sharma and K. Sagara. Latent Heat Storage Materials and Systems: A Review. *International Journal of Green Energy*, 2(1):1–56, 2005. doi: 10.1081/GE-200051299.

T. Silva, R. Vicente, N. Soares, and V. Ferreira. Experimental testing and numerical modelling of masonry wall solution with {PCM} incorporation: A passive construction solution. *Energy and Buildings*, 49:235 – 245, 2012. doi: 10.1016/j.enbuild.2012.02.010.

N. Soares, J. Costa, A. Gaspar, and P. Santos. Review of passive PCM latent heat thermal energy storage systems towards buildings' energy efficiency. *Energy and Buildings*, 59:82 – 103, 2013. doi: 10.1016/j.enbuild.2012.12.042.

N. Soares, A. Gaspar, P. Santos, and J. Costa. Multi-dimensional optimization of the incorporation of PCM-drywalls in lightweight steel-framed residential buildings in different climates. *Energy and Buildings*, 70:411 – 421, 2014. doi: 10.1016/j.enbuild.2013.11.072.

N. Soares, C. F. Reinhart, and A. Hajiah. Simulation-based analysis of the use of PCM-wallboards to reduce cooling energy demand and peak-loads in low-rise residential heavyweight buildings in Kuwait. *Building Simulation*, 10(4):481–495, 2017. doi: 10.1007/s12273-017-0347-2.

U. Stritih and P. Novak. Solar heat storage wall for building ventilation. *Renewable Energy*, 8(1):268 – 271, 1996. doi: 10.1016/0960-1481(96)88860-4.

V. R. Voller, C. R. Swaminathan, and B. G. Thomas. Fixed grid techniques for phase change problems: A review. *International Journal for Numerical Methods in Engineering*, 30(4): 875–898, 1990. doi: 10.1002/nme.1620300419.

T. Whiffen and S. Riffat. A review of PCM technology for thermal energy storage in the built environment: Part I. *International Journal of Low-Carbon Technologies*, 8(3):147–158, 2013. doi: 10.1093/ijlct/cts021.

X. Zeng and A. Faghri. Temperature-transforming model for binary solid-liquid phase-change problems. Part I: Mathematical modeling and numerical methodology. *Numerical Heat Transfer, Part B: Fundamentals*, 25(4):467–480, 1994. doi: 10.1080/10407799408955931.

Y. Zhang, Y. Jiang, and Y. Jiang. A simple method, the T-history method, of determining the heat of fusion, specific heat and thermal conductivity of phase-change materials. *Measurement Science and Technology*, 10(3):201, 1999. doi: 10.1088/0957-0233/10/3/015.

Y. Zhang, K. Lin, R. Yang, H. Di, and Y. Jiang. Preparation, thermal performance and application of shape-stabilized pcm in energy efficient buildings. *Energy and Buildings*, 38 (10):1262 – 1269, 2006. doi: 10.1016/j.enbuild.2006.02.009.

Y. Zhang, G. Zhou, K. Lin, Q. Zhang, and H. Di. Application of latent heat thermal energy storage in buildings: State-of-the-art and outlook. *Building and Environment*, 42(6):2197 – 2209, 2007. doi: 10.1016/j.buildenv.2006.07.023.

D. Zhou, C. Zhao, and Y. Tian. Review on thermal energy storage with phase change materials (PCMs) in building applications . *Applied Energy*, 92:593 – 605, 2012. doi: 10.1016/j.apenergy.2011.08.025.

G. Zhou, Y. Zhang, X. Wang, K. Lin, and W. Xiao. An assessment of mixed type PCM-gypsum and shape-stabilized PCM plates in a building for passive solar heating. *Solar Energy*, 81(11):1351 – 1360, 2007. doi: 10.1016/j.solener.2007.01.014.

G. Zhou, Y. Zhang, K. Lin, and W. Xiao. Thermal analysis of a direct-gain room with shape-stabilized PCM plates. *Renewable Energy*, 33(6):1228 – 1236, 2008. doi: 10.1016/j.renene.2007.06.024.

N. Zhu, S. Wang, Z. Ma, and Y. Sun. Energy performance and optimal control of air-conditioned buildings with envelopes enhanced by phase change materials. *Energy Conversion and Management*, 52(10):3197 – 3205, 2011. doi: 10.1016/j.enconman.2011.05.011.